

DIPLOMA THESIS ASSIGNMENT FORM

I. PERSONAL AND STUDY DATA

Surname: MORITZ Name: MASON Personal number: 520838

Assigning Department: Department of Mechanics

Study programme: Civil Engineering

Study branch/spec.: Advanced Masters in Structural Analysis of Monuments and Historical Constructions

II. DIPLOMA THESIS DATA

Diploma Thesis (DT) title: Vliv tuhosti tradičních tesařských spojů na distribuci vnitřních sil v historických dřevěných konstrukcích

Diploma Thesis title in English: The influence of carpentry joint stiffness and modelling techniques on internal forces distribution in traditional timber structures

Instructions for writing the thesis:

Since the realistic modelling of timber structures is an important part of a sensitive repair design, the analysis of the influence of different joints to the overall stiffness of the structure is needed. As timber members have high stiffness in comparison to the joints and connections present in the structure, the joints mechanical response is of significant importance for the load distribution in the structure. The study should focus on three main historic construction types present in Europe (will be specified). These constructions should be modelled in 2D using standard structural analysis software and in each of them the sensitivity study of influence of boundary conditions and joint stiffness should be made. Moreover, the description of missing information of several traditional timber joint types and their stiffness response should be addressed and questioned. The thesis shall serve as a preliminary study for a broader research in timber joints and their influence in overall structural response. Valuable results are expected: typology of joints and their mechanical representation in the model; literature review of existing resources regarding traditional timber joints; guidelines for further research in a practice-driven topic

List of recommended literature:

Carpentry joints, Manfred Gerner (in Czech), 2003, Grada. Kunecký, Jiří - Hasníková, Hana - Kloiber, Michal - Milch, J. - Sebera, V. - Tippner, J. Structural assessment of a lapped scarf joint applied to historical timber constructions in central Europe. International Journal of Architectural Heritage. Roč. 12, č. 4 (2018), s. 666-682

Milch, J. - Tippner, J. - Sebera, V. - Kunecký, Jiří - Kloiber, Michal - Navrátil, M.

The numerical assessment of a full-scale historical truss structure reconstructed with use of traditional all-wooden joints. Journal of Cultural Heritage. Roč. 21, September-October (2016), s. 759-766.

Wald F., Mareš J., Sokol Z., Drdác M. (2000) Component Method for Historical Timber Joints. In: Baniotopoulos C.C., Wald F. (eds) The Paramount Role of Joints into the Reliable Response of Structures. NATO Science Series (Series II: Mathematics, Physics and Chemistry), vol 4. Springer, Dordrech

Name of Diploma Thesis Supervisor: Jiří Kunecký

DT assignment date: 14.3.2023

DT submission date in IS KOS: 6.7.2023

see the schedule of the current acad. year

DT Supervisor's signature

Head of Department's signature

III. ASSIGNMENT RECEIPT

I declare that I am obliged to write the Diploma Thesis on my own, without anyone's assistance, except for provided consultations. The list of references, other sources and consultants' names must be stated in the Diploma Thesis and in referencing I must abide by the CTU methodological manual "How to Write University Final Theses" and the CTU methodological instruction "On the Observation of Ethical Principles in the Preparation of University Final Theses".

4/4/2023

Assignment receipt date

Mason Moritz

Student's name

DECLARATION

Name: Mason Moritz

Email: mcmsahc@gmail.com | masonmoritz@gmail.com

Title of the Msc Dissertation: The influence of carpentry joint stiffness and modelling techniques on internal forces distribution in traditional timber structures

Supervisor(s): Jiří Kunecký

Year: 2023

I hereby declare that all information in this document has been obtained and presented in accordance with academic rules and ethical conduct. I also declare that, as required by these rules and conduct, I have fully cited and referenced all material and results that are not original to this work.

I hereby declare that the MSc Consortium responsible for the Advanced Masters in Structural Analysis of Monuments and Historical Constructions is allowed to store and make available electronically the present MSc Dissertation.

University: Czech Technical University in Prague

Date: 06/07/2023

Signature: Mason Moritz_____

Dedication-

I would like to express my deepest gratitude and appreciation to all those who have contributed to the completion of this thesis, which examines the field of structural engineering within the context of historic structures. Without their unwavering support, invaluable guidance, and encouragement, this work would not have been possible.

First and foremost, I would like to extend my heartfelt thanks to my parents for their endless love, encouragement, and sacrifices throughout my academic journey. Their unwavering belief in me has been a constant source of inspiration, and I am truly grateful for them and everything they do.

To my sister, whose unwavering belief in my abilities has been a constant source of motivation, I am deeply grateful. Your encouragement, constructive feedback, and endless support have been invaluable to me, and I cannot thank you enough.

Last but certainly not least, I want to express my heartfelt appreciation to my supportive girlfriend, Charmae. Your love, patience, and understanding have been an anchor in my life, especially during the demanding phases of this thesis. Your unwavering belief in my abilities and your willingness to lend an ear and offer support have been invaluable. I am deeply grateful for your presence in my life.

Your belief in me, encouragement, and assistance have been crucial in bringing this thesis to fruition. Thank you all for being an integral part of my success and for making this experience truly remarkable.

This page is left blank on purpose.

This page is left blank on purpose.

ACKNOWLEDGEMENTS

I am indebted to my supervisor Jiří Kunecký, whose expertise and guidance has shaped my understanding of timber, carpentry, and FEA in the context of historic structures. Your mentorship has been instrumental in shaping my research, and I am grateful for your patience, wisdom, and willingness to share your knowledge.

A special mention goes to Jiri Blaha, who provided the AutoCAD drawings from each of the structures. They were instrumental and much appreciated

I would also like to extend my gratitude to the SAHC Consortium, from whom I was privileged to be awarded a generous scholarship that has allowed me to follow my passions and make lifelong friends.

In conclusion, I would like to acknowledge the contributions of all those who have supported and taught me on this academic journey.

This page is left blank on purpose.

ABSTRACT

This thesis will focus on the evaluating the sensitivity of historic timber trusses to various stiffness parameters and boundary conditions. Values including rotational stiffness, axial tension stiffness, and compressive stiffness are utilized for this purpose. Three different historic trusses from the Czech Republic were modeled including a collar rafter roof with scissor braces, an interior truss from a ‘Stehender stuhl’ roof, and a ležatá stolice truss with a typical inner supporting frame. It was found that the typical assumption that joints can be modelled as rotational hinges is valid when stiffness is evenly distributed through a structure. Where numerous elements connect at one location and create a rigid zone in the truss the hinges struggle to accurately predict the interactions and of the members involved. Axial stresses were the most commonly accurate measure, with the hinged model often overconservative by just over 10%. Moment was underestimated by the hinge assumption in the cases of supporting struts which could not adequately have the bending stresses imposed from the internal components of the roof. The hinged connection assumption is acceptable for truss configurations that are regularly loaded and have a clear load path to the supports.

This page is left blank on purpose.

RESUMO

Vliv tuhosti tradičních tesařských spojů na distribuci vnitřních sil v historických dřevěných konstrukcích

Tato práce se zaměřuje na popis vlivu různých parametrů, jako jsou tuhosti spojů a okrajových podmínek, na distribuci sil v dřevěných historických konstrukcích. Pro tento účel se používá variování hodnot rotační tuhosti, axiální tuhosti v tahu a tuhosti v tlaku. Byly vymodelovány tři historické krovy z České republiky, a to zejména jedna kroevní soustava s ondřejskými kříži reprezentující středověké krovy, dále pak jedna ležatá a jedna stojatá stolice, každá typická pro jisté období. Bylo zjištěno, že typický předpoklad, že spoje mohou být modelovány jako kloubové styčníky, platí, zejména když je tuhost rovnoměrně rozložena v konstrukci. Tam, kde se mnoho prvků spojuje na jednom místě a vytváří tuhou zónu v příhradovém nosníku, schopnost předpovědět zapojení jednotlivých nosníků je v tomto způsobu modelování omezená. Porovnání normálových sil bylo nejčastěji kritériem, přičemž kloubový model byl často více konzervativní o 10 %. Hodnota ohybového momentu byla podceňena předpokladem kloubového styčníku zejména v případech vzpěr či pásků. Předpoklad kloubového spojení je přijatelný pro konstrukce, které jsou rovnoměrně zatíženy a kde přenos sil probíhá přímo bez dalšího větvení od zatížení k podporám.

This page is left blank on purpose.

This page is left blank on purpose.

TABLE OF CONTENTS

Contents

1.	Introduction.....	15
2.	Historical context	17
2.1	Timber as a Historic Building Material.....	17
2.2	Timber Roof Construction in the Czech Republic.....	18
2.3	Case Study Structures	21
2.3.1	House in Slavonice (1835)	21
2.3.2	Church of the Holy Trinity, Třebíč (1563).....	23
2.3.3	Doksy Chateau (1828)	25
3.	Literature review	29
3.1	Limitation on standardization	31
3.2	Semi-rigid Joint Theory.....	32
4.	CONNECTION TYPOLOGIES AND INVENTORY	35
4.1	Crossing Joints (X Joints)	35
4.1.1	Lap Joints.....	35
4.2	Corner or Angle Joints (L Joints).....	36
4.2.1	Forked Bridle Joint	36
4.3	Encounter Joints (T-Joints).....	37
4.3.1	Mortise and tenon.....	37
4.3.2	Rafter Ends	38
4.3.2.1	Oblique tenon joint.....	38
4.3.2.2	Notched Rafter	38
4.3.3	Dovetail Joints.....	39
5.	Materials and methods.....	41
5.1	Numerical Model Description	41
5.2	Material and Mechanical Properties	44
5.3	Estimation of Joint Stiffness	45
5.4	Loading.....	48
6.	results.....	51
6.1	Třebíč Truss Model.....	51
6.2	Slavonice Truss Model.....	54
6.3	Doksy Truss Model	60
7.	Conclusion.....	62
8.	References	64
9.	AppendICES	66
9.1	Appendix A	66
9.2	Appendix B	68
9.3	Appendix C: Expanded Images from Figure 30.....	70
9.4	Appendix D: Expanded Images from Figure 31.....	74
9.5	Appendix E: Expanded Images from Figure 34.....	77
9.6	Appendix F: Expanded Images from Figure 35.....	81
9.7	Appendix G: Expanded Images from Figure 36.....	85
9.8	Appendix H: Expanded Images from Figure 38.....	87

Figure 1. Wood species use in the Czech Republic constructions over time	18
Figure 2. Typological example of a purlin roof.....	19
Figure 3. Typological example of a rafter roof with a queen strut inner frame.....	19
Figure 4. Case study structure locations on a map of the Czech Republic (original map per Wikimedia Commons).....	21
Figure 5. B. Němcové 543 Slavonice baroque house.....	22
Figure 6. Satellite view of the house in Slavonice (per Google Earth)	22
Figure 7. The queen post and passing brace truss (top) and simplified collar truss (bottom)	23
Figure 8. Church of the Holy Trinity in Třebíč.....	24
Figure 9. Satellite view of the Church of the Holy Trinity in Třebíč (per Google Earth)	25
Figure 10. Church of the Holy Trinity truss	25
Figure 11. Satellite view of the Doksy Chateau (per Google Earth).....	26
Figure 12. Doksy Chateau (per Toulava Kamera, 2019)	26
Figure 13. Ležatá stolice truss drawing from the Doksy Chateau (Bláha, n.d.).....	27
Figure 14. Pinned, semi-rigid, and fixed end conditions of a uniformly loaded beam (Fang, 2020)	32
Figure 15. Perpendicular half lap joint (Left) and notched-angle half lap joint (Right) (Gerner, 1992)	36
Figure 16. Forked bridle joint (Gerner, 1992)	37
Figure 17 Perpendicular mortise and tenon (Left) and oblique tenon joint (Right) (Gerner, 1992)	38
Figure 18 Hidden notch (Left) and hidden notch with tenon (Right) (Gerner, 1992).....	39
Figure 19. Double notched perpendicular lapped dovetail (Left), and angled single notch lapped dovetail (Right) (Gerner, 1992).....	40
Figure 20. Třebíč truss and connection typology identification	41
Figure 21. Slavonice truss and connection typology identification.....	42
Figure 22. Doksy Chateau truss and connection typology identification	42
Figure 23. BEAM188 cross-section cells (left) and geometry (right) (ANSYS Inc., 2023b) ...	43
Figure 24. COMBIN14 Element geometry (ANSYS Inc., 2023b)	43
Figure 25. Doksy Chateau truss model configuration where the blue springs indicate a triad of 1D spring elements.....	44
Figure 26. – Spring equivalents for perpendicular to grain deformations.....	46
Figure 27. Subsidence factor equation per (Kitamori et al., 2009).....	46
Figure 28. Wind loading zones of dual-pitched roof 9 (CEN, 2005).....	50
Figure 29. Flat snow loads map for the Doksy Chateau (GACR Project, n.d.)	50
Figure 30. (From top) Trebic deflection, axial force, bending moment, and shear force distributions for the spring model (left) and hinged model (right)	52
Figure 31. (From top) Trebic roof deflection, axial force, and bending moment, distributions for the spring model with a pin and roller (left) and a pin at each end (right)	54
Figure 32. Boundary condition at rafter base influence on collar tie forces (Branco & Descamps, 2015).....	55
Figure 33. (From top) Absolute deflection, shear force, bending moment, and axial force distributions for the spring model (left) and hinged model (right)	56
Figure 34 (From top) Absolute deflection, shear force, bending moment, and axial force distributions for the semi-rigid model with a roller (left) and a pins (right)	58
Figure 35. Absolute deflection, shear force, bending moment, and axial force distributions for the spring model at collar tie axial force inflection point.....	59
Figure 36 convergence of rafter end spring truss to the boundary conditions.....	59
Figure 37. Image capture of the collar and subcollar overlapping.....	60
Figure 38. Absolute deflection, shear force, bending moment, and axial force distributions for the spring model at collar tie axial force inflection point.....	61

1. INTRODUCTION

The ability to realistically model timber joinery and connections is critical in the assessment and repair of sensitive existing structures. Timber truss roofs exemplify the diversity of joint types with varying complexity, different types of force distributions, and a variety of inherent structural properties. Additionally, due to the typical static indeterminacy of trusses, the actual behaviour of these connections can have huge implications on force distribution to the various components.

Current standards such as Eurocode 5 (EC5) and the American Wood Council's NDS give little to no guidance on the handling of traditional wood joints and rather focus on modern mechanical connections. In addition, preservation and maintenance organisations such as ICOMOS dictate mechanical compatibility and ideally the duplication of traditional woodworking joints in the case of repair or prosthesis of historical timber structures (ICOMOS, 1999). A recent questionnaire of practitioners in Europe regarding the connections chapter of EC5 revealed that more than half (55%) of the practitioners surveyed think that connections require excessive effort to design according to the current standards, 26% think that the present methods could lead to uneconomic construction, 28% feel that the section is lacking complete coverage of the topic, and 52% believe that the connections chapter contains incorrect or inaccurate information (Cabrero et al., 2018). In each of these categories, connections were the most common response, revealing a dearth of knowledge of traditional wood joints.

In engineering practice, wood joints are often simplified and assumed to behave as hinges, and on occasion, as fully rigid. However, most timber joints behave somewhere in between and can be described as semi-rigid. This assumption is attractive because it simplifies the overall modelling process and can drastically speed up the computation time when dealing with complex structures and loading configurations. This decision can drastically overestimate the calculated demand on a timber connection and could lead to unnecessary work being carried out in the name of safety and preservation (Branco, 2008). For this reason, it is necessary to develop a framework and understanding of how the modeling method and assigned stiffness properties of timber joints in historical timber roofs influence their behavior and internal force distributions under realistic service loads. This study will aim to model and compare three historical truss roofs from the Czech Republic that represent common typologies seen

throughout central Europe and iterate on the boundary conditions and joints to evaluate their behavior.

2. HISTORICAL CONTEXT

2.1 Timber as a Historic Building Material

The first timber trusses are estimated to have been utilised in the construction of primitive lake dwellings during the Bronze Age around 2500 BC. They were widely adopted by the ancient Greeks for roofs and were typical during the Middle Ages. Some of the earliest plans and drawings for trusses are found in Andrea Palladio's *Four Books on Architecture*, written in 1570 (Britannica, 1998).

The popularity of wood as a building material can be attributed to several factors including its abundance, its versatility, and its favourable strength-to-weight ratio. It is an orthotropic material, meaning that it exhibits different mechanical properties in different directions. However, the primary limitation of timber is its durability. This includes sensitivity to moisture content, humidity, biological attacks, and insect infestation.

A study of wood species utilization in the Czech Republic from the 13th through 20th century found that 99.7% of historical timber constructions are made of fir, spruce, pine, or oak (Kolář et al., 2021). Fir is most common in eastern Moravia and Silesia, spruce is dominant in the western and central parts of the Czech Republic, pine and oak are more localized where they are more abundantly grown, and in central Bohemia and southern Moravia. Fir was the primary type used for construction in, and following, Medieval times. However, because of planted forests of spruce trees, spruce became much more commonly used by the end of the 19th century. Fir and spruce were the two most common wood species used in roof constructions, making up 42.5% and 41.4% of the surveyed structures respectively oak (Kolář et al., 2021). The use of these species over time can be seen in Figure 1

Below are the following types of wood most found across the greater European geography:

- Larch: high elevations of the Swiss Alps, Tetra region of Slovakia (Buentgen & et al., 2006)
- Oak: typical in situations where higher strength was demanded (such as belfries, pillars, lintels, arches) and for marine and freshwater constructions thanks to its mechanical retention at higher moisture content levels (Prokop et al., 2017)

- Pine: the Netherlands (Sass-Klaassen et al., 2008), Norway (Thun, 2005)
- Spruce: foothill regions of the Austrian Alps (Klein & Grabner, 2015)

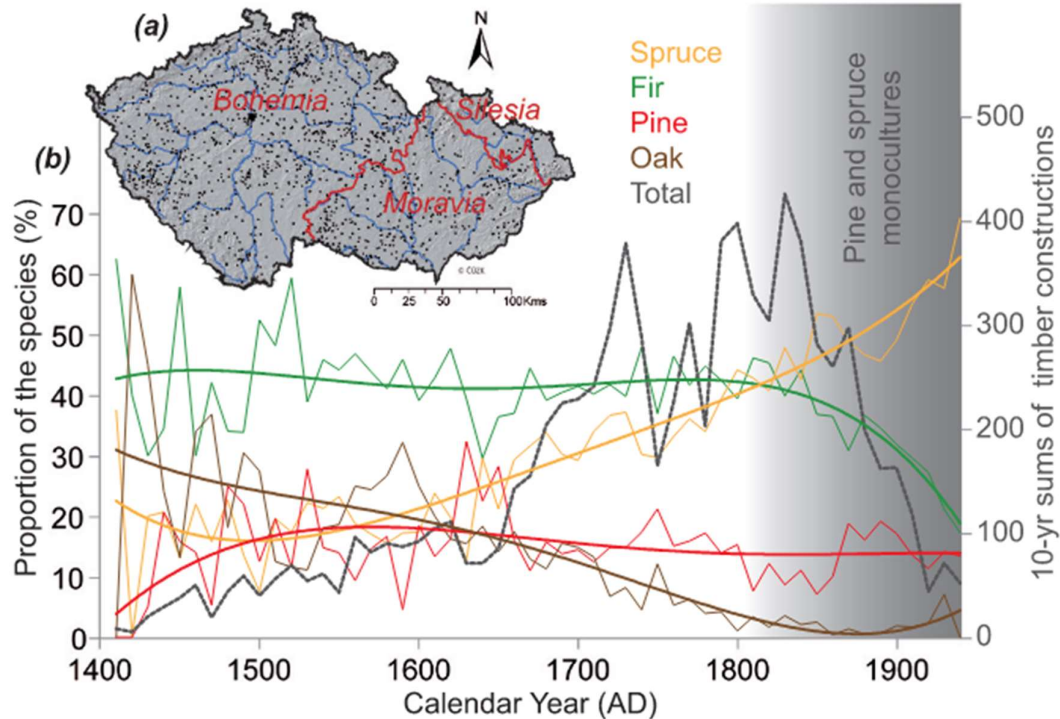


Figure 1. Wood species use in the Czech Republic constructions over time

2.2 Timber Roof Construction in the Czech Republic

Timber construction has been a staple of Czech architecture for centuries. The oldest existing trusses in the Czech Republic date back to the 14th century, circa 1320 (Narodni Technicke Muzeum, 2023). Wood was a dominant construction material throughout the Middle Ages and up until the mid-18th century when the construction of exposed wooden structures was halted over fire concerns (Škabrada, 2007). This culminated in an all-out ban on wooden constructions in 1816, forcing even rural villages into widespread adoption and dependency on masonry construction. By the time the laws were rolled back, construction workers had adapted, and masonry had become the dominant form of construction in towns, whereas timber construction was relegated to use in rural villages and farmhouses.

Before the modern advent of mechanical saws, the members of a roof would be cut down from logs and hewn into members using axes. Rafters and trusses were typically pre-

assembled on the ground of the building site or at the lumber yard itself. This preliminary construction ensured that connections had an acceptable tolerance and fit which is critical to the function and rigidity of joints as previous studies have shown that gaps and poor fits are responsible for considerable loss in stiffness of truss joints (Kunecký, 2015). At this time, pre-drilling for wood pegs would be done if needed, and assembly markings would be drawn to speed up the in-situ installation. This pre-fitting process meant that on-site erection went quickly. Softwoods were exclusively used for their workability and ease of use for carpenters. Wooden pins, also known by the German ‘*holznagel*’, were made of the hardwood of deciduous trees. Often square dowels would be used and hammered into round holes to increase the normal force and friction between them. Wood dowels remained popular until mechanical connections became widely available and codified.

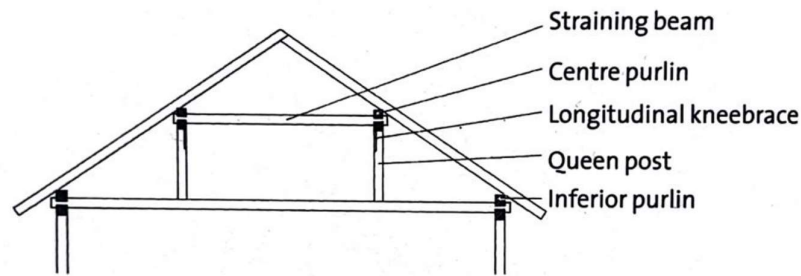


Figure 2. Typological example of a purlin roof

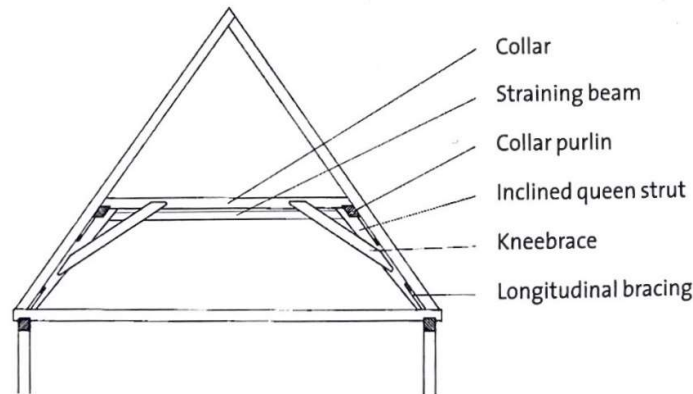


Figure 3. Typological example of a rafter roof with a queen strut inner frame

Two types of trusses are prevalent in the Czech Republic: coupled rafter (or spar) roofs and purlin roofs (Narodni Technicke Muzeum, 2023). Purlin roofs were most common up to the 1200s, whereafter coupled rafter trusses dominated construction, and purlin roofs were then relegated to use in rural areas and farmhouses. The structural system of the purlin roofs was organised such that the rafters were supported by longitudinally spanning purlins (Zwenger,

2012). Spar roofs, on the other hand, relied on a coupled rafter and sub-rafter on each side of the ridge, and a tie beam to resist thrust. Developments in construction came over time, and with the demand for greater spans came the need for innovation. More complex roof systems integrated multiple levels of collar ties, purlins, diagonal trusses, cross-braces, and various other structural components. These components served to add rigidity to the global behaviour of the roof.

One can see both a temporal and spatial distribution to roof typologies as carpentry was a very specialised vocation and master carpenters would travel from town to town, staying only as long as it took to finish a given project. Some elements, however, can be tracked to show structural trends over time. Diagonal scissor bracing was a typical addition in the 14th century for its simplicity and added rigidity. King post trusses with paired rafter bracing and queen-posts were typical in the late 15th century. Furthermore, the addition of sprockets at the truss ends provided an extra measure of protection to the rafter bases by distancing them from exposure to moisture and the environment. Often, one can find large deviations in the typologies or the combination of multiple systems together.

There are subtle differences that can be seen over time. For example, Romanesque period trusses have a lower pitch than those built during the Gothic period, and between the two the order of construction changed from building the gables prior to the roof construction to building the roof and then the gable ends (Škabrada, 2007). In addition, Gothic trusses can be noted by their more prolific use of longitudinal bracing.

The Baroque period saw an evolution in roof shape, shifting from gabled roofs to hipped and gambrel roof shapes. The roofs continued to utilize longitudinal bracing, showing an understanding of the need for lateral force-resisting systems. With this 18th-century change in roof shape came an adjustment to the principal supporting struts which gained a taper as they came into the base supports. Likely, this taper served to resist a greater moment or shear force and direct those forces into the walls. From the Baroque period on, metal connectors made from iron and steel can be found.

In the 1800s, roof framing developed because of an increased demand for economic optimization. Michael Ranek, a Hungarian carpenter living in Prague, modified the typical Baroque trusses by removing the collars through the addition of truncated principal rafters (Bláha & Ebel, 2005). These types of trusses quickly became popular due to their relative

simplicity and fast construction. Ranek's trusses have been criticized by modern engineers because too much was removed in the process of making the roofs more economical. These oversimplified trusses are notoriously harder to repair when deteriorated. In the latter half of the 19th century these fell out of fashion in favor of a return to purlin roofs. Soon after, railroads revolutionized the transportation of materials and allowed for prefabricated systems and metal hardware to become more widely available and used (Narodni Technicke Muzeum, 2023). This brought about the more modern mechanically connected trusses for which prescriptive methods for design exist.

2.3 Case Study Structures

This thesis will analyze three historic trusses from the Czech Republic.

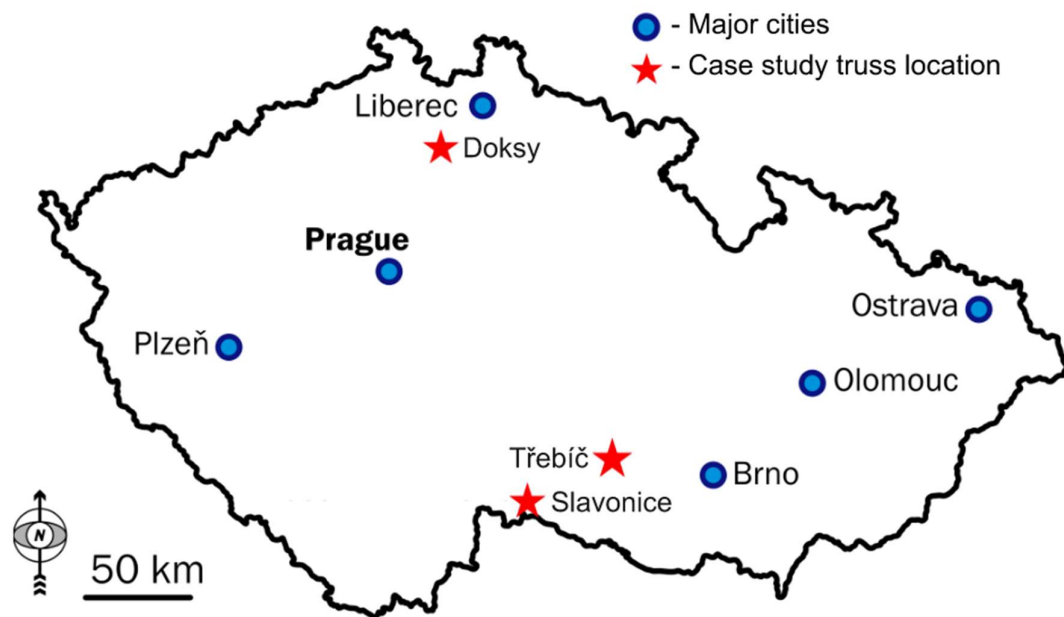


Figure 4. Case study structure locations on a map of the Czech Republic (original map per Wikimedia Commons)

2.3.1 House in Slavonice (1835)

Boženy Němcové 543 Slavonice is a residential house located in Slavonice, a southern Bohemian town near the Czech Republic's border with Austria. The town was founded in the 12th century and gained prominence and wealth in the 16th century because of its ideal location along the trade route between Prague and Vienna (CzechTourism, 2020). The house is

representative of the post-baroque, or “peasant baroque” gabled houses constructed at the turn of the 18th and 19th centuries. It is a registered cultural monument as declared by the Ministry of Culture of the Czech Republic in 2002. The existing set of plans dates the roof to 1809 and 1835.



Figure 5. B. Němcové 543 Slavonice baroque house

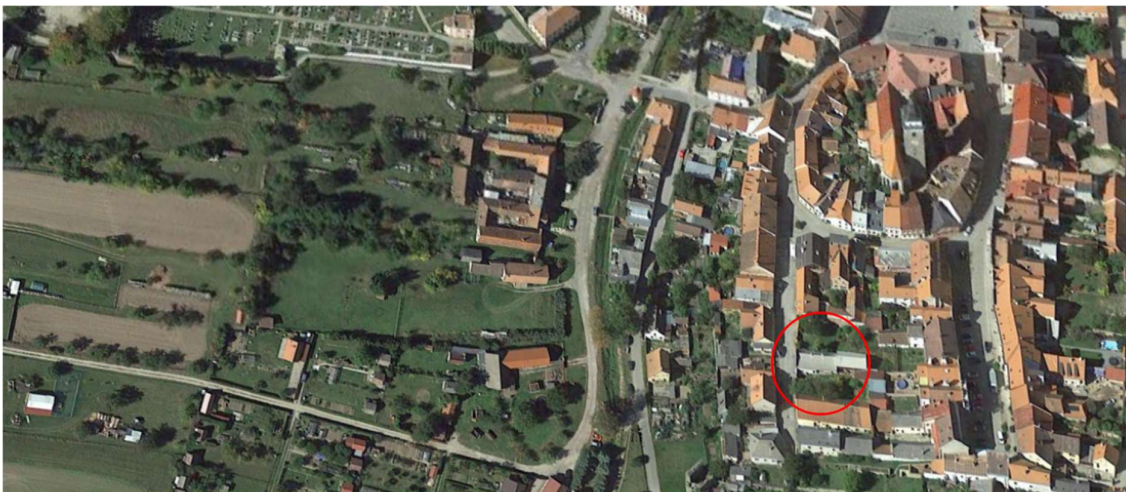


Figure 6. Satellite view of the house in Slavonice (per Google Earth)

Two types of trusses exist in this structure whose roof can be globally classified as a transition spar roof wherein the influence of purlin systems can be easily seen through the longitudinal components. The first configuration can be seen in Figure 7 (top) and consists of a primary rafter and tie beam system. A collar tie rests on longitudinally spanning collar purlins which give extra support to the interior trusses. Those collar purlins are vertically supported by queen posts which then bear on the collar tie. Additionally, a pair of diagonal passing braces run parallel to the main rafters and span from the collar to the tie beam. These trusses are spaced at 6 meters on center with three of the simplified trusses in between at 2 meters on center. The simplified trusses consist only of the rafters and collar tie, and it gains support from the collar purlins that run longitudinally. This type of truss is typical in Austria, Bavaria, and other areas of Catholic German influenced nations (Škabrada, 2007). Carpenters brought the technique to the near-border parts of the Czech Republic, and they are particularly common in Šumava and the south, referred to as “Stehender stuhl” (Binding, 1990).

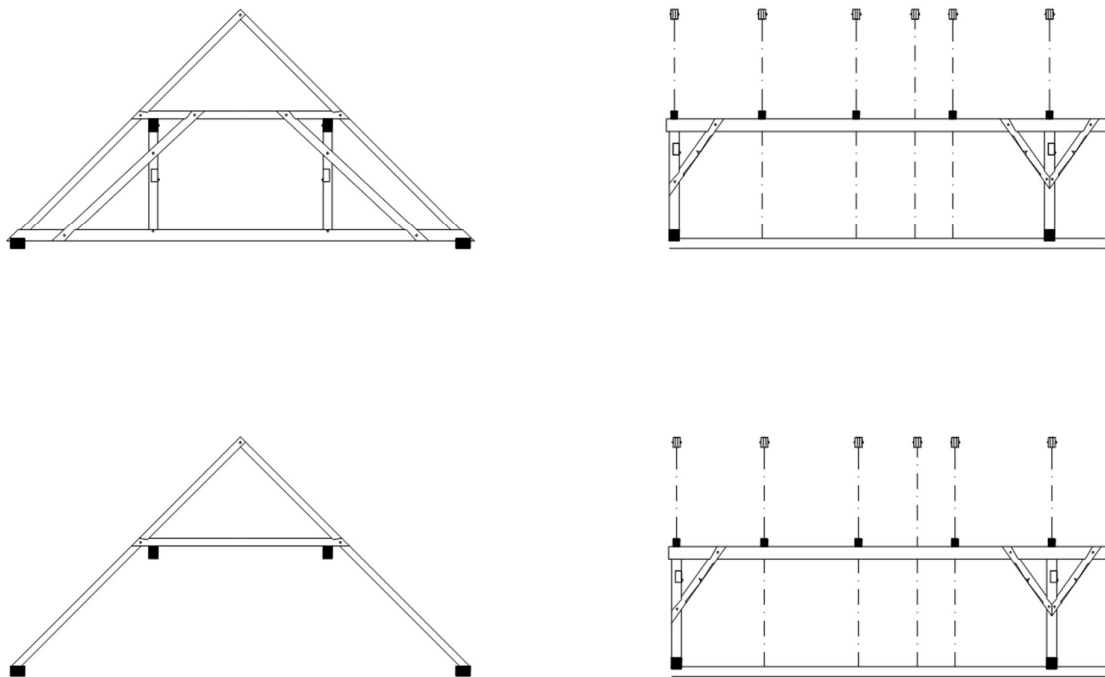


Figure 7. The queen post and passing brace truss (top) and simplified collar truss (bottom)

2.3.2 Church of the Holy Trinity, Třebíč (1563)

The Church of the Holy Trinity is in the Moravian municipality of Třebíč. It is said to have been built sometime between the 9th and 15th century, with the lack of knowledge owed to

an 1822 fire in the provincial archives in Brno (Vyhnalová, 2013). The walls of the church are made of quarry stone. A significant reconstruction is recorded to have occurred starting in 1564 to prepare the property for the incoming Hussite faction. Additional works such as modification of the sacristy and reconstruction of the church roof took place until 1575, which brought the structure to its modern state.

The church was a privileged place of worship and holy pilgrimage (Vyhnalová, 2013). In the 1930s there was an annual pilgrimage made to the church on the first Sunday of June. The church is a branch of the Roman Catholic parish of Třebíč, which falls under the diocese of Brno. Church services were held on the first Saturday of each month as well as All Souls Day. As of May 3, 1958, the church has been registered to the list of immovable cultural monuments.



Figure 8. Church of the Holy Trinity in Třebíč

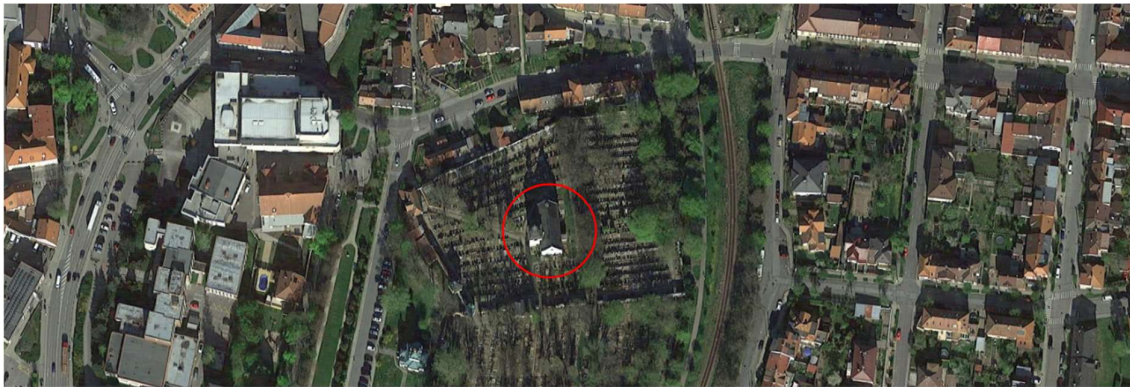


Figure 9. Satellite view of the Church of the Holy Trinity in Třebíč (per Google Earth)

The spar roof of the church is a collar-rafter roof with scissor braces, which exemplifies a typical structural arrangement popularized in the 14th century, despite being constructed roughly two centuries later. The system (see Figure 10) utilizes a bottom chord, vertical braces, scissor braces forming a St. Andrew’s cross, a collar-tie, and eave-sprockets to divert snow and rain from damaging the rafter ends. The trusses are closely spaced at about 1.1 meters on center.

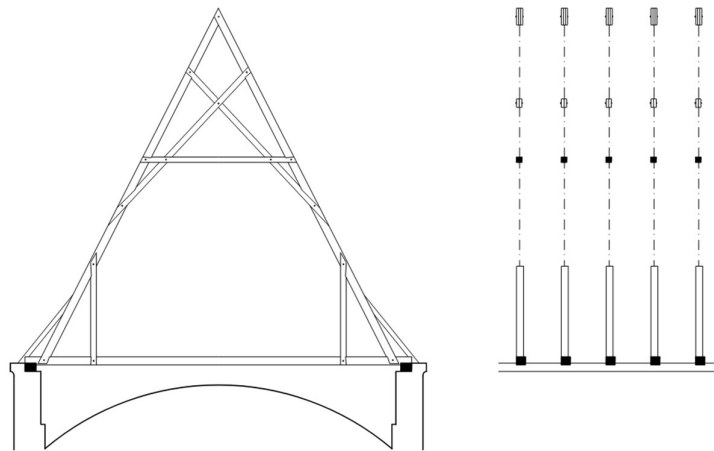


Figure 10. Church of the Holy Trinity truss

2.3.3 Doksy Chateau (1828)

The Doksy Chateau is a gothic castle that was originally constructed in the 16th century when John of Vartemberk bought the land from Emperor Rudolf II. The castle was eventually rebuilt in the 19th century to which it owes its present baroque construction and configuration to. The most modern updates were made in the early 20th century when heating, plumbing, and electrical were installed.

The Chateau construction consists of a U-shaped collection of buildings with a belfry at one corner. The main wing is at the base of the “U” and is flanked by the eastern and western wings, all of which encompass a large courtyard.



Figure 11. Satellite view of the Doksy Chateau (per Google Earth)



Figure 12. Doksy Chateau (per Toulava Kamera, 2019)

With several wings to the chateau, multiple configurations of trusses exist. A majority of them share common structural components including a tie beam, collar, straining beam, tapered queen strut, and knee braces. Spans vary from 10-16 meters, and for the purpose of this

study one of the 10-meter span, queen-strut, roof trusses was selected for more in depth analysis. This type of truss is known as “Liegende stuhl” in German or “ležatá stolice” in Czech (Škabrada, 2007).

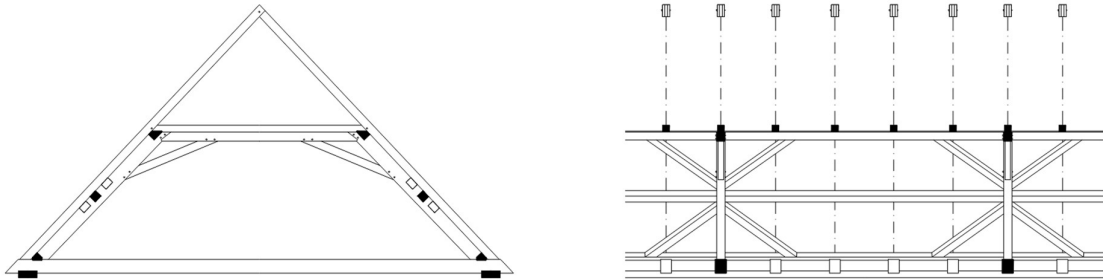


Figure 13. Ležatá stolice truss drawing from the Doksy Chateau (Bláha, n.d.)

3. LITERATURE REVIEW

Timber joinery stiffness and behaviour has been an ongoing topic of engineering interest. Many specific types of connections lack specific study and experimentation, but a plethora of campaigns have been undertaken to determine, estimate, and verify the behaviour of historic carpentry joints. Two papers were identified that provided an overview of the state of existing literature on the topic of joint rigidity and analysis. Anna Karolak summarised the current state of knowledge and sources pertaining to scarf and splice carpentry (Karolak et al., 2020) and Demi Fang collected and categorized literature that characterized analysis and behaviour of statically loaded joints. The collective sources along with those additionally collected for the present study are listed below in Table 1.

Table 1. State of methods and studies analysing and examining timber joint behaviour

Joint type	Year	Name	Experimental	Numerical	Analytical
THEORY AND BEARING					
Bearing and embedment theory	1991	Inayama (in Japanese)	✓		✓
Embedment theory	2009	Kitamori, Kataoka, and Komatsu (in Japanese)	✓	✓	✓
NUKI JOINTS					
Nuki, beam through column with wedges	2008	Guan, Kitamori, and Komatsu	✓	✓	
Continuous Nuki joint	2006	Chang, Hsu, and Komatsu	✓		✓
Continuous Nuki joint, butted Nuki joint	2007	Chang and Hsu	✓		✓
Nuki, beam through column, and mortise-and-tenon	2009	Komatsu et al.	✓	✓	✓
Dieh-Dou. stacked bracket system	2016	S.-Y. Yeo et al.	✓		✓
Nuki Joint	2020	Fang	✓	✓	✓
MORTISE-AND-TENON					
Oval mortise-and-tenon with glue line and friction (furniture scale)	2019	Hu and Guan	✓	✓	
Pegged timber frames with mortise-and-tenon, fork and tongue, and knee brace	1999	Bulleit	✓	✓	
Pegged mortise-and-tenon	2009	Shanks and Walker	✓	✓	✓
Pegged mortise-and-tenon, and full-size knee-braced timber bent frames	1985	Brungraber	✓	✓	✓

Pegged mortise-and-tenon	1997	Schmidt and Mackay	✓		✓
Mortise and tenon (furniture scale)	2005	Erdil, Kasai, and Eckelman	✓		✓
Pegged mortise-and-tenon in knee-braced frames	2003	Erikson	✓	✓	
NOTCHED JOINTS AND RAFTER-ENDS					
Notched beams	2007	Lang and Fodor	✓	✓	
Watari-ago: notched beams	2015	Ogawa, Sasaki, and Yamasaki	✓		✓
Double birdsmouth	2016	Shope	✓		✓
Birdsmouth rafter joint and strengthening interventions	2008	Branco	✓	✓	✓
Birdsmouth rafter joint with and without mortise and tenon and strengthening interventions	2012	Palma, Cruz, Ferreira	✓		
Tapered Tenon joint	2012	Koch	✓	✓	
Notched mortise-and-tenon rafter-end	2014	Feio, Lourenco, Machado	✓		✓
DOVETAIL AND LAP JOINTS					
Double and single notch dovetails	2015	Kunecky et al.	✓	✓	
Angled single notch dovetail	2000	Wald and Drdacky	✓		✓
Dovetail	2010	Sebera and Simek		✓	
Rounded dovetail	2010	Tannert, Lam, and Vallée	✓	✓	✓
Timber plates	2017	Roche	✓	✓	✓
Flexural joints/elements					
Lapped scarf joint with inclined faces	2018	Kunecký et al.	✓	✓	
Scarf joints with pins or keys	2015	Fajman et al.	✓		✓
Splice and scarf joints with pegs (under-squinted butt in halved scarf, side-halved and bridled, stop-splayed and tabled scarf with key, face halved and bridled scarf)	2008	Hirst et al.	✓		
Composite beam with stop-splayed scarf joints	2013	Mirabella-Roberti et al.		✓	
Composite beam with stop-splayed scarf joints	2015	Rug et al.	✓		✓
Halved and tabled scarfjoint and stop-splayed scarfjoint with key	2009	Sangree et al.	✓	✓	

3.1 Limitation on standardization

Semi-rigid joint behaviour has already been heavily integrated into the design of steel structures. Steel beam-column connections are typically subject to a combination of axial force, shear force, and bending moment. Deformation at the joint is most often dictated by the bending moment as it is typically much larger than the others. Most carpentry joints possess resistance to rotations and translations through bearing and can be considered semi-rigid. Literature says that clamped and hinged boundary conditions can be assumed in practice when the stiffness is sufficiently small and little moment is transferred, or if the rigidity is so high that no rotation actually occurs (Chen et al., 2011). Eurocode 3 (EC3) gives some guidance on modelling nonlinear elastic-plastic analysis seen consolidated in Table 2.

Table 2. Eurocode 3 Connection models for elastic-plastic structural analysis

Type of connection model	Classification by stiffness	Classification by strength
Continuous	Rigid	Full strength
Semi-continuous	Rigid	Partial strength
	Semi-rigid	Full strength
Simple	Nominally pinned	Partial strength
		Nominally pinned

Steel codes provide rigidity suggestions partially by nature of the material's connection ductility and predictability. The classifications are justified for nonlinear elastic-plastic analysis because the connection performance is to be based on both stiffness and strength, as opposed to elastic or rigid-plastic analysis where only one of the two is considered (Chen et al., 2011). Spring models for connection rigidity are common for steel frame analysis, but the limiting factor on development of a similar models for timber is the amount of calibration testing necessary to validate it for the variety of configurations (Larsen & Jensen, 2000). Due to the lack of standards regarding timber joinery the best source for guidance can be found in various research papers from the last century. The component method is a reliable method developed to estimate joint stiffness from only geometric and mechanical properties using the concept of the semi-infinite half space (Wald et al., 2000). This method was originally developed for steel structures but has shown success in the prediction of stiffness for carpentry joints.

3.2 Semi-rigid Joint Theory

Axial forces are typically calculated assuming pinned connections in all truss joints. While the axial design capacity of the members is unlikely to be threatened by this assumption, the effect on the joint itself could pose threats of failure. Complex carpentry joints can be stiff and brittle when rotation is imposed due to the perpendicular to the grain component of loading. Sometimes these types of joints are modelled as fixed, with infinite rigidity, which is conservative and safe, but highly uneconomical because overestimations can lead to an overly robust design (Branco, 2008).

The conceptual difference in boundary condition rigidity can be seen in the example of a uniformly loaded beam with differing end conditions in Figure 14. The maximum moment of the pinned condition is located at the midspan of the beam whereas the fixed condition experiences maximum moment at the connections and the midspan moment has decreased to a third of the pinned value. This goes to show that semi-rigid connections land somewhere in between, and end rigidity can lead to concentrated moment at the connections. Consequently, assuming pinned ends neglects the moment demand at the member ends and could easily lead to overlooking the moment demand placed on potentially brittle timber connections.

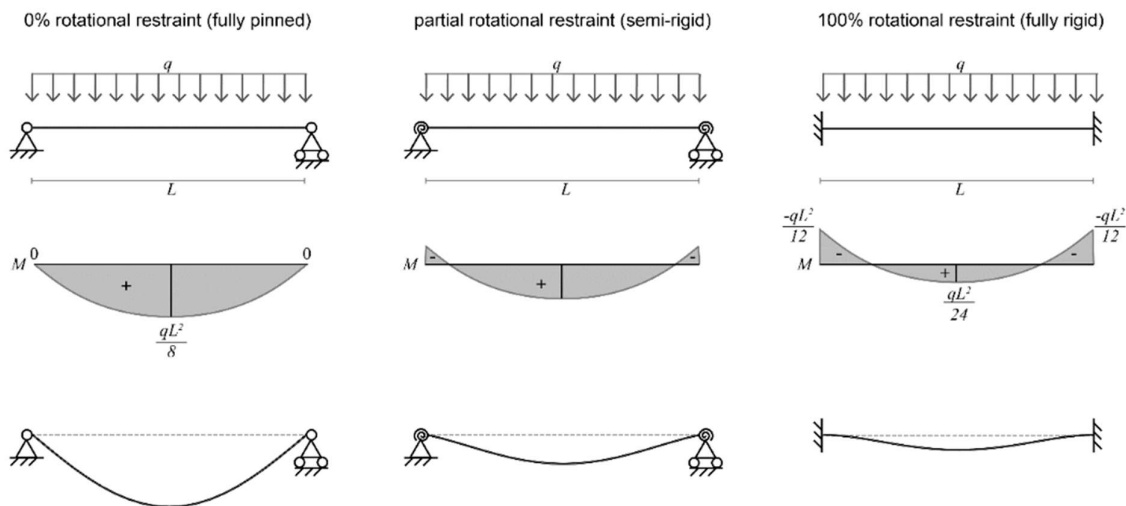


Figure 14. Pinned, semi-rigid, and fixed end conditions of a uniformly loaded beam (Fang, 2020)

The magnitude of the rotational stiffness is not what specifically determines joint behavior, but it is rather the ratio of the rotational stiffness to the flexural stiffness of the members associated:

$$\text{Joint stiffness} = \frac{kL}{EI} \quad \text{(Eq. 1)}$$

Where k =rotational stiffness, and $\frac{EI}{L}$ = flexural stiffness

It stands to reason that as the value of joint stiffness increases the joint approaches rigid behavior whereas closer to zero it approaches hinged behavior.

4. CONNECTION TYPOLOGIES AND INVENTORY

Wood coupled carpentry joints are significantly different than their mechanical counterparts in that the metal dowel fasteners can significantly change the failure mechanisms and stiffness of the connection. Wooden dowels do not have the added component of post-tension that comes with many bolted connections, adding to frictional resistance. There are several drawbacks to using metal connectors however, namely the material and mechanical incompatibilities. There can be significant stiffness and ductility discrepancies between timber and steel. There have been numerous metal-dowel type fasteners that have led to a brittle perpendicular to grain failure within timber members. In roofs especially, humidity and exposure can change drastically depending on the time of year, and the thermal differences between wood and steel mean that water condensation tends to localize at their interface causing moisture issues (Kunecký et al., 2016). Steel connectors are mostly present in structures that were built from the 20th century onwards, so within the context of historical trusses the inventory will herein concentrate on historical timber-only joints.

Traditional carpentry connections exist for a multitude of joint functions. The choice of connection was historically dependent on the forces expected to be experienced at the joint and they can be categorized as such. Variations in these connections exist depending on the member arrangement, geometry, and skill of the carpenter. The typologies presented below will include joint typologies that are represented within the three case study roof trusses chosen as well as several others that are typical or have existing research examining the use in numerical models. The following section will categorically list and describe various carpentry joints, grouped through the proposed taxonomy from the European Cooperation in Science and Technology (Sobra et al., 2015). For a more detailed and expansive description of the taxonomy see Figure A- 1. Proposed taxonomy for joint classificationFigure A- 1.

4.1 Crossing Joints (X Joints)

4.1.1 Lap Joints

Lap joints are defined by the planar intersection of two members that are joined. In a full lap, the members are simply overlapping and pinned by a dowel connector. A half lap, on

the other hand, removes material from either section, typically equal to half the depth of the lesser member (see Figure 15). Lap joints are commonly used to reduce the unbraced length of a truss member or to avoid full discontinuities of members that pass through the same point. By reducing the depth in both members, they can then have bearing surface area to resist imposed forces. A half lap joint has some rotational stiffness, but the joint is already “half-weakened” compared to the members’ original sections (Branco & Descamps, 2015). The rotational stiffness is relatively small compared to the member stiffness as will be discussed further in the modelling methods section. For this reason, it is reasonable to assume that full and half laps function as rotational hinges.

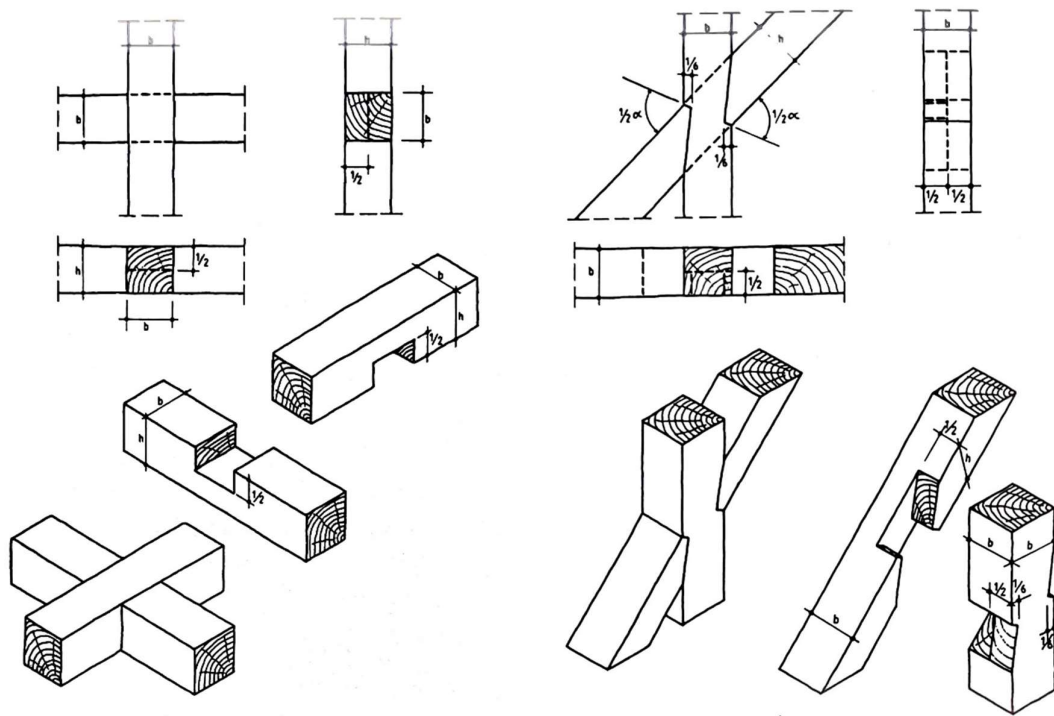


Figure 15. Perpendicular half lap joint (Left) and notched-angle half lap joint (Right) (Gerner, 1992)

4.2 Corner or Angle Joints (L Joints)

4.2.1 Forked Bridle Joint

Corner joints were primarily used at the apex of typical spar roofs, as well as locations where pitch changed in mansard or gambrel roofs. They were present in situations where no ridge-board or ridge-beam was used. Butt joints with dowels provide the simplest construction but weakest joint. Laps and bridles, however, provided a pseudo-locking mechanism to resist

rotation due to the orthogonal bearing areas as well as rotational bearing that was enabled by the dowel (Zwerger, 2012).

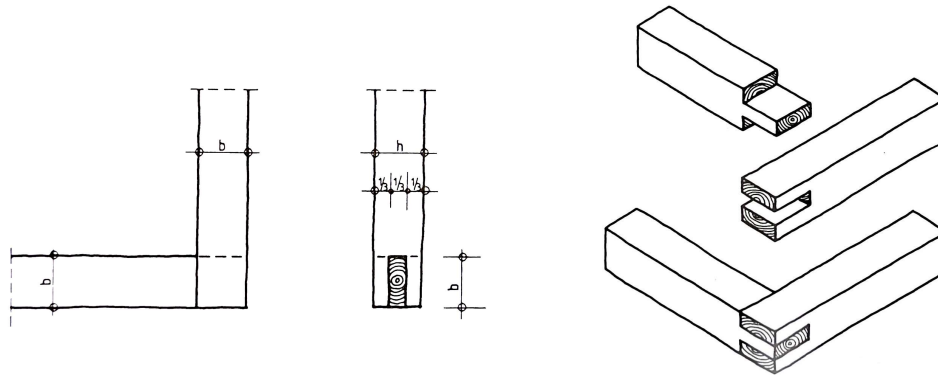


Figure 16. Forked bridle joint (Gerner, 1992)

4.3 Encounter Joints (T-Joints)

4.3.1 Mortise and tenon

Mortise-and-tenon joints (seen in Figure 17) are one of the most commonly found carpentry joints in historic constructions. It includes the shouldering of one end to form a tenon (usually $1/3$ to $1/2$ of the member width) which is then sunk into a corresponding mortise hole which is typically cut to be a very snug fit. Pins are a very common addition to mortise-and-tenon connections because the addition of one or two of them serve to lock it into place (Zwerger, 2012). Dowel pins also provide tensile capacity to the joint so that it no longer is purely dependent on friction. Doweled versions of this joint are commonly used for beam-to-column connections or smaller truss members. Additionally, tenons in angled members provide a shear plane and bearing surface area to increase its capacity. The mortise is typically slightly deeper than the tenons length to avoid stress concentrations where the tenon end would contact the base of the mortise. This also guarantees that the joint is reliant on the bearing surface area of the shoulders of the connecting member.

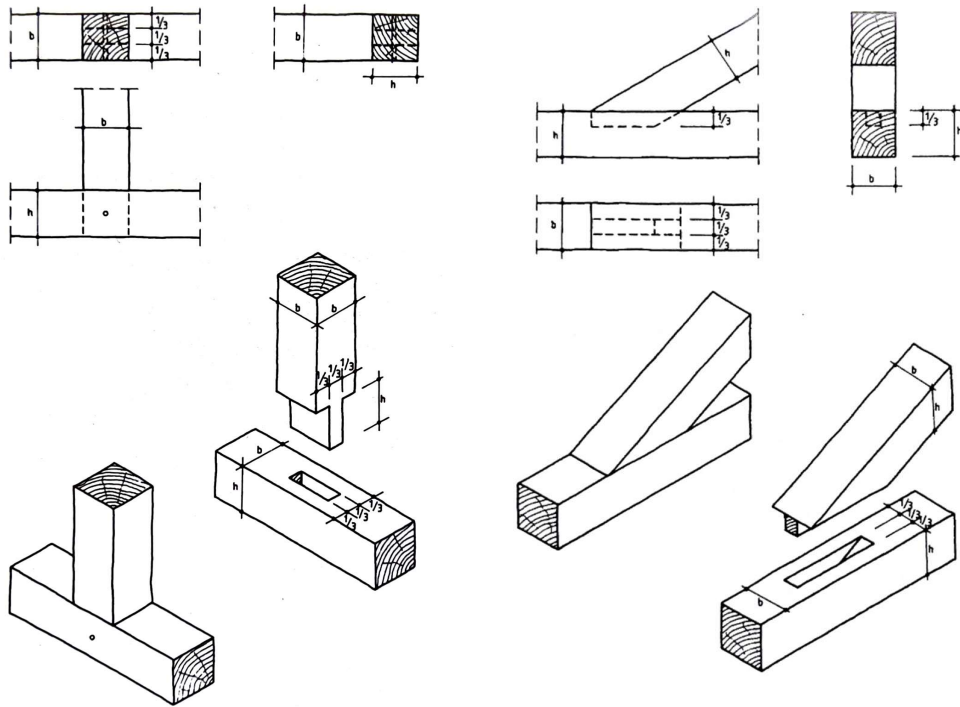


Figure 17 Perpendicular mortise and tenon (Left) and oblique tenon joint (Right) (Gerner, 1992)

4.3.2 Rafter Ends

4.3.2.1 Oblique tenon joint

The oblique tenon joint (pictured in Figure 17) was briefly a popular choice for rafter ends. It fell out of widespread use due to other variations with notches taking their place. The joint brings a rafter with a tenon into a mortise in the tie beam. This configuration resolves the axial force in the rafter to the tie beam through the shear plane in the tenon's cross section and the contact bearing area that the shoulders and tenon rest on the tie beam. The shear plane is a considerable weakness however, as it would result in a relatively brittle failure if it were to be overloaded (Zwerger, 2012). Koch (2012) conducted both experimental and numerical analyses on tapered tenon joints wherein axial characteristic stiffness values were measured and numerically validated.

4.3.2.2 Notched Rafter

As a solution to the shear resistance issues with the oblique tenon joint, notched rafters add normal bearing component where the rafter comes into the tie beam. This addition

significantly increases the strength of the connection and is extremely common in king-post frames (Branco & Descamps, 2015). The added notch also serves to change the limiting failure mechanism away from the tenon shear failure that was common for the oblique tenon joints and encourage a more ductile and controlled failure such as crushing at the notch. Some versions of the notched rafter-end also included a tenon, but it mostly served to restrict out of plane movement at the joint. Due to the prevalence of this joint in European trusses, extensive research has been conducted to determine their stiffness and cyclic behaviour. Branco et al. (2006) and Branco (2008) concluded that notched rafter-ends exhibit significant moment capacity, and the stiffness of the joint correlates with the axial stress of the rafter, the width of the member, and the friction angle.

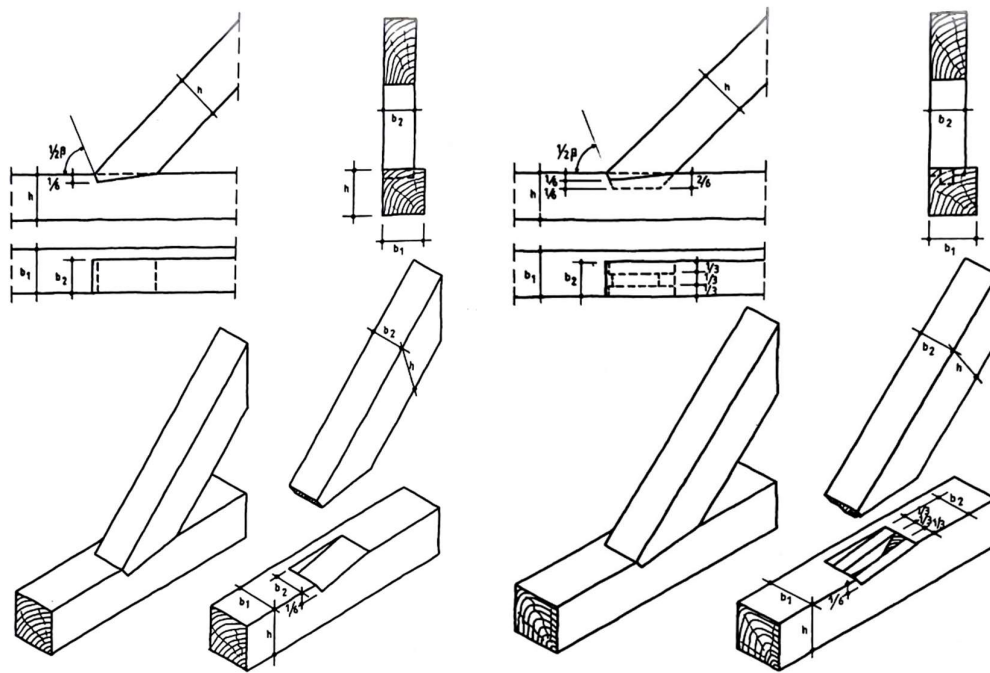


Figure 18 Hidden notch (Left) and hidden notch with tenon (Right) (Gerner, 1992)

4.3.3 Dovetail Joints

Dovetail joints have been utilized in the Czech Republic since as early as the first half of the 14th century (Zwerger, 2012). Pictured in Figure 19, single notched dovetail joints were most often employed when connecting inclined elements and would nearly always be pinned through with a wooden dowel to prevent disassembly. The dovetail is typically half, or one-third, lapped over the other member. In some configurations, the tail stops short of the full

member depth to protect the cut end of the dovetail. The notch was cut on the inside of the incline to facilitate a locking mechanism and provide extra axial bearing area. The double-notched dovetail was mostly used in perpendicular cases such as crossties and vertical struts. Dovetails were particularly popular due to their versatility and aesthetics (Gerner, 1992). Kunecký (2015) examined the axial and rotational stiffness behaviour of single and double notched dovetail joints. The experimental study found that a steeper contact angle of the mortise and tenon was positively correlated to joint stiffness, and the numerical modelling portion of the study saw minimal change in global roof behaviour when stiffness was iterated.

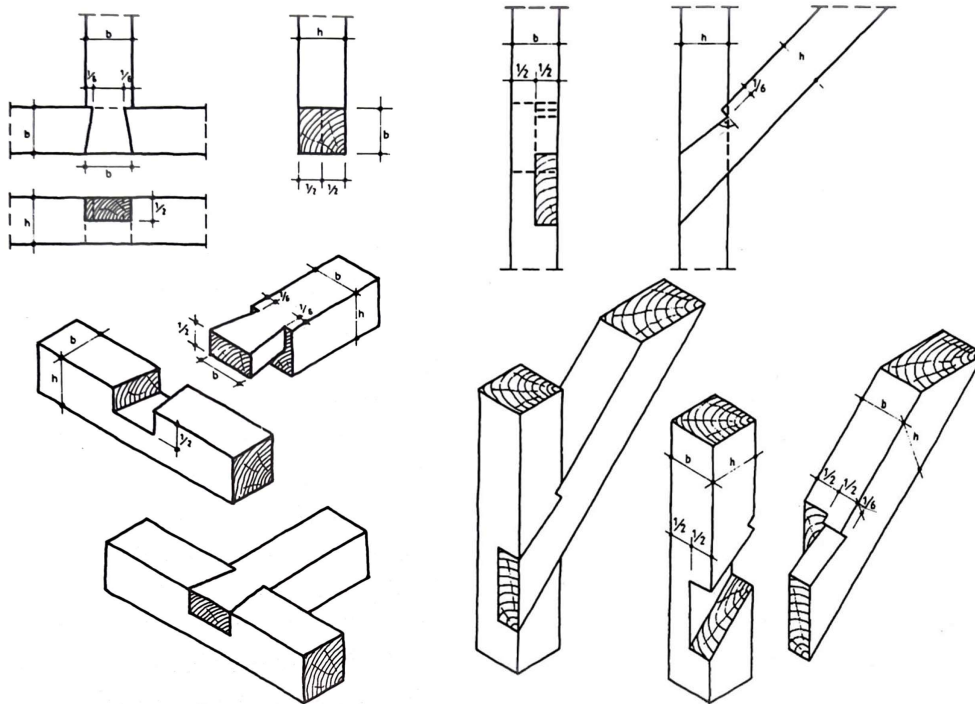


Figure 19. Double notched perpendicular lapped dovetail (Left), and angled single notch lapped dovetail (Right) (Gerner, 1992)

5. MATERIALS AND METHODS

To analyse the influence of stiffness parameters on the global behaviour of a timber roof structure, three typological models were generated based on existing structures in the Czech Republic. The numerical models were constructed using ANSYS Mechanical APDL 2023 R1, build 23.1 (ANSYS Inc., 2023a). This is a commercially available software that uses finite element modelling to discretize and solve the set of boundary value problem equations which produces the solution as displacements and internal force distributions.

5.1 Numerical Model Description

The configurations of the roof trusses chosen can be seen in Figures 20, 21, and 22 along with a visual representation of the carpentry joint inventory for each of them. For the purposes of this preliminary analytical study all models were to be generated in 2D and restricted to 3 degrees of freedom (2 translational, 1 rotational), and all nodes were fixed with respect to out of plane deformation.

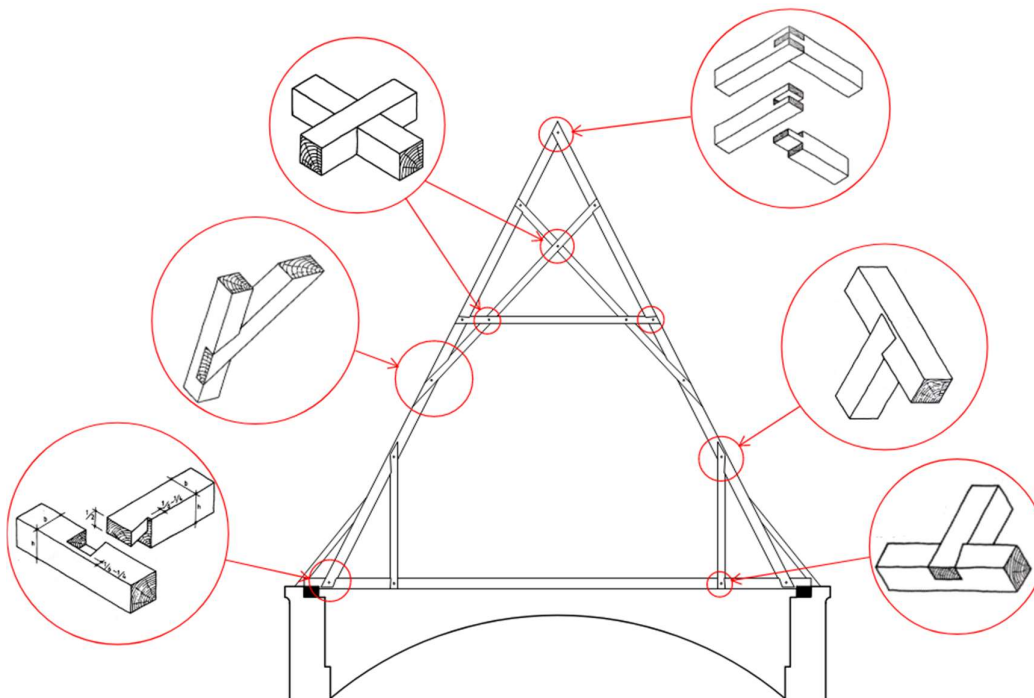


Figure 20. Třebíč truss and connection typology identification

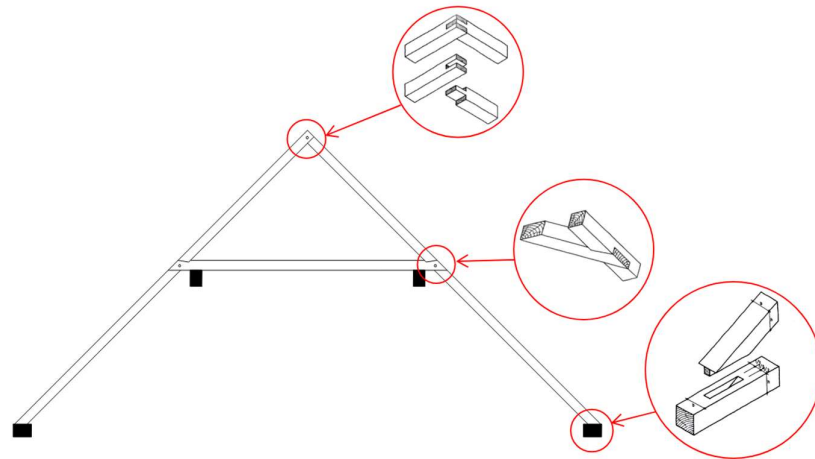


Figure 21. Slavonice truss and connection typology identification

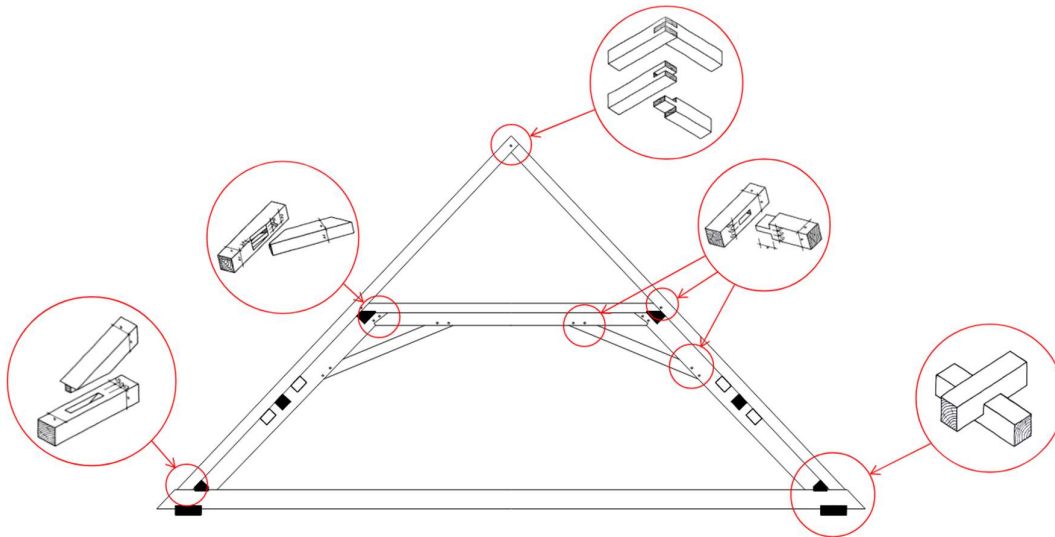


Figure 22. Doksy Chateau truss and connection typology identification

For the truss members, linear BEAM188 elements were used. The choice was made to use beam elements rather than truss elements because truss elements neglect moment and bending effects, so they were not appropriate. The beam element is based on Timoshenko beam theory and therefore includes shear contributions to deflection (ANSYS Inc., 2023b). The element is suited for slender to moderately thick beams, and its recommended global slenderness ratio is >30 . Timoshenko theory expects deformation to converge as slenderness ratio increases. The linear option for BEAM188 has one integration point along the length, and for a rectangular cross section there is a four-by-four grid of integration points along the cross section of each element. A sample cross section and the local coordinate system of BEAM188

elements can be seen in Figure 23, and the linear shape functions can be found in the Appendix equation set A1.

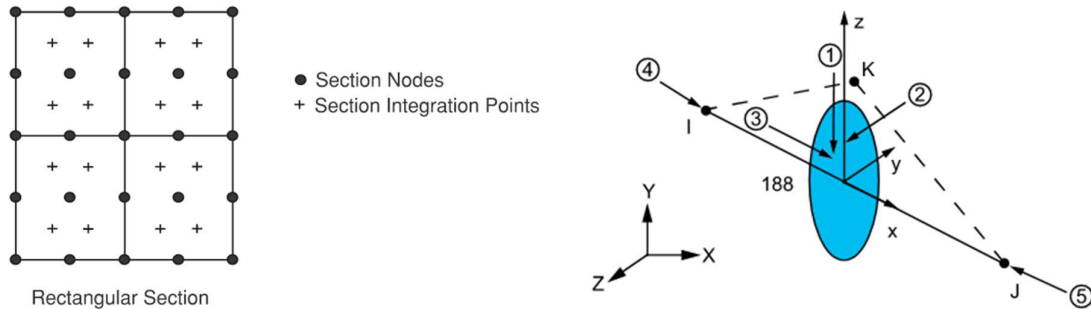


Figure 23. BEAM188 cross-section cells (left) and geometry (right) (ANSYS Inc., 2023b)

To model longitudinal and rotational stiffnesses, spring elements were modelled using COMBIN14 type elements (see Figure 24). This is a longitudinal or torsional spring that can be adjusted to be isolated to one, or multiple, degrees of freedom. Spring models are a simple representation of joints in a numerical model as most finite element programs can then generate stiffness matrices automatically rather than requiring manual input.

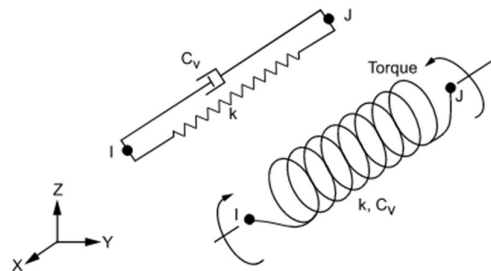


Figure 24. COMBIN14 Element geometry (ANSYS Inc., 2023b)

Three 1D springs were placed at each joint, two of which are for planar translation and the third is a rotational spring. This combination seeks to represent the normal, shear, and rotational stiffnesses inherent to a given connection. For the model, analytical methods and previous research results were used to estimate these three spring stiffnesses which were then implemented as zero-length elements “between” members. Each of the coincident nodes that served as one end of each of the springs was attached to one of the members involved in each connection. It was important to keep track of nodes that were part of a continuous member because there were also then unique boundary conditions to make sure rotation, forces, and

especially displacements were maintained across the connection and member. This concept of maintaining continuity of members demonstrated in Figure 25.

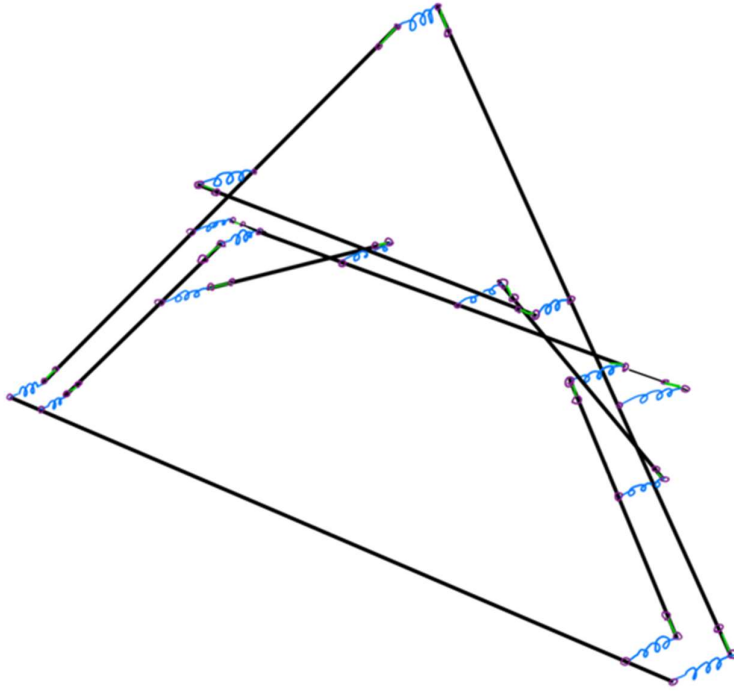


Figure 25. Doksy Chateau truss model configuration where the blue springs indicate a triad of 1D spring elements

5.2 Material and Mechanical Properties

By virtue of tree growth, the principal directions for timber follow a cylindrical coordinate system with different properties in the longitudinal, tangential, and radial directions. However, due to the variance of wood cuts and inability to consistently predict or control the positioning of the radial and tangential components during construction, the two can be averaged to reduce model uncertainty. Since this model is intended to be used in structural and component applications, assumptions of homogeneity and orthotropy are adequate at this scale. Wood can reasonably be modelled as a homogeneous material whose linear behaviour can be described by Hooke's law as a linear elastic orthotropic material. As members were generated in the model, local coordinate systems were created to align with each members longitudinal axis such that when it was meshed, the orthotropic properties were correctly applied.

For the purposes of this study, material properties for wood were defined by the mean values of class C24 timber as given in Table 1 of EN 338 (see Appendix Table A-1) as well as reference studies. The values in Table 3 are those used in the model.

Table 3. Model material properties

Material Properties		
ρ_{mean}	420	kg/m ³
E_x	11	MPa
E_y	0.4	MPa
E_z	0.4	MPa
G_{xy}	0.7	MPa
G_{yz}	0.1	MPa
G_{xz}	0.7	MPa
ν_{xy}	0.4	
ν_{yz}	0.05	
ν_{xz}	0.4	

5.3 Estimation of Joint Stiffness

Numerous connections have forces acting at some angle to the wood grain, therefore a transformation is necessary to predict the off-axis modulus of elasticity. The simplified Hankinson transformation was used for the purposes of this preliminary study. The Hankinson's formula for stress at an angle, α , to the grain can be adapted to estimate the modulus of elasticity at a given angle to the grain prior to the proportional limit being reached (Fang, 2020). It should be noted that the Hankinson transformation is merely an estimate and the elastic moduli parallel and perpendicular to the grain will differ depending on the species.

As described in the typology database, wood joints each have an inherent stiffness. Therefore, to have a more realistic model behaviour it is necessary to estimate values of rotational and translational stiffnesses for each connection type used in the real trusses. Perpendicular to grain-bearing type connection stiffnesses were approximated for the various connections that were to be modelled in compression. These approximations utilized the analytical model proposed in Kitamori (2009) and Hataj (2022) wherein the contributions of the perpendicular beam are compounded with the resistance provided by the subsidence effect of the compressed timber (see Figure 27). For each truss analysed, the analogous spring constants for the two global axes were calculated for each unique joint typology. For the Třebíč

truss, X-joints were present (half lap, forked bridle, mortise and tenon, and lapped dovetail). As these often have small resisting areas, they were assumed to be rotational hinges. Equations 1-5 were used for the perpendicular to grain stiffness formulations. In cases where no experimental results were known or reasonable, rotational stiffness was to be determined using equations 6-12.

$$K_1 = \frac{E_{0,mean} \cdot b \cdot L_2}{v} \quad (1)$$

$$K_2 = \frac{E_{90,mean} \cdot b \cdot L_2}{h} \quad (2)$$

$$K_3 = \frac{E_{90,mean} \cdot b \cdot L_{ef}}{h} \quad (3)$$

$$L_{ef} = \frac{(1 - e^{-ax})}{a} \quad (4)$$

$$a = \frac{2.5}{Z_0} \quad x = 1.5Z_0 \quad (5)$$

$$E_\alpha = \frac{E_{0,mean}}{\frac{E_{0,mean}}{E_{90,mean}} \cdot \sin^2(\alpha) + \cos^2(\alpha)} \quad (6)$$

$$A = \frac{b_T \cdot h_T}{\sin(\alpha)} \quad (7)$$

Where b is the width of the perpendicular grain member, L_2 is the length along the span of the member where contact is made, and h is the member depth.

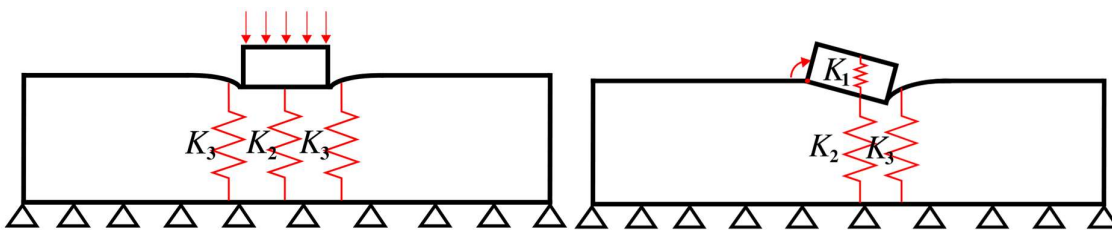


Figure 26. – Spring equivalents for perpendicular to grain deformations

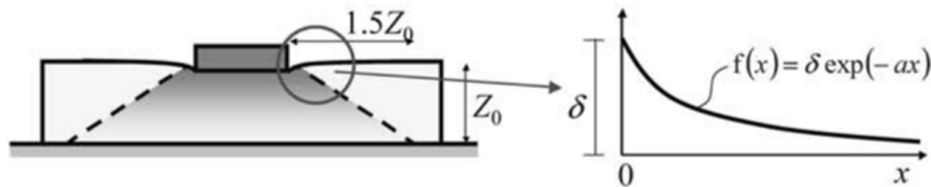


Figure 27. Subsidence factor equation per (Kitamori et al., 2009)

$$X_p = \frac{2l^3 + 3hl^2}{3l^2 + 6hl + 6h/a} \quad (8)$$

$$N_1 = \frac{y_p X_p E_{90}}{2Z_0} \quad (9)$$

$$N_2 = \frac{y_p (1 - X_p)^2 E_{90}}{2Z_0} \quad (10)$$

$$C_1 = \frac{y_p X_p E_{90}}{aZ_0} \quad (11)$$

$$a = \frac{5.5}{Z_0} \quad (12)$$

$$k_r = \frac{2}{3}(l - X_p)N_2 + \frac{2}{3}X_p N_1 + X_p C_1 \quad (13)$$

$$E_{90} = \frac{E_0}{29.2} \quad (14)$$

Where l is the longitudinal length of the deformed area, h is the depth of the triangular embedment due to rotation, X_p is the distance from the end of the triangular displacement to the centre of rotation, N_1 and N_2 are the resultant forces of the triangular embedment area, C_1 is the resultant force from the subsidence effect, a is an adjustment factor, and k_r is the estimated rotational stiffness.

Where values existed for axial or rotational stiffnesses from previous studies, they were used. As this is a parametric study, the values should be on the correct scale and justifiable for the size of the members. When members could be expected to change from tension to compression, or vice versa, spring constants had to be available for both cases. Table 4 details the stiffness values used for springs in the various models. The rotational values were sourced from Kunecký et al (2016) for dovetail joints. The analytical values for other typologies trended around these values so it was applied to all of them for simplicity. The Hataj methodology for bearing perpendicular to grain was utilized for the longitudinal stiffnesses, and typically the K_1 contributions were small. These values were rounded to the nearest 10 kN/mm for compression uses. 20mm dowels were assumed for tensile cases, and the stiffness values were interpolated according to the results of Hasníková et al. (2020) for 18mm and 22mm diameter dowels in single shear.

Table 4. Connection model stiffness parameters

Trebic			
Connection Type	K_x [kN/mm]	K_y [kN/mm]	K_r [Nm/rad]
Lapped Dovetail (Comp.)	50	50	40000
Single Dowel Lapped Dovetail (Tens.)	1.2	1.2	120000
Continuous lap joint	50	50	-
Mortise-and-tenon (rafter-end)	60	60	40000
Forked bridle joint	50	50	40000
Doksy			
Connection Type	K_x [kN/mm]	K_y [kN/mm]	K_r [Nm/rad]
(1) Dowel Lap Dovetail (Comp./+ rot)	50	40	40000
(1) Dowel Lap Dovetail (Comp./- rot)	50	40	120000
(1) Dowel Lapped Dovetail (Tens.)	1.2	1.2	40000
(2) Dowel Lap Dovetail (Comp./+ rot)	60	30	40000
(2) Dowel Lap Dovetail (Comp./- rot)	50	50	120000
(2) Dowel Lapped Dovetail (Tens.)	2.4	2.4	40000
Continuous lap joint	50	50	-
Mortise-and-tenon (Comp./+ rot)	40	80	40000
Mortise-and-tenon (Comp./- rot)	40	80	120000
Forked bridle joint	50	50	40000
Slavonice			
Connection Type	K_x [kN/mm]	K_y [kN/mm]	K_r [Nm/rad]
(1) Dowel Lap Dovetail (Comp./+ rot)	50	50	40000
(1) Dowel Lap Dovetail (Comp./- rot)	50	40	120000
(1) Dowel Lapped Dovetail (Tens.)	1.2	1.2	40000
Continuous lap joint	50	50	-
Mortise-and-tenon/wedge (Comp./+ rot)	60	60	40000
Mortise-and-tenon/wedge (Comp./- rot)	60	60	120000
Forked bridle joint	50	50	40000

5.4 Loading

Loads were determined according to EN-1991 standards (EN 1991-1-1, EN 1991-1-3, and EN 1991-1-4). Self-weight, live loads, snow load, and wind actions were considered where applicable. The self-weight of the structure was applied as a gravitational acceleration where the beam elements had been assigned a cross sectional area and the C24 mean density. Static loads beyond self-weight were applied to account for a typical roofing material including slate, timber battens, and felt cover. This additional static load summed to 0.55 kN/m^2 .

For all the roofs, a category H roof live load was considered, resulting in a 0.6 kN/m^2 impermanent load applied (Cobb, 2015). Loads were added to each rafter node after meshing

such that they were adequately distributed across the roof. The ultimate limit state load combinations below were compared, and the worst-case loads were those considered in analysis.

Ultimate Load State load combinations:

$$\sum \gamma_{G,j} \cdot G_{k,j} + \gamma_{G,j} \cdot Q_{k,1} + \sum \gamma_{Q,i} \cdot \Psi_{k,j}$$

$$ULS1: E_d = \gamma_{g,1}G_{k,1} + \gamma_{g,2}G_{k,2} + \gamma_{q,1}Q_{k,1} + \gamma_{q,2}Q_{k,2}$$

$\gamma_{g,1}$ and $\gamma_{g,2}$ equal 1.35, $G_{k,1}$ is self-weight, $G_{k,2}$ is dead load, $\gamma_{q,1}$ is 1.5 (representing a dominant action), $Q_{k,1}$ is wind load, $\gamma_{q,2}$ is 0.75, and $Q_{k,2}$ is snow load.

$$ULS2: E_d = \gamma_{g,1}G_{k,1} + \gamma_{g,2}G_{k,2} + \gamma_{q,1}Q_{k,1} + \gamma_{q,2}Q_{k,2}$$

$\gamma_{g,1}$ and $\gamma_{g,2}$ equal 1.35, $G_{k,1}$ is self-weight, $G_{k,2}$ is dead load, $\gamma_{q,1}$ is 1.5 (representing a dominant action), $Q_{k,1}$ is snow load, $\gamma_{q,2}$ is 0.9, and $Q_{k,2}$ is wind load.

The flat snow loads were determined using the Technika Univerzita Ostrava digital snow load map tool (GACR Project, n.d.). Finally, external pressure coefficients for a dual-pitch roof were used for finding the EN 1991-1-4 loads (see Appendix Table A-2).

Table 5. Loading table for Třebíč

Dead Load	
Slate, timber battens, felt	0.55 kN/m ²
Self weight	-
Live Load	
Category H EC1 roof live load	0.6 kN/m ²
Snow Load	
Characteristic snow load	0.9 kN/m ²
angle factor	0
Applicable snow load	0 kN/m ²

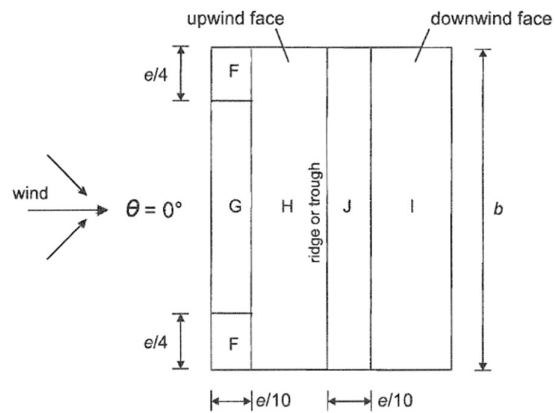


Figure 28. Wind loading zones of dual-pitched roof 9 (CEN, 2005)

Table 6. Wind loading table for the Trebic roof

Area	Width [m]	Depth [m]	$c_{pe,10}$ [m]	$c_{pe,1}$ [m]	w_e [N]
F	6	2.4	0.7	0.7	273
G	12	2.4	0.7	0.7	273
H	24	2.6	0.7	0.7	273
I	24	2.6	-0.2	-0.2	-78
J	24	2.4	-0.3	-0.3	-117

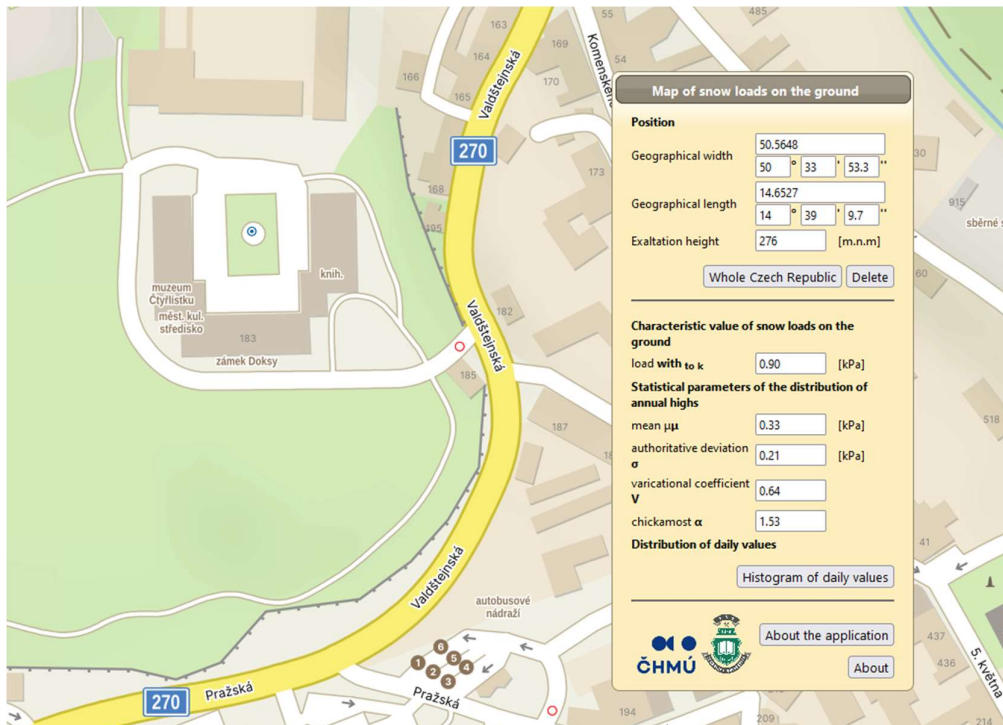


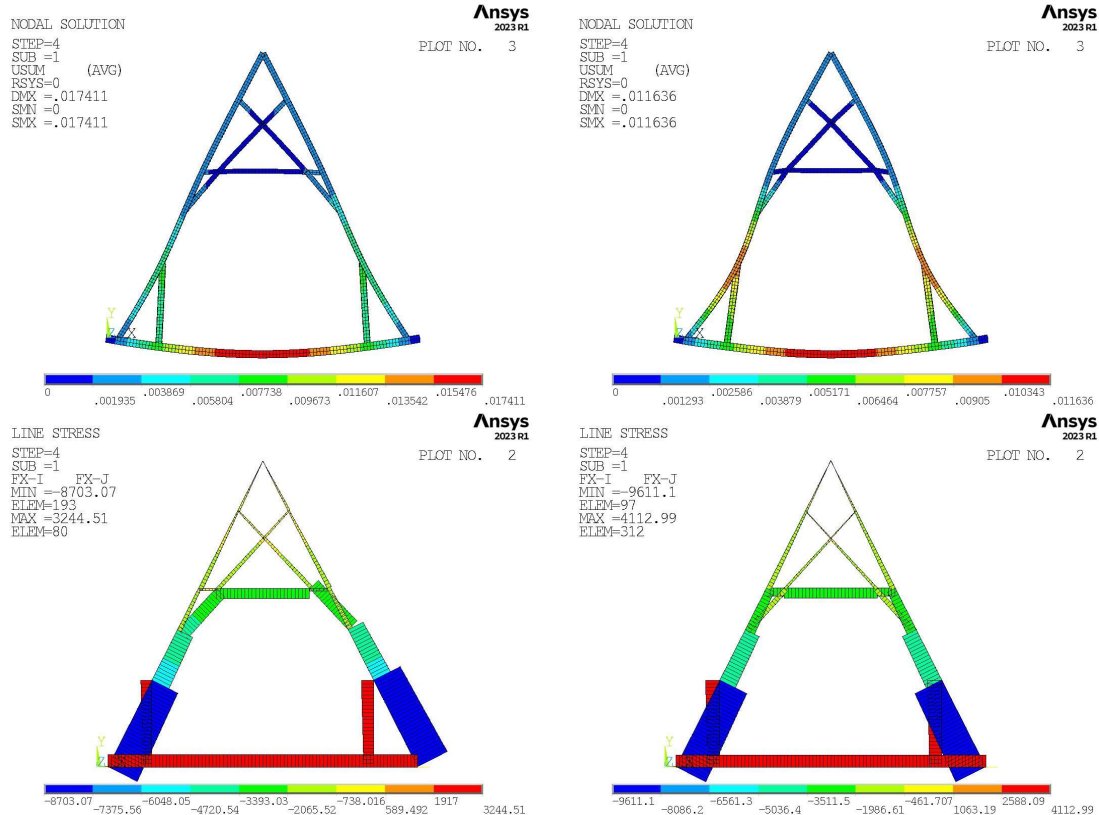
Figure 29. Flat snow loads map for the Doksy Chateau (GACR Project, n.d.).

6. RESULTS

For all models and graphical outputs in this section, units for various forces shall be considered base SI units. Displacements will be given in meters, forces in newtons, and moments in newton-meters. Tables may show different units, but they will be labeled as such. For larger and more detailed plots of the roof models refer to the Appendix. Additionally, a sample ANSYS APDL script is included which was used for the semi-rigid Třebíč truss.

6.1 Třebíč Truss Model

For the Třebíč truss, the angle of the roof exceeds 60 degrees and therefore is considered steep enough that snow would slide off. Therefore, the wind load combination always governed. The boundary conditions imposed include a pin at the far-left side of the bottom chord and a roller at the far-right side.



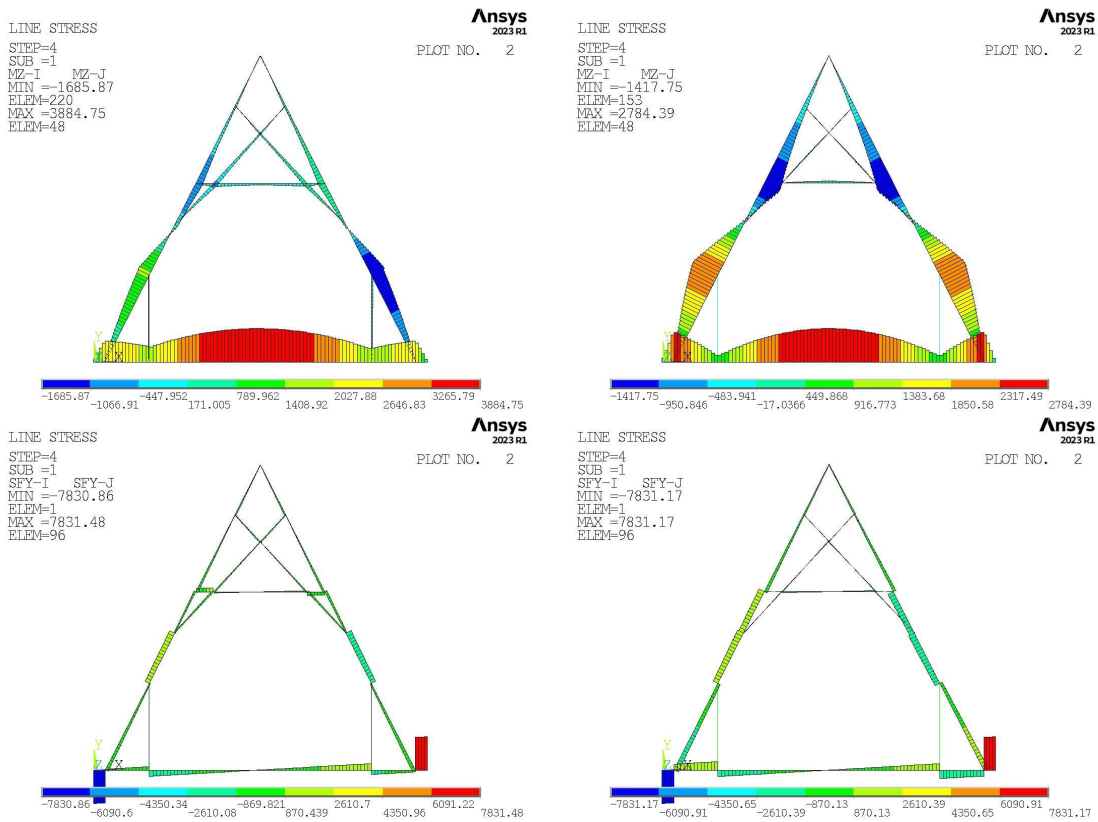


Figure 30. (From top) Trebič deflection, axial force, bending moment, and shear force distributions for the spring model (left) and hinged model (right)

When evaluating the sensitivity of the Trebič roof it was found that in transitioning from the semi-rigid to hinged case there were notable differences in the distribution of moment and axial forces. Table 7 shows the internal force minimums and maximums for both the semi-rigid and hinge models, as well as the percentage of relative difference in the values.

Table 7. Trebič member internal forces and relative differences between models

		Semi-Rigid			Rotational Hinge			Relative Difference		
		A [N]	M [Nm]	V [N]	A [N]	M [Nm]	V [N]	A	M	V
Global	MIN	-8703.1	-1685.9	-7830.9	-9611.1	-1417.8	-7831.2	-10%	16%	0%
	MAX	3244.5	3884.7	7831.5	4113	2784.4	7831.2	-27%	28%	0%
Bottom Chord	MIN	-8.3E-09	320.38	-7830.9	-1.3E-10	320.39	-7831.2	98%	0%	0%
	MAX	3244.5	3884.7	7831.5	3360.2	2784.4	7831.2	-4%	28%	0%
Rafter	MIN	-8478.5	-765.73	-721.49	-9611.1	-1417.8	-1109.6	-13%	-85%	-54%
	MAX	10.031	1468.4	1346.6	30.449	2318.1	1502.3	-204%	-58%	-12%
Collar tie	MIN	-2666.3	-376.77	-839.73	-2952.7	1.6471	-232.31	-11%	100%	72%
	MAX	-605.55	-22.086	897.96	-2362.6	154.78	232.31	-290%	801%	74%
Cross-brace	MIN	-3460.8	-457.39	-302.78	-1541.8	2.8782	-122.9	55%	101%	59%
	MAX	-340	37.04	399.87	-102.74	60.74	122.9	70%	-64%	69%
Vertical strut	MIN	2288.2	93.431	9.818	3509.3	2.84E-11	-4.47E-10	-53%	100%	100%
	MAX	2891.9	115.82	9.818	4113	4.03E-10	1.43E-09	-42%	100%	100%

The maximum compressive axial force is seen at the rafter bases. The rafter of the semi-rigid model has a lower magnitude, with a relative difference of 13%. This is in line with what is expected, and the hinged model will therefore be more conservative. This deviation could potentially be explained by the small triangle region where the collar tie and the cross brace meet with the rafter. In the semi-rigid model, this area will have a high rigidity compared to the rest of the structure, so it distributes the forces among them as seen by the axial force that the lower part of the cross brace takes on. In the hinged model the axial force is much more direct and force flow favors the rafters.

In both models, the vertical struts and bottom chord (tie beam) are the tension members. The bottom chord sees the highest tension and the difference between the two is minimal, at 4% where the semi-rigid model is slightly more conservative than the hinged model.

The bottom chord sees the highest magnitude of moment, and in the hinged model the magnitude is about 28% lower than in the semi-rigid model. As this is the global maximum moment and bending is typically one of the greater concerns with timber, this does not support the hinged assumption because it would mean that in practice the actual demand on the member is over a quarter larger than the designed demand. On the other hand, the rafter saw the next highest magnitude of moment, and the semi-rigid model showed a lower maximum moment by 58%. This can be related to the force flow favoring the rafters in the hinged model, as mentioned previously. Since the semi-rigid model can pass moment across joints, more members are able to participate and take on those forces. The deflection of the semi-rigid truss was almost 33% greater than its hinged counterpart, which can be attributed to the same phenomenon as with the increased moment.

In general, the axial members were conservatively overestimated by the hinged model. Compressive members were conservatively represented by a margin typically just over 10% as in the cases of the rafter and collar tie. The main member that was misrepresented was the cross brace which was underestimated by about 55%.

In addition to assessing the stiffness, a change in the base boundary conditions was also simulated for the spring model, where the roller on the right side was swapped out for a pin. The resulting plots can be seen in Figure 31. With the contribution of the bottom chord, the roller model is almost identical to the pin-pin model and has less than 1% difference in the measurable maximum forces and displacements.

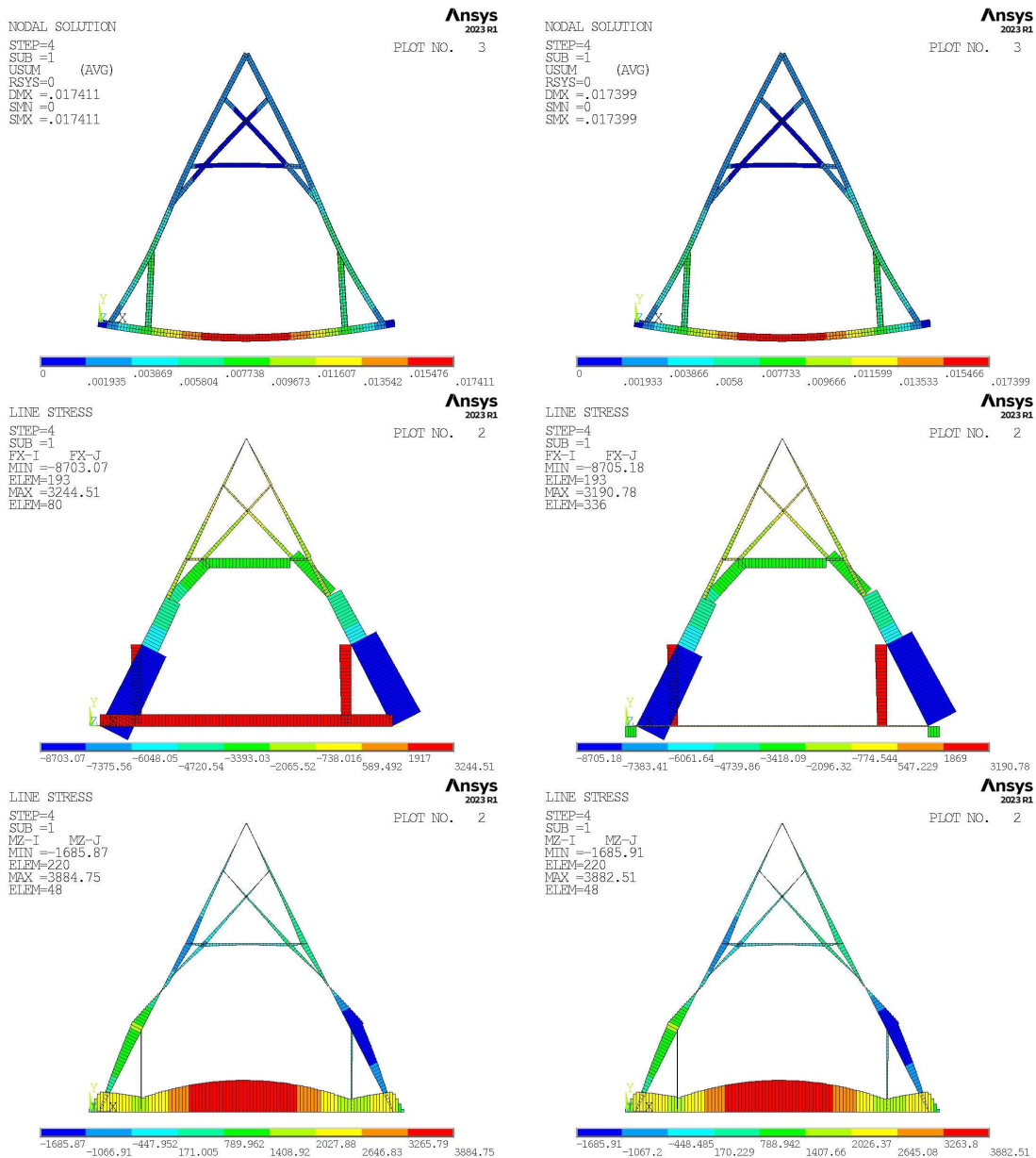


Figure 31. (From top) Trebic roof deflection, axial force, and bending moment, distributions for the spring model with a pin and roller (left) and a pin at each end (right)

6.2 Slavonice Truss Model

The Slavonice truss is has a unique composition in the context of the typological examples because it does not have a bottom chord. This trait implies that the exterior boundary conditions will be more influential. As this truss was iterated upon, the tension values of collar tie connection stiffness had to be interchanged with compressive stiffness values when the

inflection point was found where the axial force changed directions. In future studies it is recommended to have elements with a “birth” and “death” depending on the force experienced.

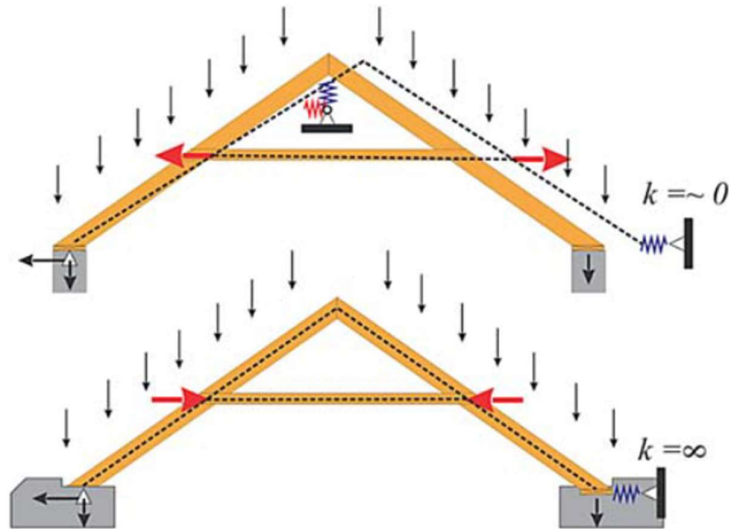
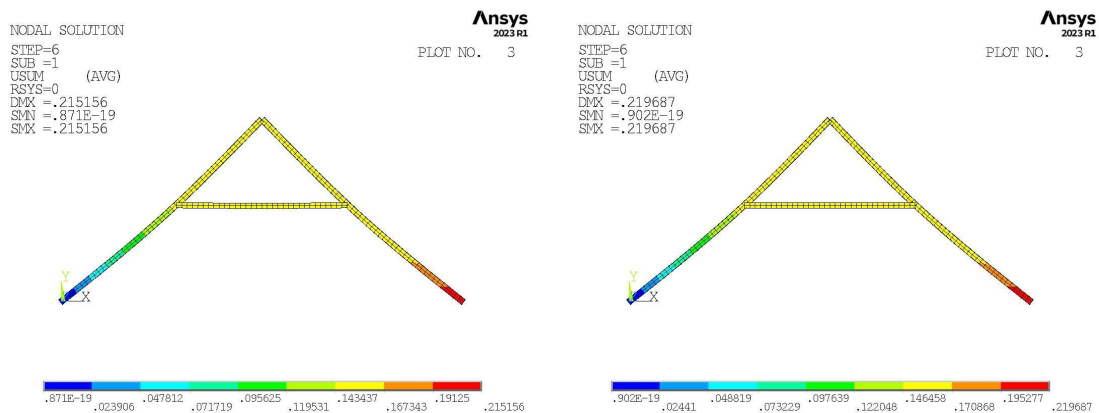


Figure 32. Boundary condition at rafter base influence on collar tie forces (Branco & Descamps, 2015)

The angle of the roof is roughly 45 degrees and therefore both snow and wind must be compared. Therefore, the wind load combination always governed. The boundary conditions imposed include a pin at the far-left side of the bottom chord and a roller at the far right side. The load distribution and magnitudes of both load combinations were relatively close, so for the remainder of the analyses, the snow dominant load-case (ULS2) was applied.



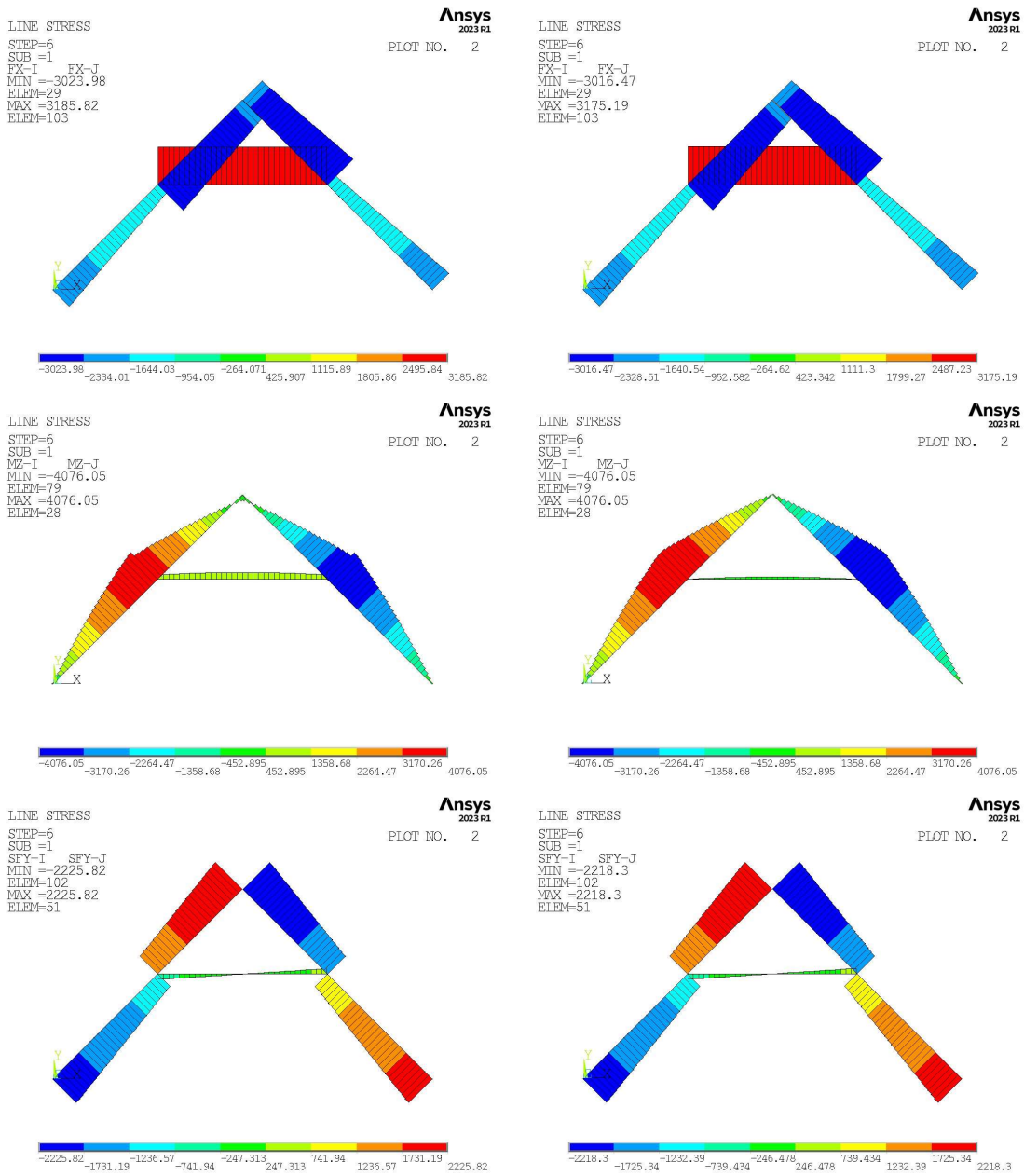


Figure 33. (From top) Absolute deflection, shear force, bending moment, and axial force distributions for the spring model (left) and hinged model (right)

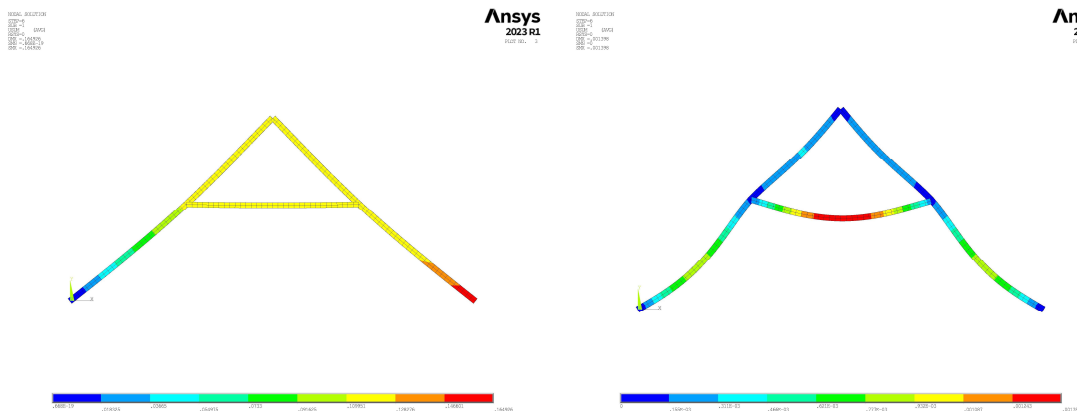
Table 8. Slavonice truss member internal forces and relative differences between models

		Semi-Rigid			Rotational Hinge			Relative Difference		
		A [N]	M [Nm]	V [N]	A [N]	M [Nm]	V [N]	A	M	V
Global	MIN	-3024	-4076.1	-2225.8	-3016.5	-4076.1	-2218.3	0.25%	0.00%	0.34%
	MAX	3185.8	4076.1	2225.8	3175.2	4076.1	2218.3	0.33%	0.00%	0.34%
Collar	MIN	3185.8	512.17	-306.07	3175.2	15.091	-306.07	0.33%	97.05%	0.00%
	MAX	3185.8	745.84	306.07	3175.2	248.76	306.07	0.33%	66.65%	0.00%
Rafter	MIN	-3024	-405.71	-1949.1	-3016.5	96.477	-1949.1	0.25%	123.78%	0.00%
	MAX	-1028.6	4076.1	2225.8	-1028.6	4076.1	2218.3	0.00%	0.00%	0.34%

The comparison of the semi-rigid and hinged model can be seen above in Table 8. Given the predictability of the load path and the simplicity of the model, it makes sense that the relative differences for meaningful magnitudes of internal forces are incredibly close. For simple cases like this, the hinged assumption is very accurate.

It should be noted that while this 2D representation of the truss is simple, the entire roof system is more complicated. In future studies, it would be beneficial to model all typologies utilized in the same roof. In this typology especially, purlins run longitudinally and realistically provide support for the truss. For a more accurate model, the deflection of the purlins could have been estimated and combined with the Hataj method of perpendicular bearing to model them as in plane vertical springs. This would allow the model to maintain the 2D configuration and still have a representative semi-rigid model.

In addition to the semi-rigid and hinge cases, the external boundary conditions are also of note. In order to see where the collar changes from tension to compression between the outer bounds of the pinned and roller conditions, a spring was attached to the footing to see at what stiffness the shift occurs.



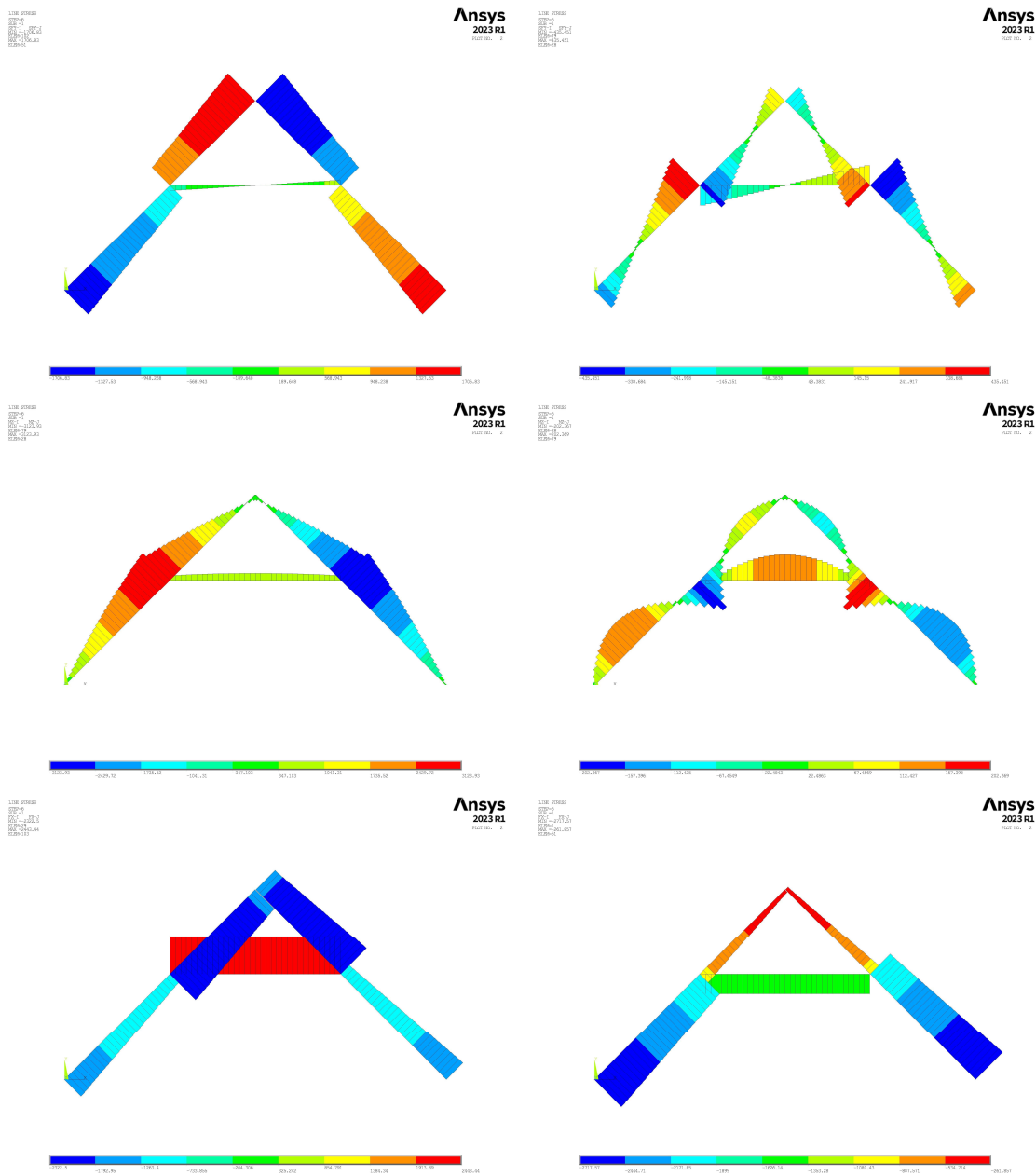


Figure 34 (From top) Absolute deflection, shear force, bending moment, and axial force distributions for the semi-rigid model with a roller (left) and a pins (right)

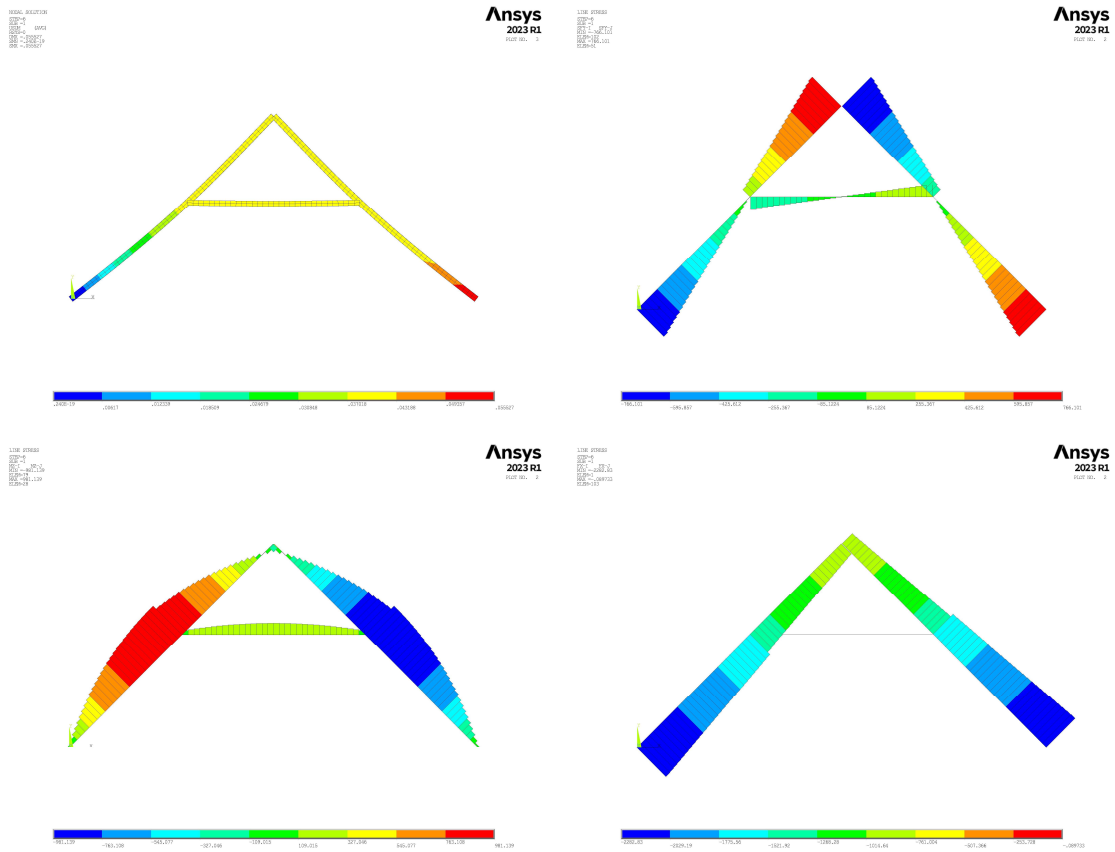


Figure 35. Absolute deflection, shear force, bending moment, and axial force distributions for the spring model at collar tie axial force inflection point

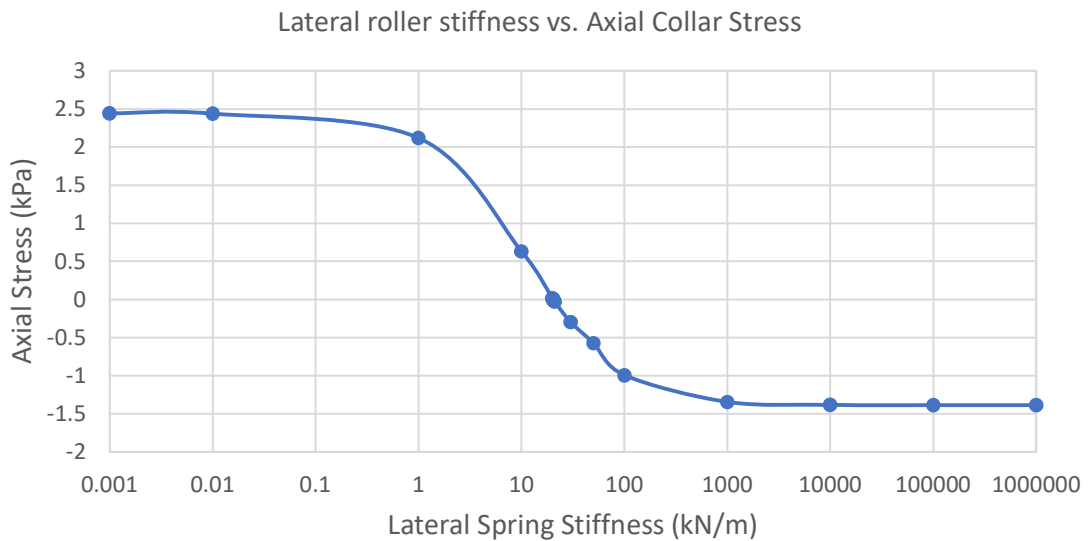


Figure 36 convergence of rafter end spring truss to the boundary conditions

6.3 Doksy Truss Model

The Doksy truss model, similar to previous cases, was governed by the snow loaded combination. One of the main difficulties in the modelling of this truss was in organizing the connectivity. It should be noted that by virtue of the use of line elements and springs, there is limited ability to control contact stresses other than by applying boundary conditions that tell the nodes not to pass through one another. However, as seen in figure the collar-tie and sub-collar overlap when stressed. The elements are in contact with one another in-situ, so realistically there should be moment transfer from the upper to the lower column. Adding boundary conditions that restricted the nodes in these members from relative UY displacement helped to transfer some of the actions, however a contact surface may be a more successful alternative to use in the future.

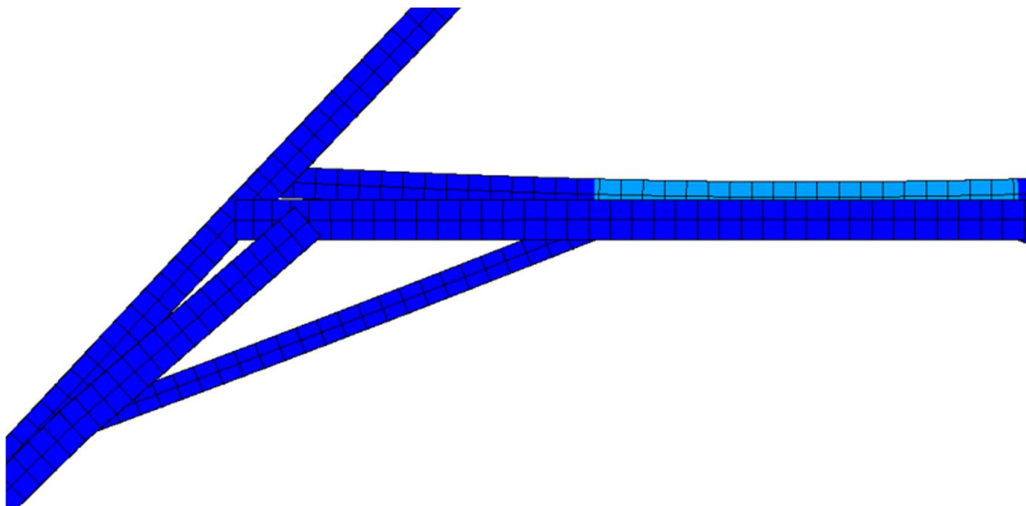
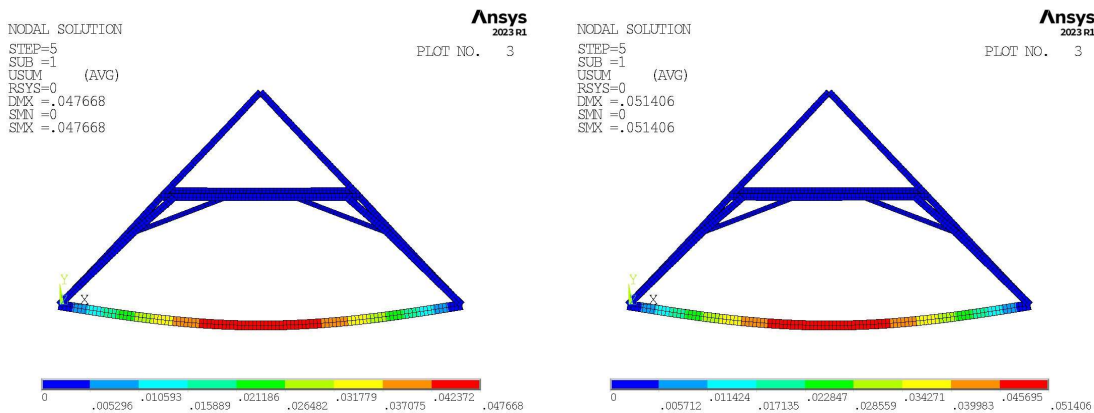


Figure 37. Image capture of the collar and sub-collar overlapping



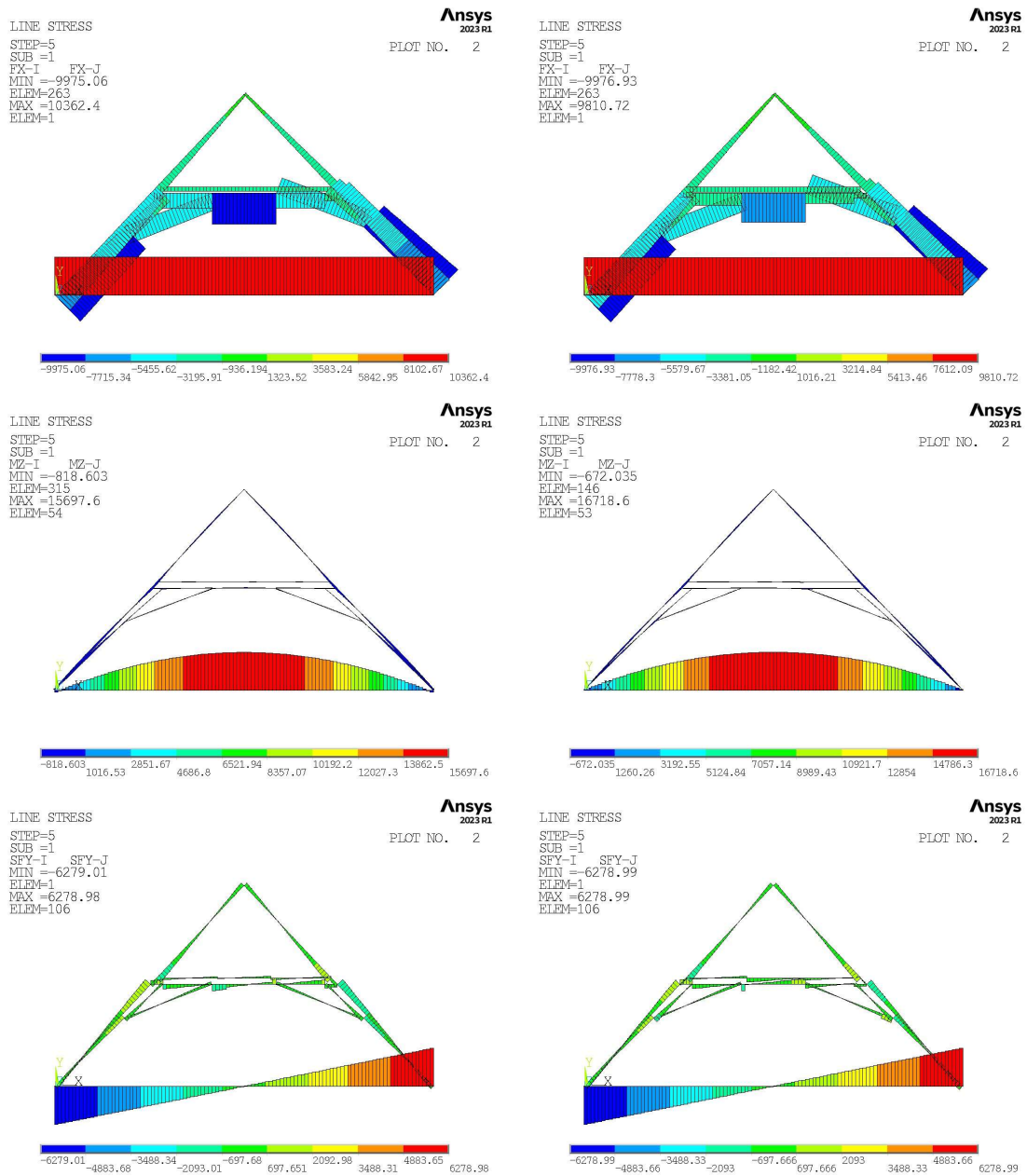


Figure 38. Absolute deflection, shear force, bending moment, and axial force distributions for the spring model at collar tie axial force inflection point

Table 9. The Doksy roof member internal forces and relative differences between models

		Semi-Rigid			Rotational Hinge			Relative Difference		
		A [N]	M [Nm]	V [N]	A [N]	M [Nm]	V [N]	Axial	Moment	Shear
Global	MIN	-9975.1	-818.6	-6279	-9976.9	-672.03	-6279	0%	18%	0%
	MAX	10362	15698	6279	9810.7	16719	6279	5%	-7%	0%
Collar	MIN	-1106.1	-7.857	-296.08	-1393.5	-172.66	-641.34	-26%	-2098%	-117%
	MAX	-1106.1	144	313.68	-1393.5	216.33	315.79	-26%	-50%	-1%
Subcollar	MIN	-8437.7	-248.92	-1030.3	-7622.9	-357.26	-1104.8	10%	-44%	-7%
	MAX	-1709.1	385.81	1055.5	-975.11	328.71	906.43	43%	15%	14%
Knee Brace	MIN	-4773.6	-230.91	-308.14	-4893.8	-87.498	-284.86	-3%	62%	8%
	MAX	-4470.4	139.73	485.61	-4622.6	141.8	425.28	-3%	-1%	12%
Subrafter	MIN	-9975.1	-188.17	-606.47	-9976.9	-418.48	-786.9	0%	-122%	-30%
	MAX	-2866.6	814.85	1154.6	-2756.4	401.7	1037	4%	51%	10%
Rafter	MIN	-5813.3	-805.69	-947.9	-5283.5	-672.03	-924.2	9%	17%	3%
	MAX	-579.03	788.16	1181.4	-561.22	507.35	990.69	3%	36%	16%

From the internal force distributions of the Doksy Chateau roof truss (Table 9), several notable trends are apparent. The axial forces were somewhat well predicted by the hinged model. When the semi-rigid model expects a higher compressive force, the hinged model often was conservative. There was a 3% overestimation of the knee brace axial compression, and a 26% higher value achieved for the main collar tie.

The only tensile member in the model is the bottom tie beam. The semi-rigid model was about 5% higher than the hinged model, so in this case it failed to be the conservative estimate. In bending, the hinged model overestimated the bottom chord's moment by 7%, showing that when the rafters tie directly into the footings where they meet the tie beam, the hinged model may be better suited as an assumption.

The inner queen strut had the worst relative difference between the models. The moment predicted in the hinged model was more than 50% lower than in the semi-rigid model. This is a critical member to this typology of truss as the main supporting member of the inner frame. If it cannot adequately have moment transferred to it, then it should not be considered a reasonable proxy in the model.

7. CONCLUSION

This thesis has evaluated the influence of rigidity on the internal force distributions of three different historic timber trusses. It was found that the typical assumption that joints can be modelled as rotational hinges is valid when stiffness is evenly distributed through a structure.

Where numerous elements connect at one location and create a rigid zone in the truss the hinges struggle to accurately predict the interactions and of the members involved. Axial stresses were the most commonly accurate measure, with the hinged model often overconservative by just over 10%. Moment was underestimated by the hinge assumption in the cases of supporting struts which. The hinged connection assumption is acceptable for truss configurations that are regularly loaded and have a clear load path to the supports. When there are rigidity concentrations or significant geometric discontinuities, the assumption of hinges in a historic truss model fails to give accurate, and even conservative, results.

8. REFERENCES

- ANSYS Inc. (2013). *ANSYS Mechanical APDL Theory Reference*.
- ANSYS Inc. (2023a). *ANSYS Mechanical APDL (23.1)*. ANSYS Inc.
- ANSYS Inc. (2023b). *ANSYS Mechanical APDL Element Reference*.
- Binding, G. (1990). *Fachterminologie für den historischen Holzbau. Fachwerk – Dachwerk*. (Vol. 15). Veröffentlichung der Abteilung Architekturgeschichte des Kunsthistorischen Instituts der Universität zu Köln.
- Bláha, J. (n.d.). *Typological AutoCAD drawings of timber trusses in the Czech Republic*.
- Bláha, J., & Ebel, M. (2005). Historic Roof Timber Structures of Prague Carpenter Michael Ranek - Aspects of their structural design. *The Conservation of Historic Wooden Structures*, 193–205.
- Branco, J. M. (2008). *Influence of the joints stiffness in the monotonic and cyclic behaviour of traditional timber trusses. Assessment of the efficacy of different strengthening techniques* [Doctoral Thesis]. Universidade do Minho.
- Branco, J. M., & Descamps, T. (2015). Analysis and strengthening of carpentry joints. *Construction and Building Materials*, 97, 34–47. <https://doi.org/10.1016/j.conbuildmat.2015.05.089>
- Britannica, T. E. of E. (1998). Truss. In *Encyclopedia Britannica*. <https://www.britannica.com/technology/truss-building>
- Buentgen, U., & et al., et al. (2006). 700 years of settlement and building history in the Loetschental, Switzerland. *Erdkunde*, 2(60), 96–112. <https://doi.org/10.3112/erdkunde.2006.02.02>
- Cabrero, J. M., Stepinac, M., Ranasinghe, K., & Kleiber, M. (2018). Results from a questionnaire for practitioners about the connections chapter of Eurocode 5. *Design of Connections in Timber Structures*.
- CEN. (2005). *Eurocode 1: Actions on structures - Part 1-4: General actions -Wind actions* .
- Chen, W.-F., Kishi, N., & Komuro, M. (2011). *Semi-Rigid Connections Handbook*. Ross Publishing Inc.
- CzechTourism. (2020). *Ve Slavonicích si užijete skvělé letní dny*. Kudyznudy.Cz. <https://www.kudyznudy.cz/aktuality/ve-slavonicich-si-uzijete-skvely-vikendovy-program>
- Fang, D. L. (2020). *Timber joinery in modern construction: Mechanical behavior of wood-wood connection* [Master's thesis]. Massachusetts Institute of Technology.
- GACR Project. (n.d.). *Map of snow load on the ground*. <https://clima-maps.info/snehovamapa/>
- Gerner, M. (1992). *Tesarske Spoje*. Grada Publishing.
- Hasníková, H. , Kunecký, J., Hataj, M., Tyrová, M., & Milch, J. (2020). *Dubový spojovací prostředek v dřevěných konstrukcích: podklady pro normativní ukotvení*.
- Hataj, M., Posta, J., Hasnikova, H., & Kunecky, J. (2022). ANALYTICAL MODEL OF JOINT LOADED PERPENDICULAR TO WOODEN GRAIN . *6th International Conference on Structural Health Assessment of Timber Structures* .
- ICOMOS. (1999). *Principles for the Preservation of Historic Timber Structures*.
- Karolak, A., Jasieńko, J., & Raszczuk, K. (2020). Historical scarf and splice carpentry joints: state of the art. *Heritage Science*, 8(1), 105. <https://doi.org/10.1186/s40494-020-00448-2>
- Kitamori, A., Mori, T., Kataoka, Y., & Komatsu, K. (2009). EFFECT OF ADDITIONAL LENGTH ON PARTIAL COMPRESSION PERPENDICULAR TO THE GRAIN OF WOOD. *Journal of Structural and Construction Engineering (Transactions of AIJ)*, 74(642), 1477–1485. <https://doi.org/10.3130/aijs.74.1477>

- Klein, A., & Grabner, M. (2015). Analysis of Construction Timber in Rural Austria: Wooden Log Walls. *International Journal of Architectural Heritage*, 9(5), 553–563. <https://doi.org/10.1080/15583058.2013.804608>
- Kolář, T., Dobrovolný, P., Szabó, P., Mikita, T., Kyncl, T., Kyncl, J., Sochová, I., & Rybníček, M. (2021). Wood species utilization for timber constructions in the Czech lands over the period 1400–1900. *Dendrochronologia*, 70, 125900. <https://doi.org/10.1016/j.dendro.2021.125900>
- Kunecký, J., Arciszewska-Kędzior, A., Sebera, V., & Hasníková, H. (2016). Mechanical performance of dovetail joint related to the global stiffness of timber roof structures. *Materials and Structures*, 49(6), 2315–2327. <https://doi.org/10.1617/s11527-015-0651-1>
- Larsen, H. J., & Jensen, J. L. (2000). Influence of semi-rigidity of joints on the behaviour of timber structures. *Progress in Structural Engineering and Materials*, 2, 267–277.
- Narodni Technicke Muzeum. (2023). *Exhibition Krovky*.
- Prokop, O., Kolář, T., Kyncl, T., & Rybníček, M. (2017). Updating the Czech Millennia-Long Oak Tree-Ring Width Chronology. *Tree-Ring Research*, 73(1), 47–52. <https://doi.org/10.3959/1536-1098-73.1.47>
- Sass-Klaassen, U., Vernimmen, T., & Baittinger, C. (2008). Dendrochronological dating and provenancing of timber used as foundation piles under historic buildings in The Netherlands. *International Biodeterioration & Biodegradation*, 61(1), 96–105. <https://doi.org/10.1016/j.ibiod.2007.07.013>
- Škabrada, J. (2007). *Konstrukce historických staveb*. Argo.
- Sobra, K., Ferreira, C. F., Riggio, M., D’Ayala, D., Arriaga, F., & Aira, J.-R. (2015). A New Tool for the Structural Assessment of Historic Carpentry Joints. *3rd International Conference on Structural Health Assessment of Timber Structures*.
- Technical Committee CEN/TC 124. (2003). *EN 338 Structural Timber - Strength Classes*.
- Thun, T. (2005). Norwegian conifer chronologies constructed to date historical timber. *Dendrochronologia*, 23(2), 63–74. <https://doi.org/10.1016/j.dendro.2005.08.002>
- Vyhnalová, J. (2013). *Kostel Nejsvětější Trojice v Třebíči*. Masarykova univerzita Filozofická fakulta.
- Wald, F., Mareš, J., Sokol, Z., & Drdácký, M. (2000). Component Method for Historical Timber Joints. In *The Paramount Role of Joints into the Reliable Response of Structures* (Vol. 4, pp. 417–424).
- Zwinger, K. (2012). *Wood and Wood Joints: Building Traditions in Europe, Japan, and China* (2nd ed.). Birkbauser, Basel.

9. APPENDICES

9.1 Appendix A

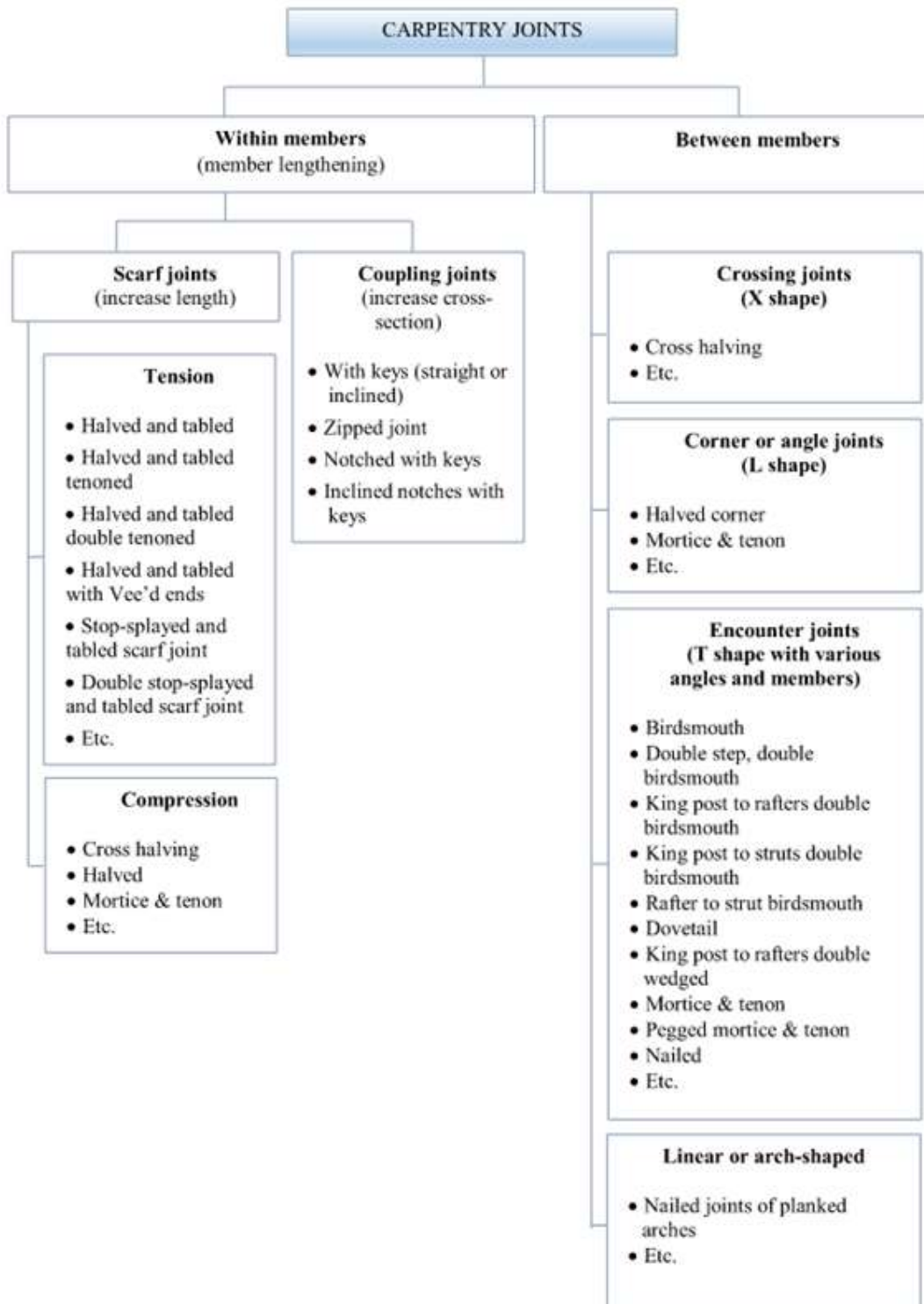


Figure A- 1. Proposed taxonomy for joint classification

Equation Set A1 – Shape functions for BEAM188 Element (ANSYS Inc, 2013)

$$u = \frac{1}{2} \left(u_I(1 - s) + u_J(1 + s) \right)$$

$$v = \frac{1}{2} \left(v_I \left(1 - \frac{s}{2} (3 - s^2) \right) + v_J \left(1 + \frac{s}{2} (3 - s^2) \right) \right) \\ + \frac{L}{8} \left(\theta_{z,I} (1 - s^2) (1 - s) - \theta_{z,J} (1 - s^2) (1 + s) \right)$$

$$w = \frac{1}{2} \left(w_I \left(1 - \frac{s}{2} (3 - s^2) \right) + w_J \left(1 + \frac{s}{2} (3 - s^2) \right) \right) \\ - \frac{L}{8} \left(\theta_{y,I} (1 - s^2) (1 - s) - \theta_{y,J} (1 - s^2) (1 + s) \right)$$

$$\theta_x = \frac{1}{2} \left(\theta_{x,I} (1 - s) + \theta_{x,J} (1 + s) \right)$$

These shape functions are for 3-D 2-node line elements with RDOF

9.2 Appendix B

	Softwood species										Hardwood species										
	C14	C16	C18	C20	C22	C24	C27	C30	C35	C40	C45	C50	D18	D24	D30	D35	D40	D50	D60	D70	
Strength properties (in N/mm²)																					
Bending	14	16	18	20	22	24	27	30	35	40	45	50	18	24	30	35	40	50	60	70	
Tension parallel	$f_{m,k}$	8	10	11	12	13	14	16	18	21	24	27	30	11	14	18	21	24	30	36	42
Tension perpendicular	$f_{t,0,k}$	0,4	0,4	0,4	0,4	0,4	0,4	0,4	0,4	0,4	0,4	0,4	0,4	0,6	0,6	0,6	0,6	0,6	0,6	0,6	0,6
Compression parallel	$f_{c,0,k}$	16	17	18	19	20	21	22	23	25	26	27	29	18	21	23	25	26	29	32	34
Compression perpendicular	$f_{c,90,k}$	2,0	2,2	2,2	2,3	2,4	2,5	2,6	2,7	2,8	2,9	3,1	3,2	7,5	7,8	8,0	8,1	8,3	9,3	10,5	13,5
Shear	$f_{v,k}$	3,0	3,2	3,4	3,6	3,8	4,0	4,0	4,0	4,0	4,0	4,0	4,0	3,4	4,0	4,0	4,0	4,0	4,0	4,5	5,0
Stiffness properties (in kN/mm²)																					
Mean modulus of elasticity parallel	$E_{0,mean}$	7	8	9	9,5	10	11	11,5	12	13	14	15	16	9,5	10	11	12	13	14	17	20
5 % modulus of elasticity parallel	$E_{0,05}$	4,7	5,4	6,0	6,4	6,7	7,4	7,7	8,0	8,7	9,4	10,0	10,7	8	8,5	9,2	10,1	10,9	11,8	14,3	16,8
Mean modulus of elasticity perpendicular	$E_{90,mean}$	0,23	0,27	0,30	0,32	0,33	0,37	0,38	0,40	0,43	0,47	0,50	0,53	0,63	0,67	0,73	0,80	0,86	0,93	1,13	1,33
Mean shear modulus	G_{mean}	0,44	0,5	0,56	0,59	0,63	0,69	0,72	0,75	0,81	0,88	0,94	1,00	0,59	0,62	0,69	0,75	0,81	0,88	1,06	1,25
Density (in kg/m³)																					
Density	ρ_k	290	310	320	330	340	350	370	380	400	420	440	460	475	485	530	550	620	700	900	
Mean density	ρ_{mean}	350	370	380	390	410	420	450	460	480	500	520	550	570	580	640	650	660	750	840	1080
<p>NOTE 1 Values given above for tension strength, compression strength, shear strength, 5 % modulus of elasticity, mean modulus of elasticity perpendicular to grain and mean shear modulus, have been calculated using the equations given in Annex A.</p> <p>NOTE 2 The tabulated properties are compatible with timber at a moisture content consistent with a temperature of 20 °C and a relative humidity of 65 %.</p> <p>NOTE 3 Timber conforming to classes C45 and C50 may not be readily available.</p> <p>NOTE 4 Characteristic values for shear strength are given for timber without fissures, according to EN 408. The effect of fissures should be covered in design codes.</p>																					

Table A- 1. Timber strength classes and characteristic values (Technical Committee CEN/TC 124, 2003)

Pitch Angle α	Zone for wind direction $\theta = 0^\circ$									
	F		G		H		I		J	
	$C_{pe,10}$	$C_{pe,1}$	$C_{pe,10}$	$C_{pe,1}$	$C_{pe,10}$	$C_{pe,1}$	$C_{pe,10}$	$C_{pe,1}$	$C_{pe,10}$	$C_{pe,1}$
-45°	-0,6		-0,6		-0,8		-0,7		-1,0	-1,5
-30°	-1,1	-2,0	-0,8	-1,5	-0,8		-0,6		-0,8	-1,4
-15°	-2,5	-2,8	-1,3	-2,0	-0,9	-1,2	-0,5		-0,7	-1,2
-5°	-2,3	-2,5	-1,2	-2,0	-0,8	-1,2	+0,2		+0,2	
							-0,6		-0,6	
5°	-1,7	-2,5	-1,2	-2,0	-0,6	-1,2	-0,6		+0,2	
	+0,0		+0,0		+0,0				-0,6	
15°	-0,9	-2,0	-0,8	-1,5	-0,3		-0,4		-1,0	-1,5
	+0,2		+0,2		+0,2		+0,0		+0,0	+0,0
30°	-0,5	-1,5	-0,5	-1,5	-0,2		-0,4		-0,5	
	+0,7		+0,7		+0,4		+0,0		+0,0	
45°	-0,0		-0,0		-0,0		-0,2		-0,3	
	+0,7		+0,7		+0,6		+0,0		+0,0	
60°	+0,7		+0,7		+0,7		-0,2		-0,3	
75°	+0,8		+0,8		+0,8		-0,2		-0,3	

Table A- 2. Recommended values of external pressure coefficients for dual-pitch roofs (per EN 1991-1-4)

	Slavonice Members			Doksy members	
	b [cm]	h [cm]		b [cm]	h [cm]
Rafter	11	11	Tie beam	24	30
Collar	10	12	Rafter	16	18
Subrafter	10	14	Subrafter	18	31
Column	16	14	Subcollar	18	20
			Collar	14	15
			Knee brace	12	17

	Trebic Members	
	b [cm]	h [cm]
Tie beam	22	20
Rafter	15	19
Vertical Strut	17	14
Cross-brace	13	14
Collar tie	13	13

Model Beam Cross Sections

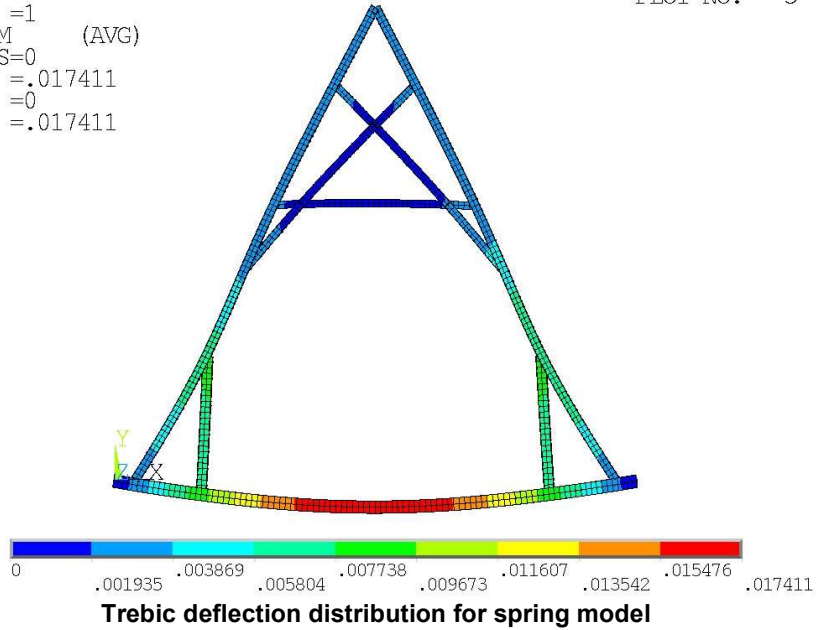
9.3 Appendix C: Expanded Images from Figure 30

NODAL SOLUTION

STEP=4
SUB =1
USUM (AVG)
RSYS=0
DMX =.017411
SMN =0
SMX =.017411

Ansys
2023 R1

PLOT NO. 3

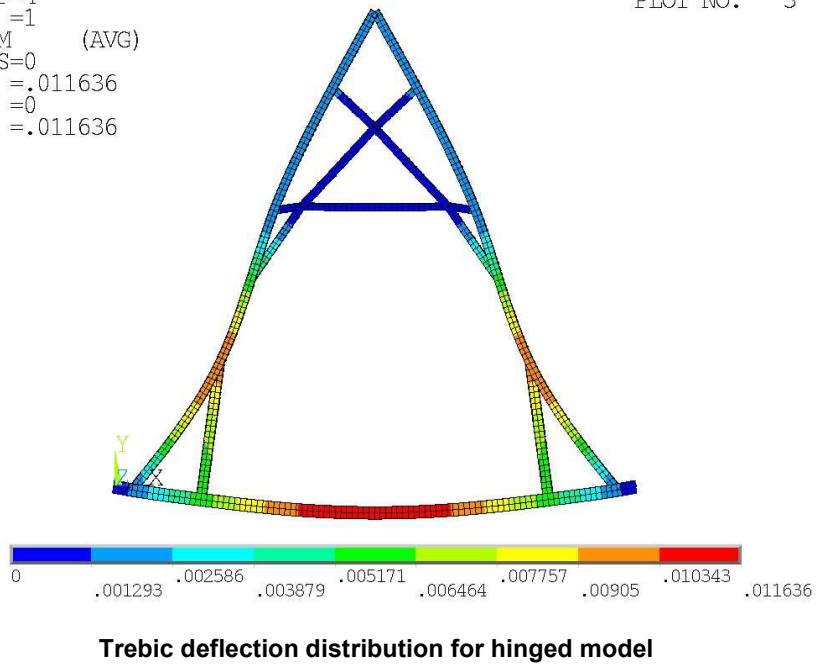


NODAL SOLUTION

STEP=4
SUB =1
USUM (AVG)
RSYS=0
DMX =.011636
SMN =0
SMX =.011636

Ansys
2023 R1

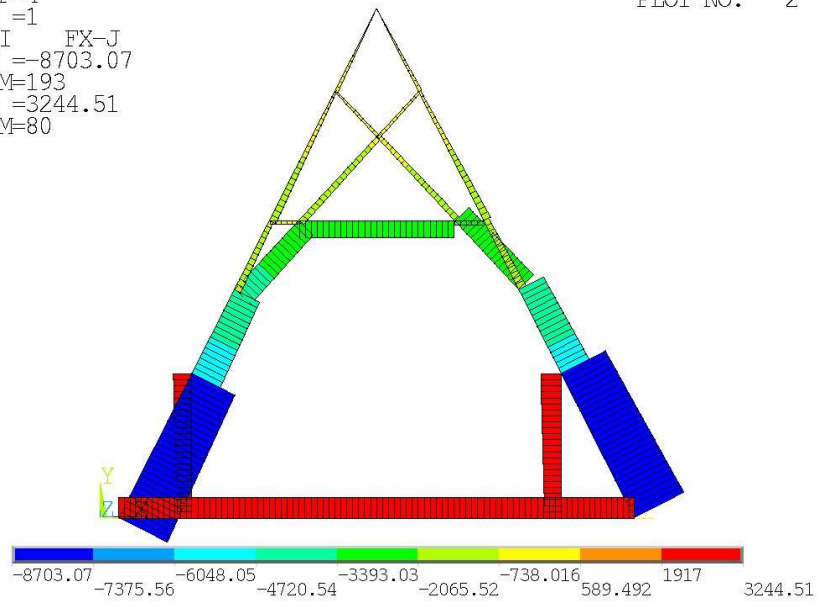
PLOT NO. 3



LINE STRESS
STEP=4
SUB =1
FX-I FX-J
MIN =-8703.07
ELEM=193
MAX =3244.51
ELEM=80

Ansys
2023 R1

PLOT NO. 2

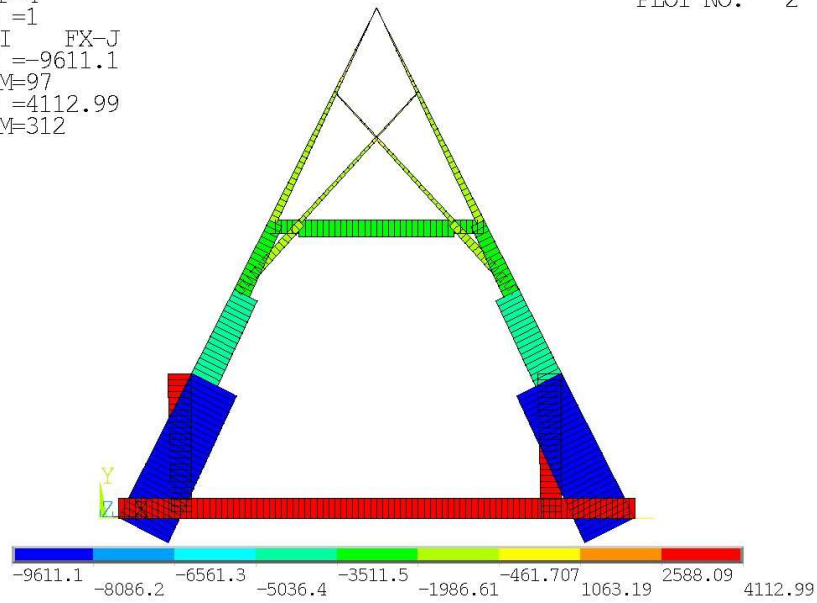


Axial force distribution for spring model

LINE STRESS
STEP=4
SUB =1
FX-I FX-J
MIN =-9611.1
ELEM=97
MAX =4112.99
ELEM=312

Ansys
2023 R1

PLOT NO. 2

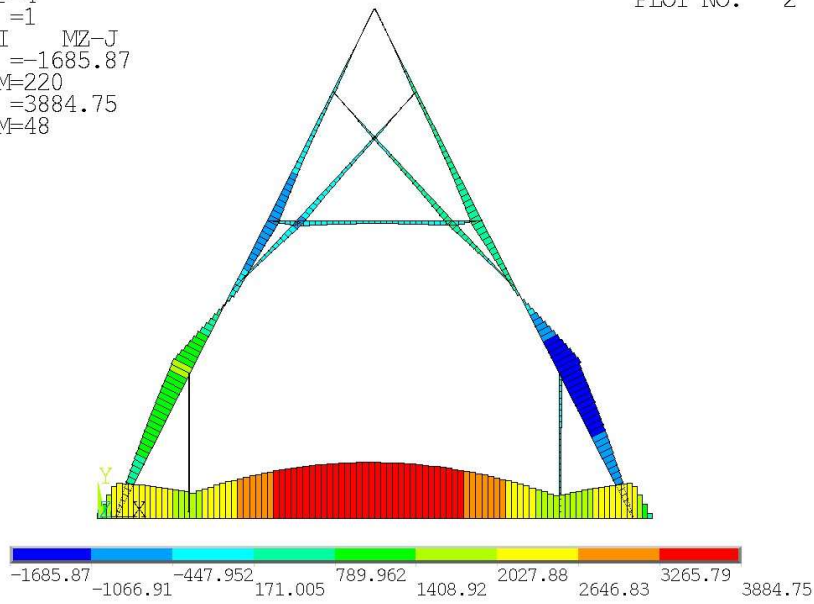


Axial force distribution for hinged model

LINE STRESS
STEP=4
SUB =1
MZ-I MZ-J
MIN =-1685.87
ELEM=220
MAX =3884.75
ELEM=48

Ansys
2023 R1

PLOT NO. 2

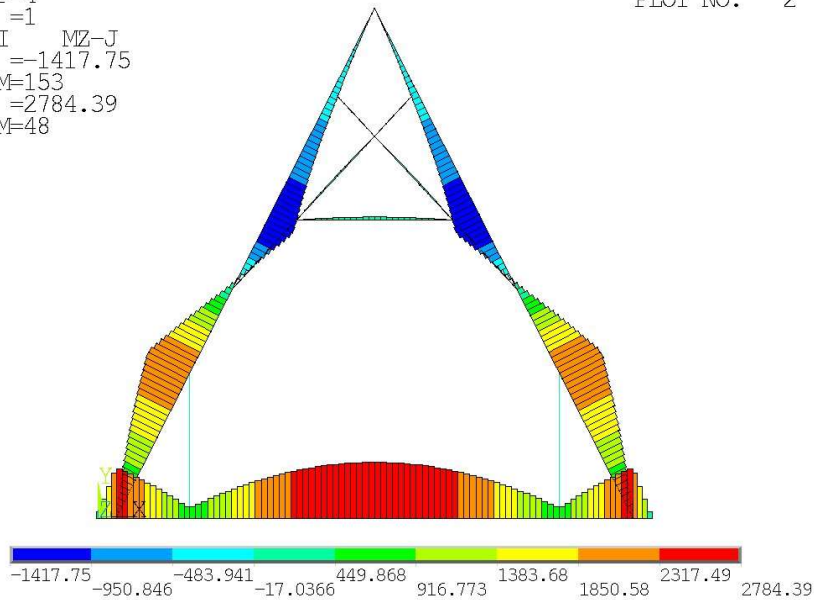


Bending moment distribution for spring model

LINE STRESS
STEP=4
SUB =1
MZ-I MZ-J
MIN =-1417.75
ELEM=153
MAX =2784.39
ELEM=48

Ansys
2023 R1

PLOT NO. 2



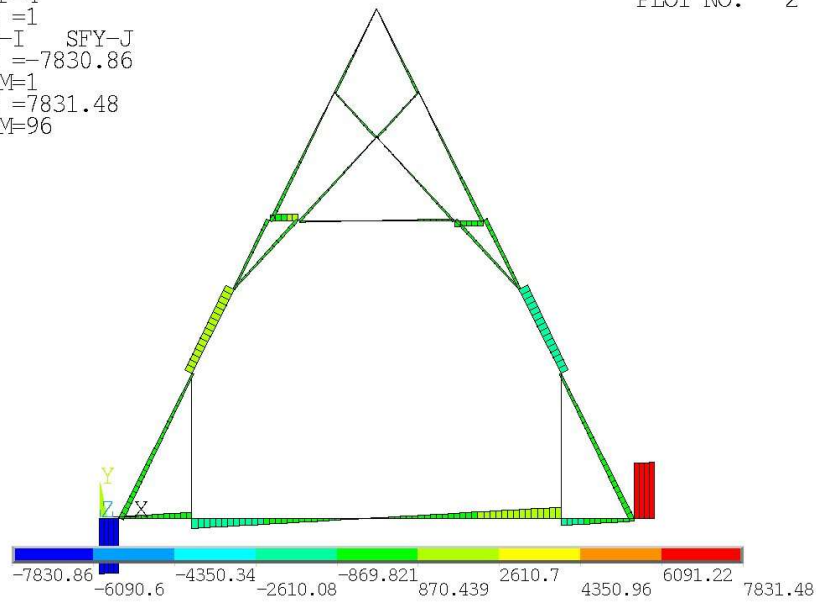
Bending moment distribution for hinged model

LINE STRESS

STEP=4
SUB =1
SFY-I SFY-J
MIN =-7830.86
ELEM=1
MAX =7831.48
ELEM=96

Ansys
2023 R1

PLOT NO. 2



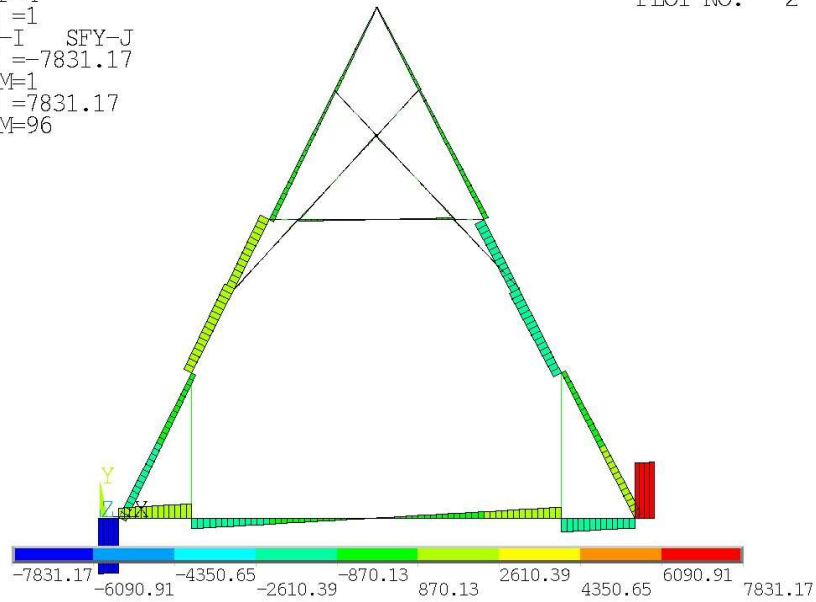
Shear force distribution for spring model

LINE STRESS

STEP=4
SUB =1
SFY-I SFY-J
MIN =-7831.17
ELEM=1
MAX =7831.17
ELEM=96

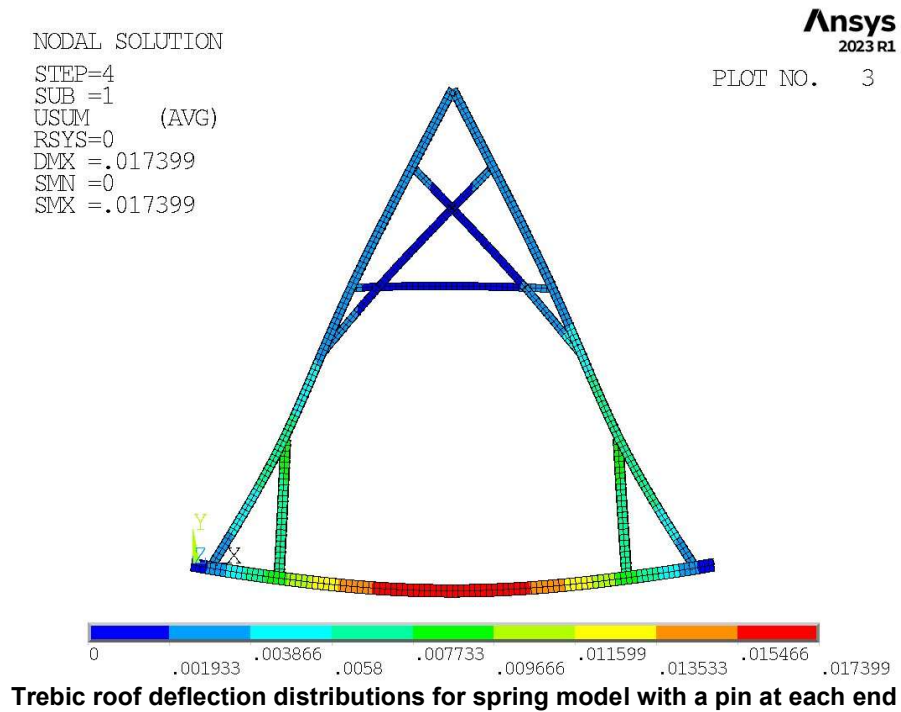
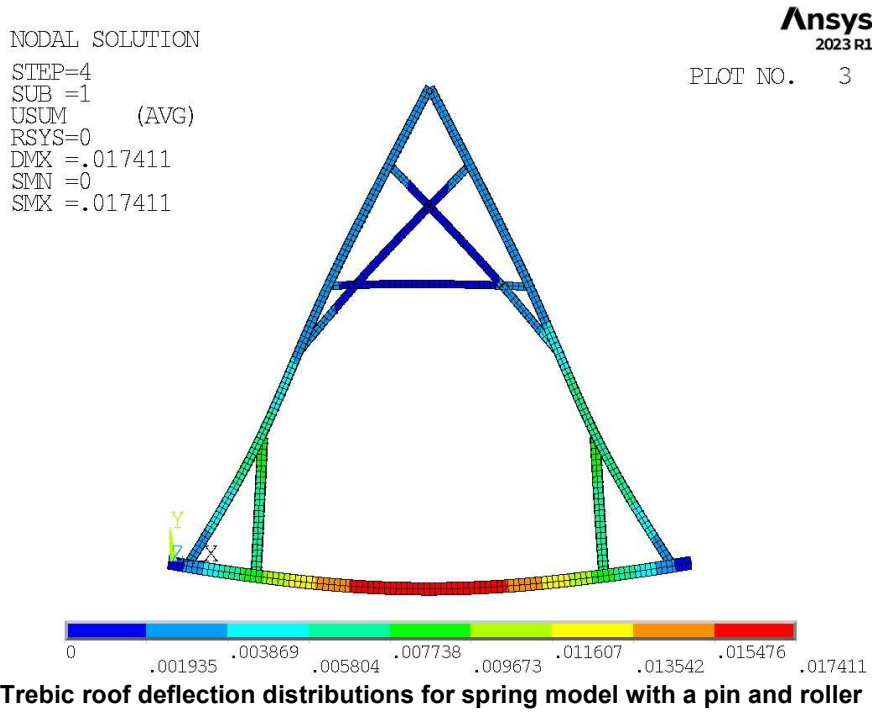
Ansys
2023 R1

PLOT NO. 2



Shear force distribution for hinged model

9.4 Appendix D: Expanded Images from Figure 31

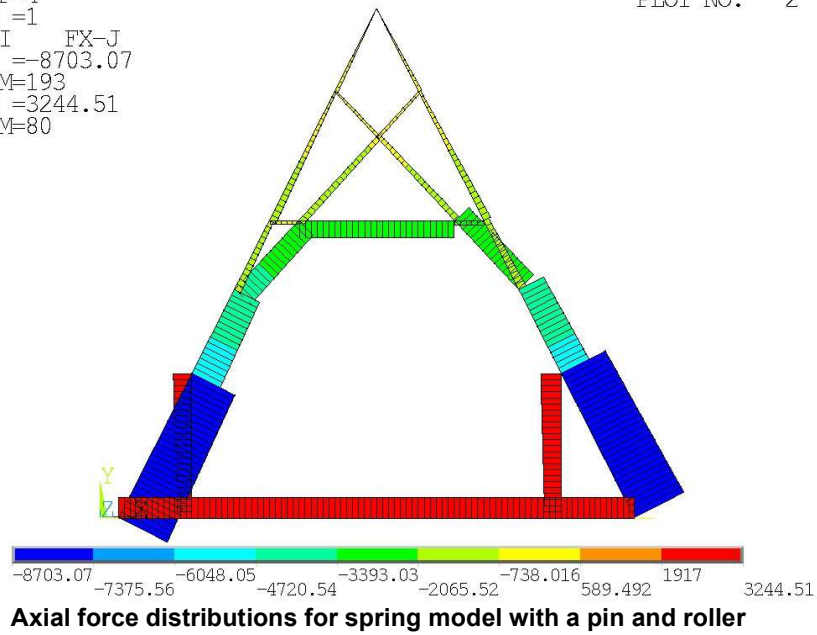


LINE STRESS

STEP=4
SUB =1
FX-I FX-J
MIN =-8703.07
ELEM=193
MAX =3244.51
ELEM=80

Ansys
2023 R1

PLOT NO. 2

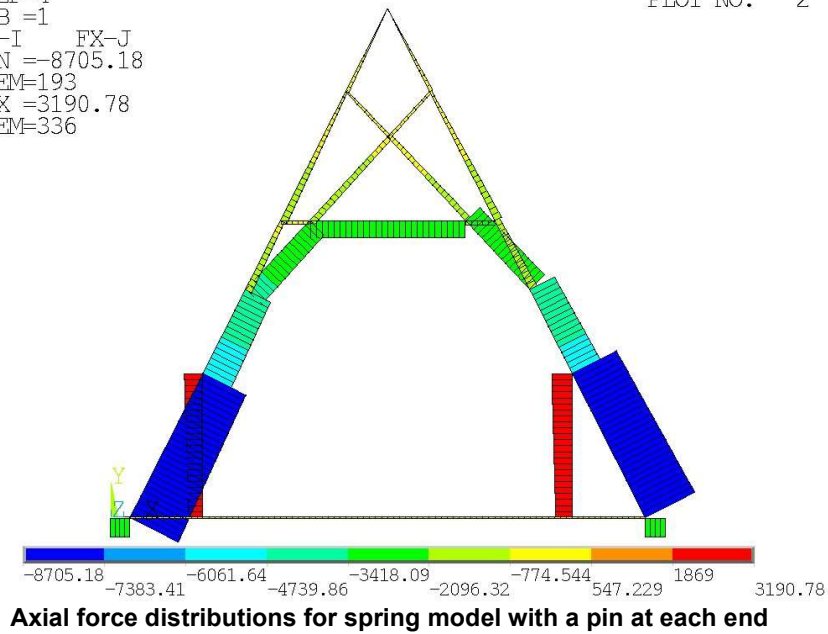


LINE STRESS

STEP=4
SUB =1
FX-I FX-J
MIN =-8705.18
ELEM=193
MAX =3190.78
ELEM=336

Ansys
2023 R1

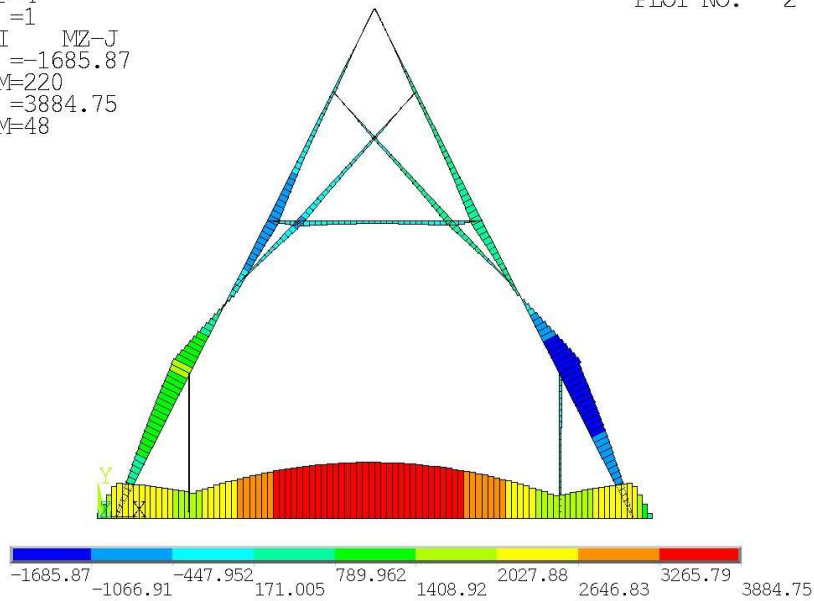
PLOT NO. 2



LINE STRESS
STEP=4
SUB =1
MZ-I MZ-J
MIN =-1685.87
ELEM=220
MAX =3884.75
ELEM=48

Ansys
2023 R1

PLOT NO. 2

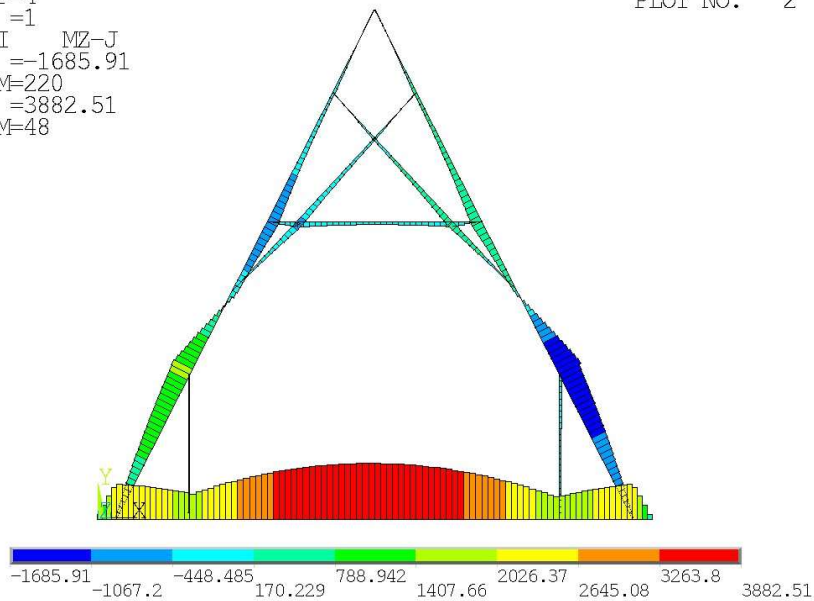


Bending moment distributions for spring model with a pin and roller

LINE STRESS
STEP=4
SUB =1
MZ-I MZ-J
MIN =-1685.91
ELEM=220
MAX =3882.51
ELEM=48

Ansys
2023 R1

PLOT NO. 2



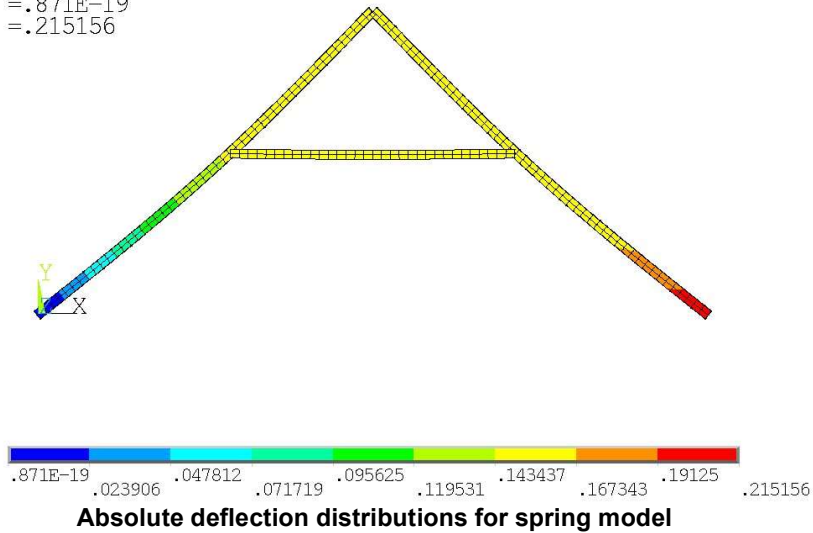
Bending moment distributions for spring model with a pin at each end

9.5 Appendix E: Expanded Images from Figure 34

NODAL SOLUTION
STEP=6
SUB =1
USUM (AVG)
RSYS=0
DMX =.215156
SMN =.871E-19
SMX =.215156

Ansys
2023 R1

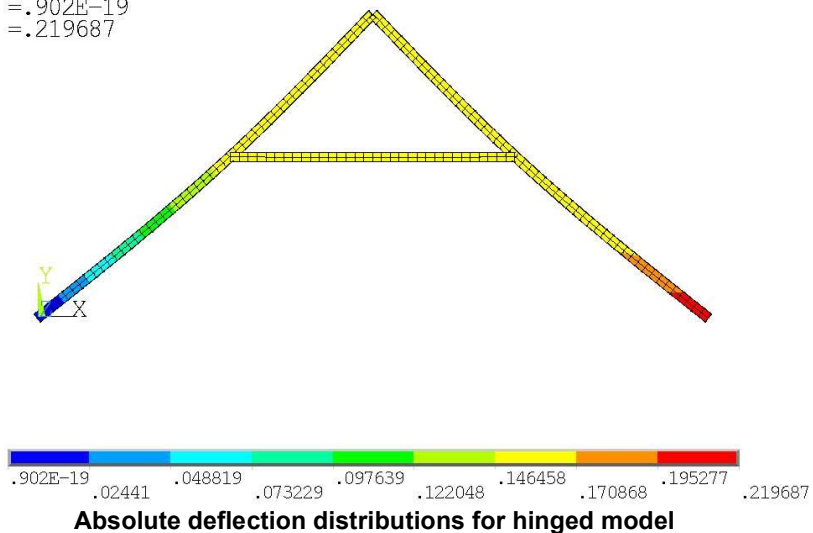
PLOT NO. 3



NODAL SOLUTION
STEP=6
SUB =1
USUM (AVG)
RSYS=0
DMX =.219687
SMN =.902E-19
SMX =.219687

Ansys
2023 R1

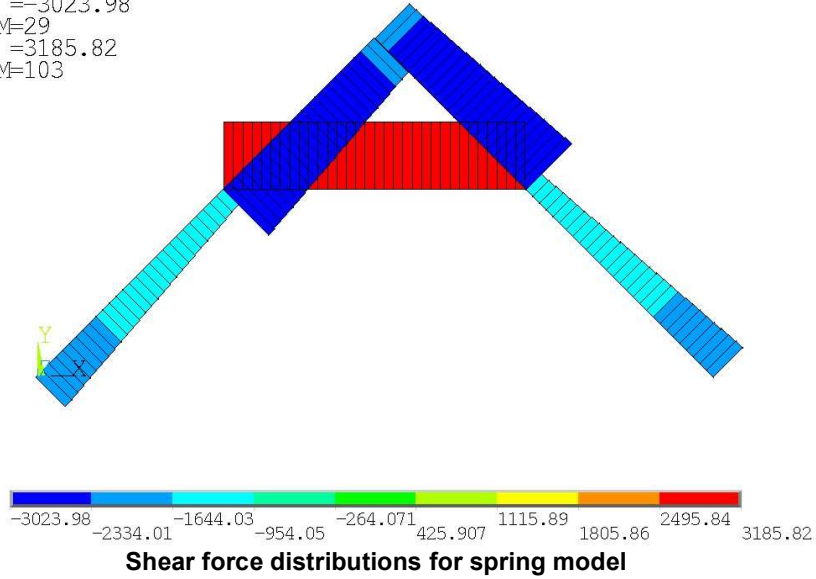
PLOT NO. 3



LINE STRESS
STEP=6
SUB =1
FX-I FX-J
MIN =-3023.98
ELEM=29
MAX =3185.82
ELEM=103

Ansys
2023 R1

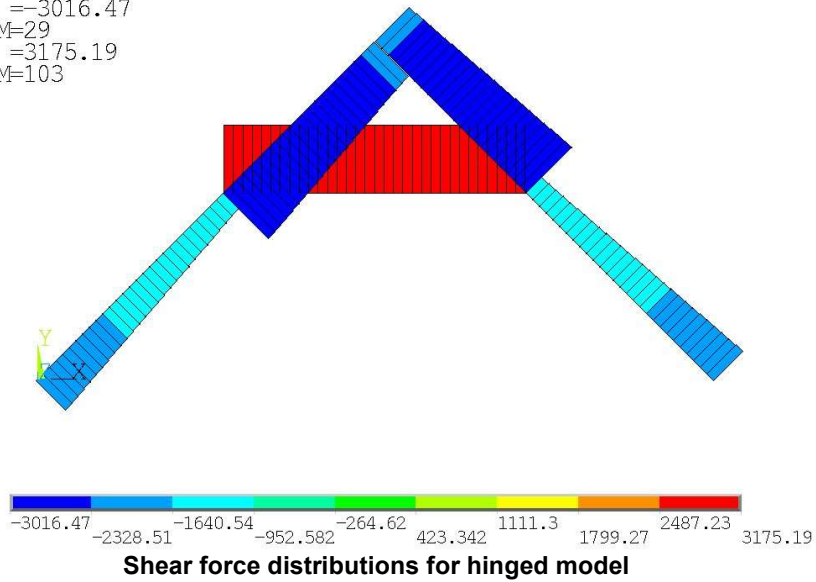
PLOT NO. 2



LINE STRESS
STEP=6
SUB =1
FX-I FX-J
MIN =-3016.47
ELEM=29
MAX =3175.19
ELEM=103

Ansys
2023 R1

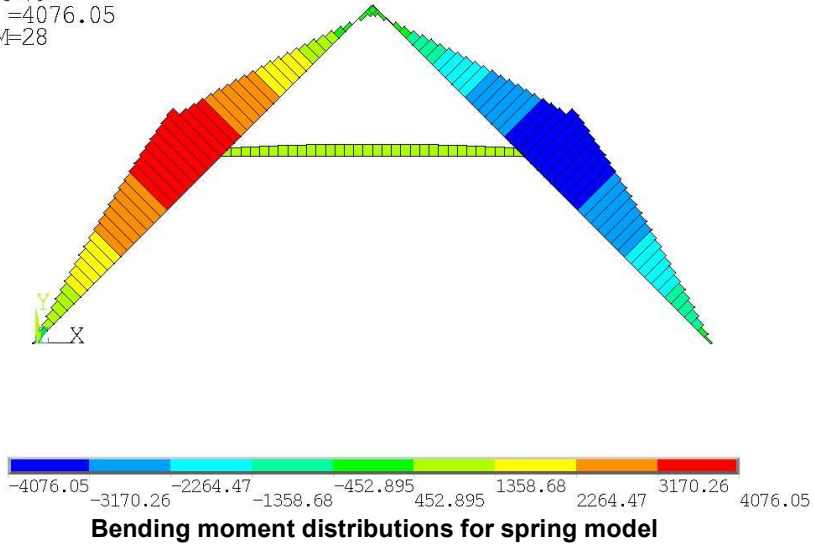
PLOT NO. 2



LINE STRESS
STEP=6
SUB =1
MZ-I MZ-J
MIN =-4076.05
ELEM=79
MAX =4076.05
ELEM=28

Ansys
2023 R1

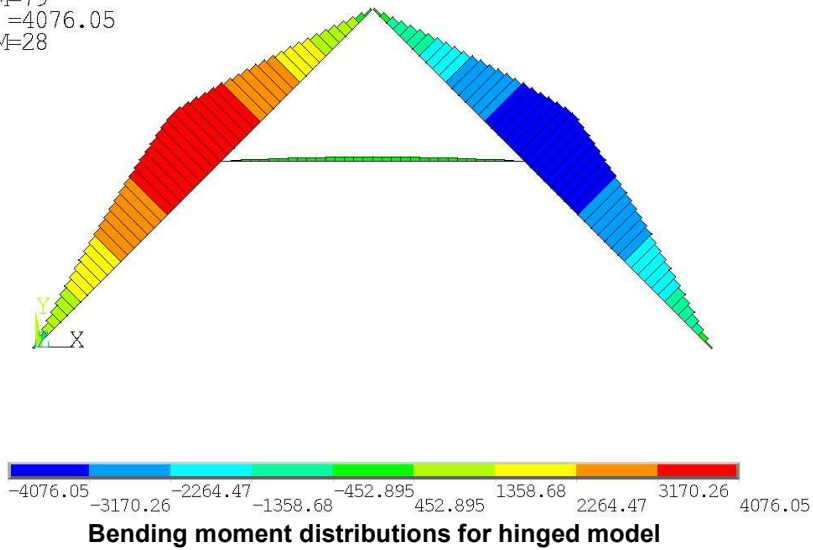
PLOT NO. 2



LINE STRESS
STEP=6
SUB =1
MZ-I MZ-J
MIN =-4076.05
ELEM=79
MAX =4076.05
ELEM=28

Ansys
2023 R1

PLOT NO. 2

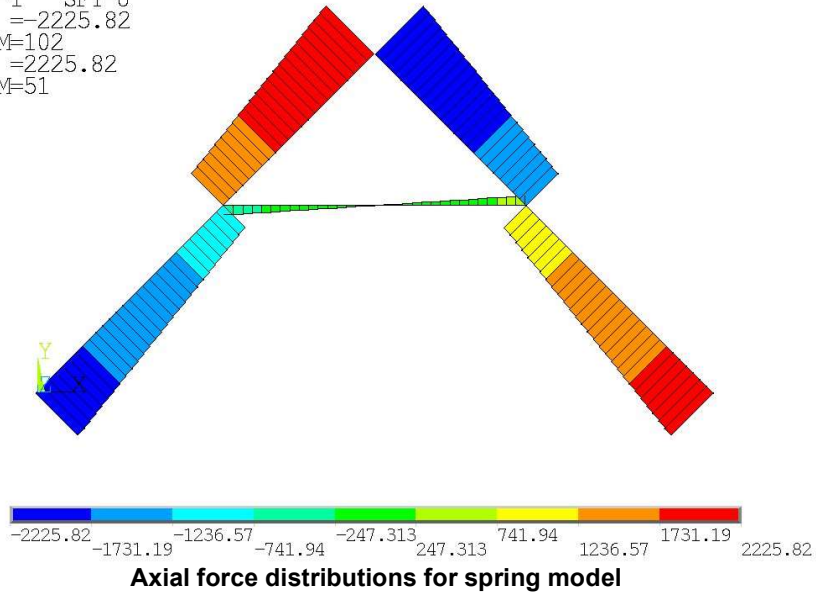


LINE STRESS

STEP=6
SUB =1
SFY-I SFY-J
MIN =-2225.82
ELEM=102
MAX =2225.82
ELEM=51

Ansys
2023 R1

PLOT NO. 2

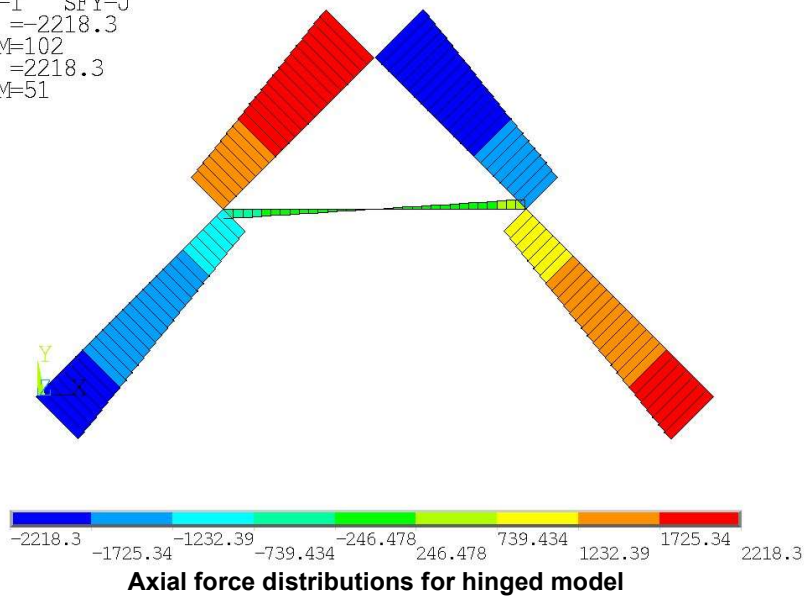


LINE STRESS

STEP=6
SUB =1
SFY-I SFY-J
MIN =-2218.3
ELEM=102
MAX =2218.3
ELEM=51

Ansys
2023 R1

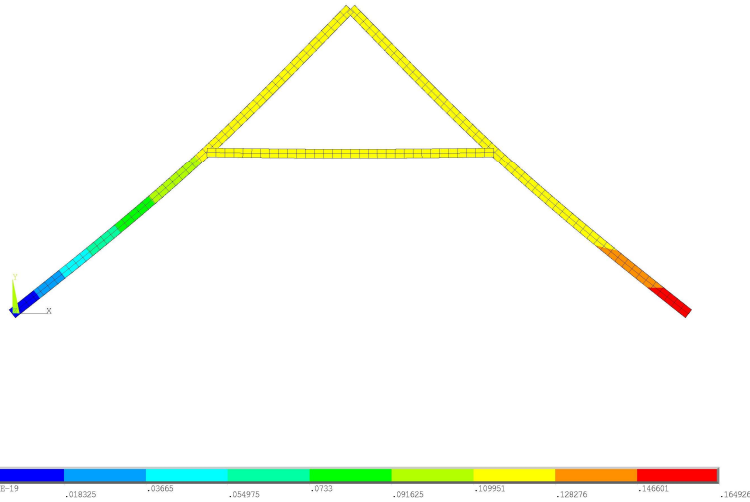
PLOT NO. 2



9.6 Appendix F: Expanded Images from Figure 35

```
MODEL SOLUTION
STEP=6
SUB=1
LOAD
TIME=0 (AVG)
NODS=164926
SIF=4980139
SDE=-1.64926
SDE=-1.64926
```

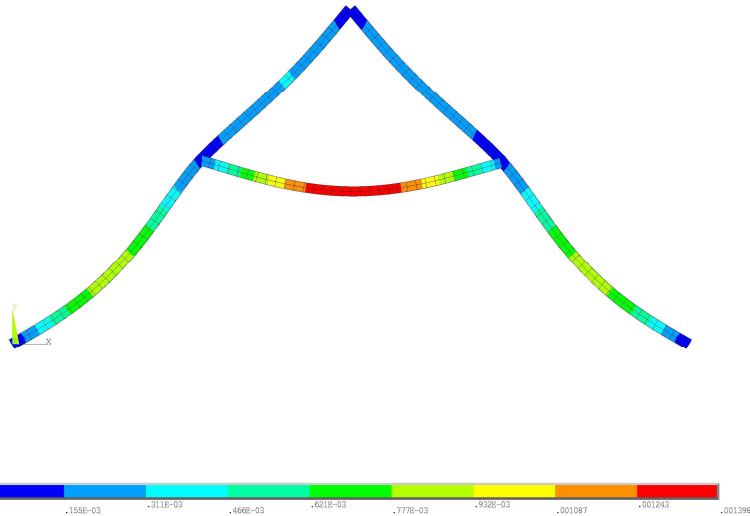
Ansys
2023 R1
FILE NO. 3



Absolute deflection distributions for semi-rigid model with a roller

```
MODEL SOLUTION
STEP=6
SUB=1
LOAD
TIME=0 (AVG)
NODS=164926
SIF=4980139
SDE=-0.001398
SDE=-0.001398
```

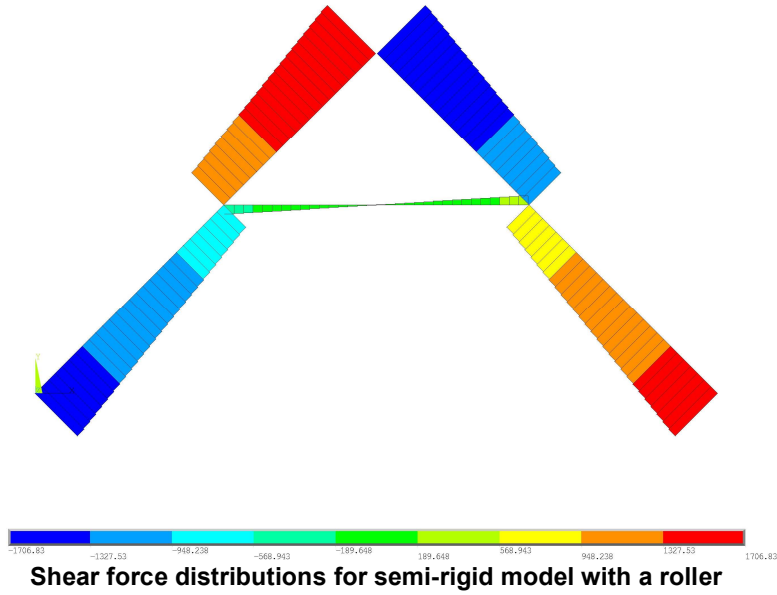
Ansys
2023 R1
FILE NO. 3



Absolute deflection distributions for semi-rigid model with a pin

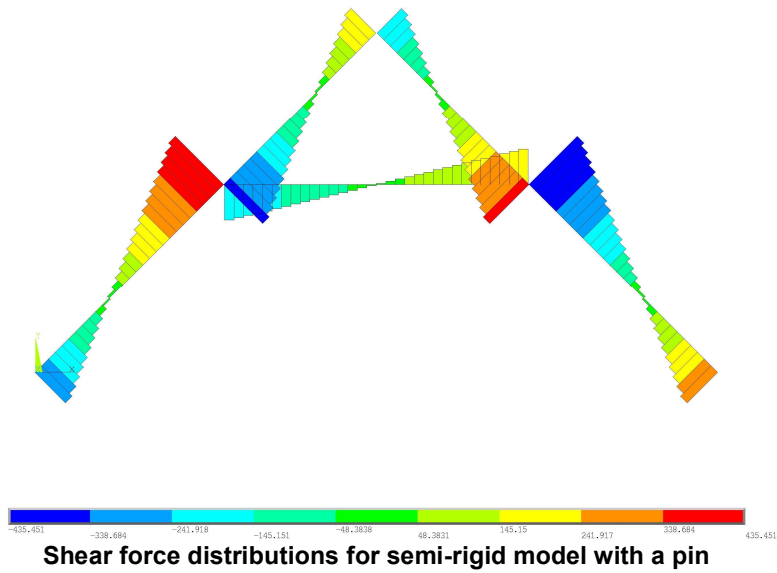
```
LINE STRESS  
STEP=6  
SUB=1  
SPY=1 SPY=2  
SIF=-106.83  
ELEM=102  
NODE=1706.83  
ELEM=51
```

Ansys
2023 R1
PLOT NO. 2



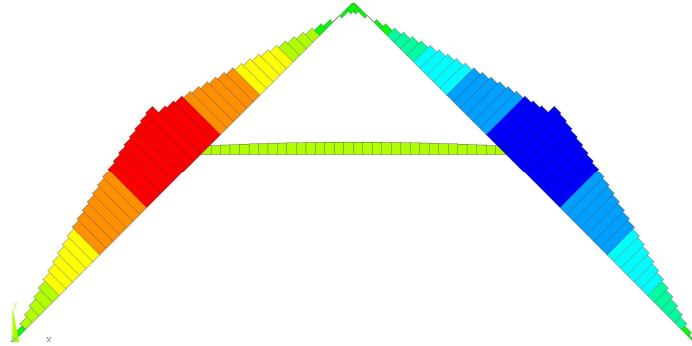
```
LINE STRESS  
STEP=6  
SUB=1  
SPY=1 SPY=2  
SIF=-435.451  
ELEM=78  
NODE=338.684  
ELEM=28
```

Ansys
2023 R1
PLOT NO. 2



LINE STRESS
S123=6
S11=1
S2=-1 102-1
E11=-3123.93
E12=79
E22=-3123.93
E13=28

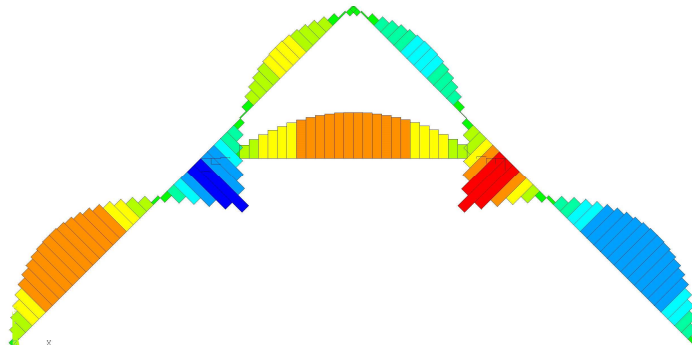
Ansys
2023 R1
PLT# NO. 2



Bending moment distributions for semi-rigid model with a roller

LINE STRESS
S123=6
S11=1
S2=-1 102-1
E11=-202.267
E12=28
E22=-202.269
E13=79

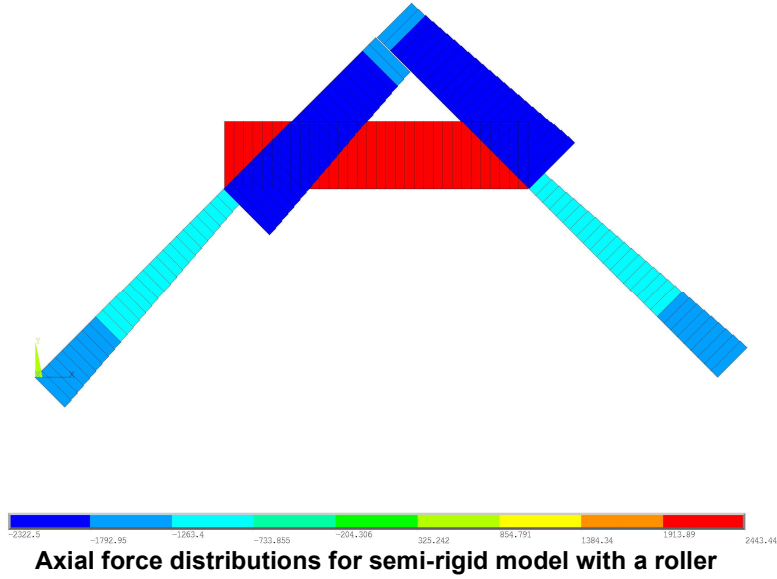
Ansys
2023 R1
PLT# NO. 2



Bending moment distributions for semi-rigid model with a pin

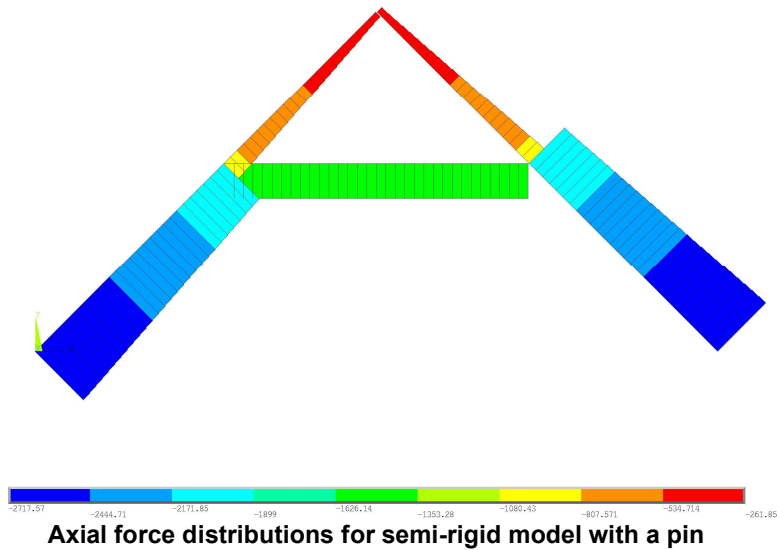
LINE STRESS
STEP=6
SUB=1
PC=1
PL1=-2322.5
PL2=-2322.5
SOL=-3383.44
ELEM=103

Ansys
2023 R1
ELOT NO. 2



LINE STRESS
STEP=6
SUB=1
PC=1
PL1=-2717.57
PL2=-2717.57
SOL=-261.857
ELEM=51

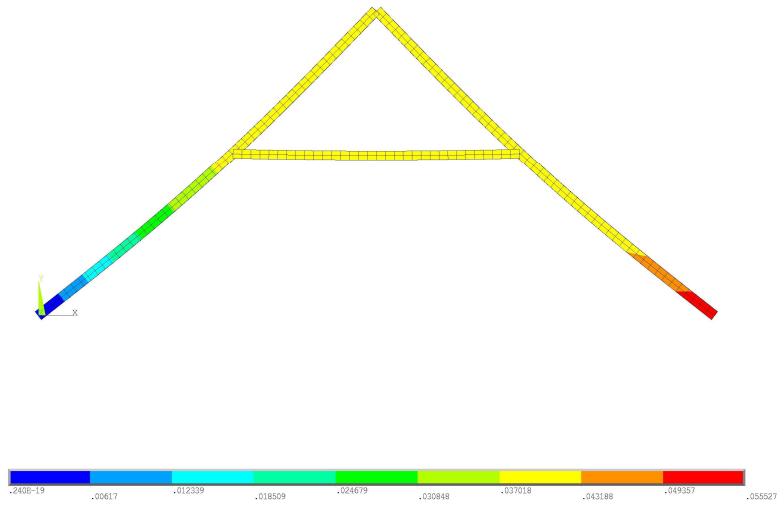
Ansys
2023 R1
ELOT NO. 2



9.7 Appendix G: Expanded Images from Figure 36

```
MODEL SOLUTION  
STEP=6  
SUB=1  
USDF  
USDF (ANG)  
NSYS=9  
NIN=0.055527  
NEX=0.055527  
NEX=0.055527
```

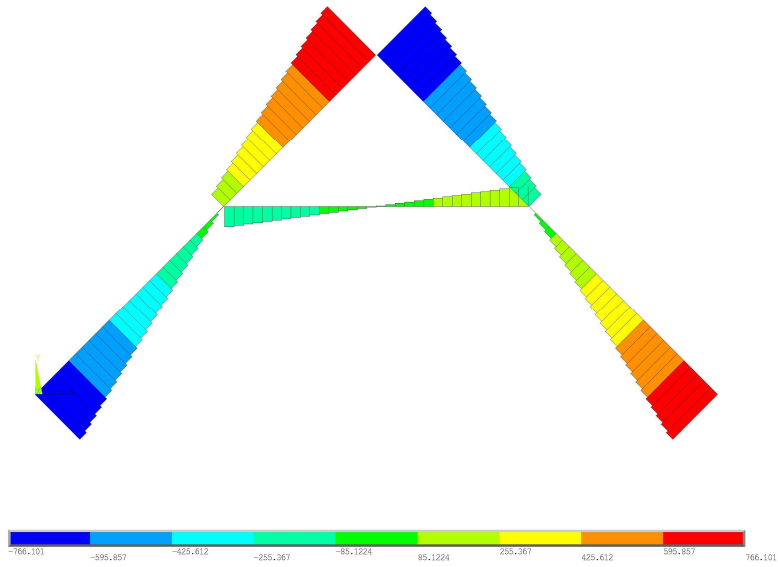
Ansys
2023 R1
FIG. NO. 3



Absolute deflection distributions for the spring model at collar tie axial force inflection point

```
LINE STRESS  
STEP=6  
SUB=1  
SPY=7  
E11=166.101  
E12=1.02  
E33=166.101  
E13=0.01
```

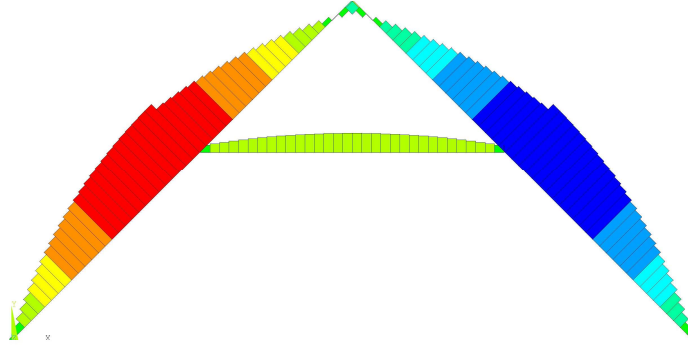
Ansys
2023 R1
FIG. NO. 2



Shear force distributions for the spring model at collar tie axial force inflection point

```
LINE STRESS  
STEP=6  
SUB=1  
PC=1 PK=J  
MIN=-981.139  
MAX=981.139  
ELEM=28
```

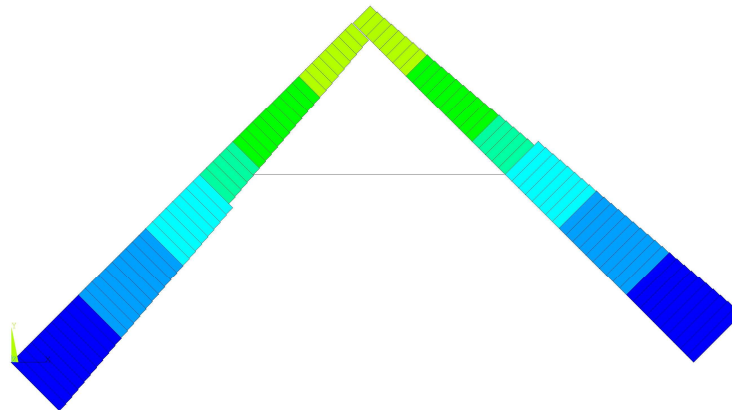
Ansys
2023 R1
PLOT NO. 2



Bending moment distributions for the spring model at collar tie axial force inflection point

```
LINE STRESS  
STEP=6  
SUB=1  
PC=1 PK=J  
MIN=-2282.83  
MAX=-.089723  
ELEM=103
```

Ansys
2023 R1
PLOT NO. 2



Axial force distributions for the spring model at collar tie axial force inflection point

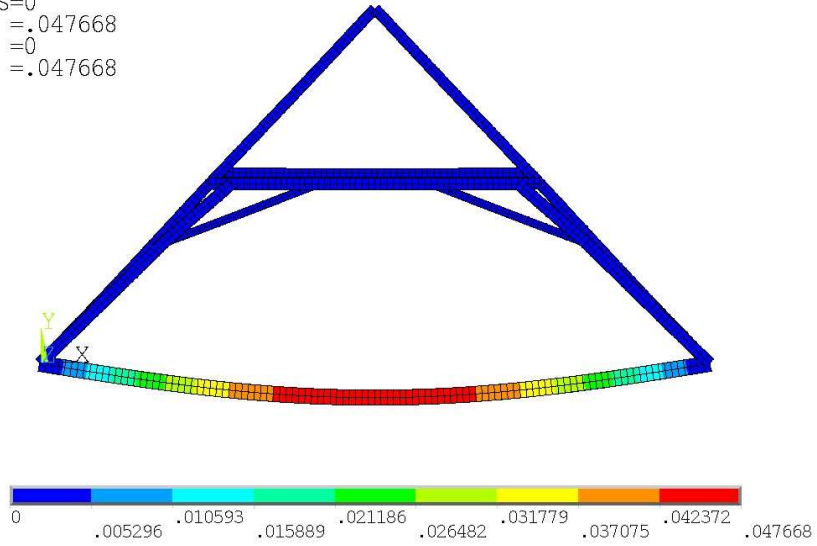
9.8 Appendix H: Expanded Images from Figure 38

NODAL SOLUTION

STEP=5
SUB =1
USUM (AVG)
RSYS=0
DMX =.047668
SMN =0
SMX =.047668

Ansys
2023 R1

PLOT NO. 3

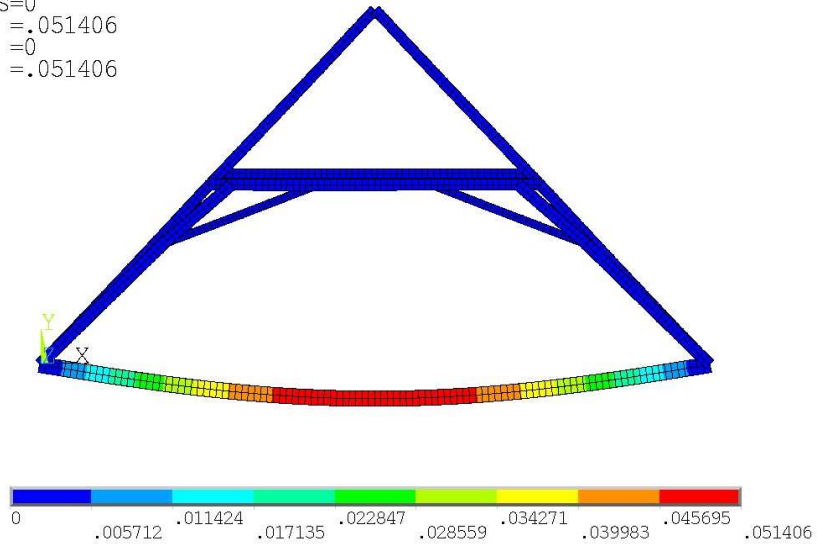


NODAL SOLUTION

STEP=5
SUB =1
USUM (AVG)
RSYS=0
DMX =.051406
SMN =0
SMX =.051406

Ansys
2023 R1

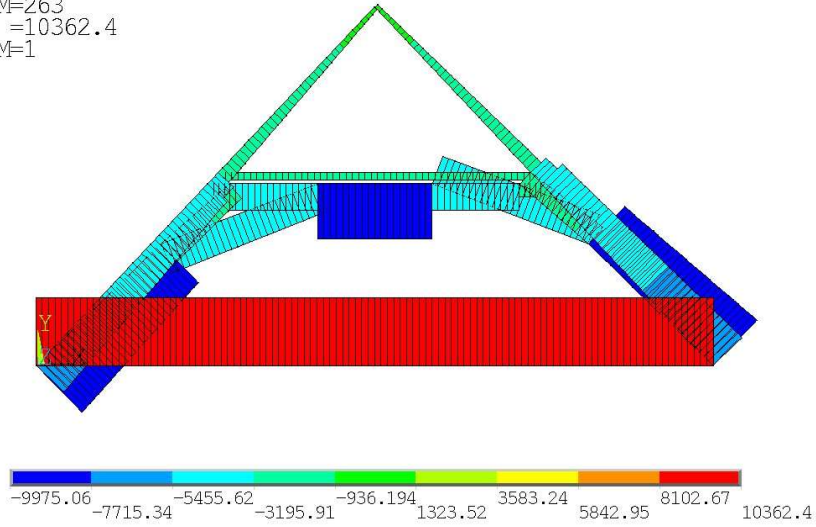
PLOT NO. 3



LINE STRESS
STEP=5
SUB =1
FX-I FX-J
MIN =-9975.06
ELEM=263
MAX =10362.4
ELEM=1

Ansys
2023 R1

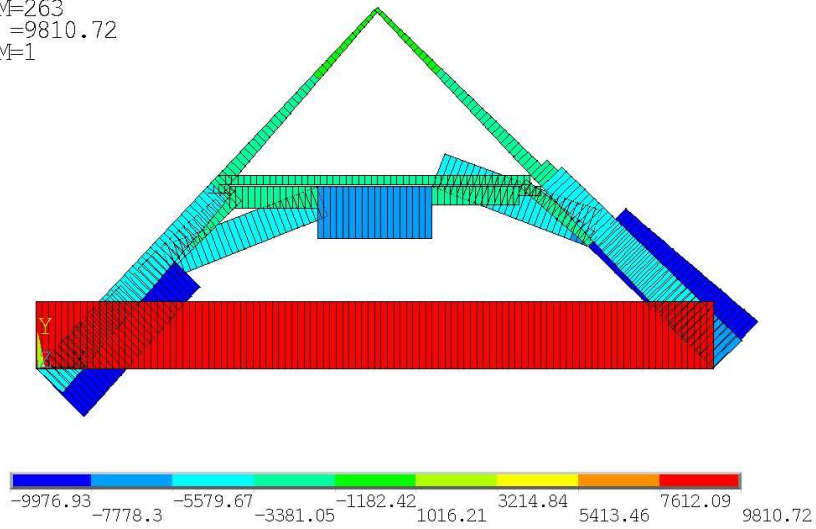
PLOT NO. 2



LINE STRESS
STEP=5
SUB =1
FX-I FX-J
MIN =-9976.93
ELEM=263
MAX =9810.72
ELEM=1

Ansys
2023 R1

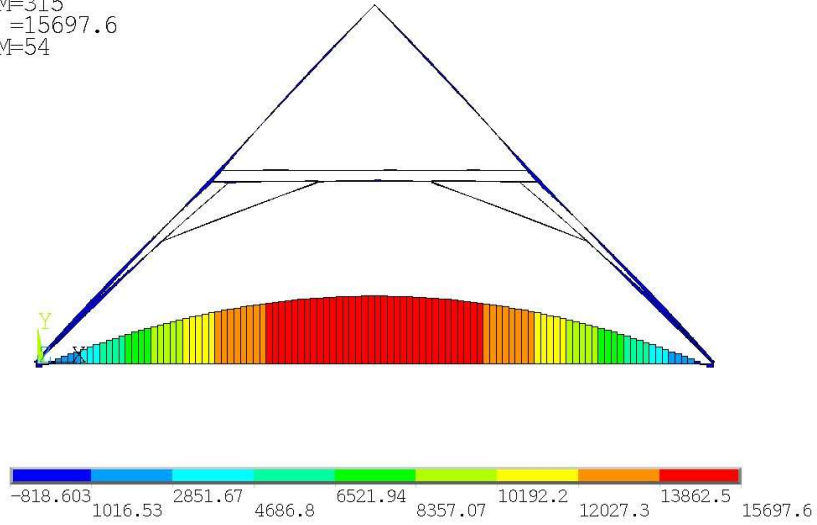
PLOT NO. 2



LINE STRESS
STEP=5
SUB =1
MZ-I MZ-J
MIN =-818.603
ELEM=315
MAX =15697.6
ELEM=54

Ansys
2023 R1

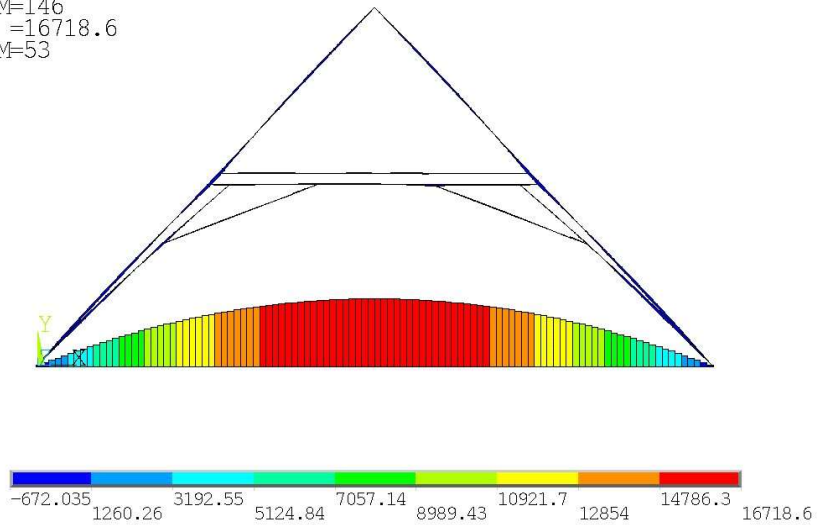
PLOT NO. 2



LINE STRESS
STEP=5
SUB =1
MZ-I MZ-J
MIN =-672.035
ELEM=146
MAX =16718.6
ELEM=53

Ansys
2023 R1

PLOT NO. 2

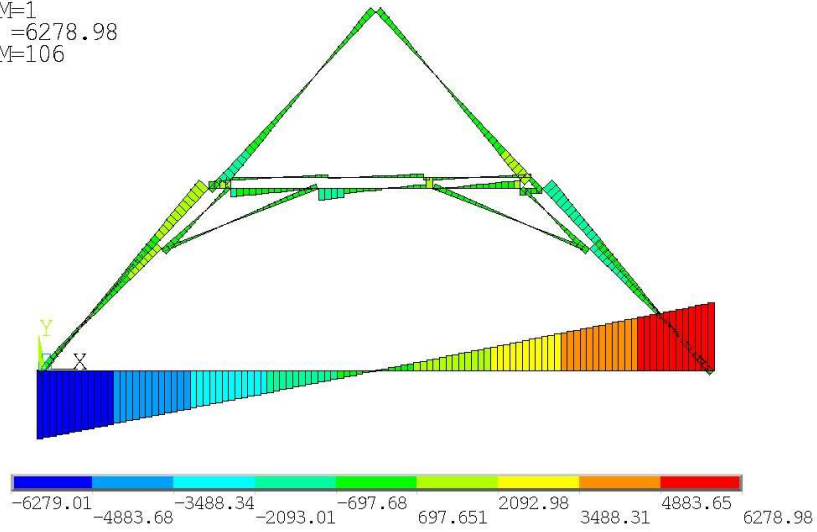


LINE STRESS

STEP=5
SUB =1
SFY-I SFY-J
MIN =-6279.01
ELEM=1
MAX =6278.98
ELEM=106

Ansys
2023 R1

PLOT NO. 2

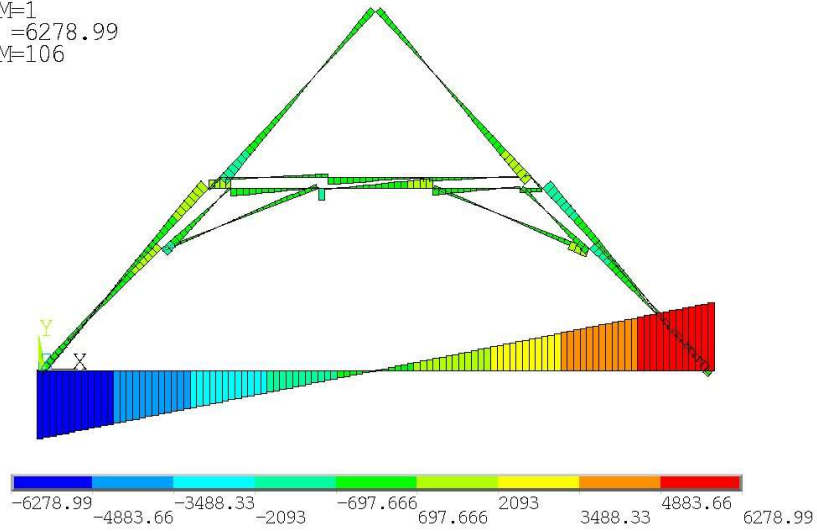


LINE STRESS

STEP=5
SUB =1
SFY-I SFY-J
MIN =-6278.99
ELEM=1
MAX =6278.99
ELEM=106

Ansys
2023 R1

PLOT NO. 2



ANSYS APDL script for Třebíč roof truss with semi-rigid joints:

Input File:

```
! Start by clearing the database and setting graphics as desired
FINISH
/CLEAR
*AFUN,DEG
/input,01_geom ! Geometry for collar-rafter truss with cross braces
/SOLU
/input,02_CEs
/input,03_BCs
solve
/input,04_loads
LSSOLVE,1,3
finish
/POST1
/input,05_post
```

01_geom:

```
/PNUM,KP,1
/PNUM,LINE,1
/NUMBER,0
```

```
! Enter preprocessing mode
/PREP7
```

```
! ITERATIVE INPUT
spacing=10e-3 ! size of hinge segments and = 1/10 of element size
```

```
!! GEOMETRY !!
```

```
!-----
```

```
! VARIABLES
```

```
z=0      ! zero
h=8.4483 ! Y - apex height
span=9.23 ! X - end of bottom chord
rbc=.3273 ! X - rafter to bottom chord
midsp=span/2 ! X - rafter apex
vbc=1.545 ! X - vertical to bottom chord
vr=2.3993 ! Y - vertical to rafter
trbx=2.2503 ! X - truss to rafter bottom connection
trby=3.7889 ! Y - truss to rafter bottom connection
trtx=3.9162 ! X - truss to rafter top connection
trty=7.0714 ! Y - truss to rafter top connection
cr=2.8319 ! X - collar tie to rafter
col=4.935 ! Y - collar tie height
ct=3.3199 ! X - collar tie to diagonal truss intersection x-coord
tt=6.3226 ! Y - intersection of diagonals
```

```
lrafang=atan(h/(midsp-rbc)) ! left rafter angle
```

```

rrafang=atan(h/(midsp-rbc))+180+2*atan((midsp-rbc)/h) ! right rafter angle
lcbang=atan((trty-trby)/(span-trtx-trbx)) ! left cross brace angle
rcbang=atan((trty-trby)/(span-trtx-trbx))+180+2*atan((span-trtx-trbx)/(trty-trby)) ! right cross brace angle

```

```
! Define Geometry of Truss in 2D
```

```
! GENERATE KEYPOINTS AND LINES
```

```
! First, define keypoints to be the nodes and offset nodes for later joint use
```

```
! Offset by 1mm using the KBETW command
```

```
!-----
```

```
!Define variables for keypoint/node numbering
```

```
n1=10
```

```
n2=20
```

```
n3=30
```

```
n4=40
```

```
n5=50
```

```
n6=60
```

```
n7=70
```

```
n8=80
```

```
n9=90
```

```
n10=100
```

```
n11=110
```

```
n12=120
```

```
n13=130
```

```
n14=140
```

```
n15=150
```

```
n16=160
```

```
! Bottom chord-----
```

```
K,n1,z,z ! K10 left end of bc
```

```
K,n1+1,rbc,z ! K11 L rafter intersects bottom chord
```

```
K,n1+2,vbc,z ! K12 L vertical intersects bottom chord
```

```
K,n1+3,span-vbc,z ! K13 R vertical intersects bottom chord
```

```
K,n1+4,span-rbc,z ! K14 R rafter intersects bottom chord
```

```
K,n2,span,z ! K20 right end of bc
```

```
L,n1,n1+1 ! L1
```

```
L,n1+1,n1+2 ! L2
```

```
L,n1+2,n1+3 ! L3
```

```
L,n1+3,n1+4 ! L4
```

```
L,n1+4,n2 ! L5
```

```
! Left rafter keypoints-----
```

```
K,n3,rbc,z ! K30 start of rafter at int with bottom chord
```

```
K,n4,midsp,h ! K40 Apex for Left rafter
```

```
KBETW,n3,n4,n3+1,Dist,spacing ! K31
```

```
K,n3+2,vbc,vr ! K32
```

```
K,n3+3,trbx,trby ! K33
```

```
K,n3+4,cr,col ! K34
```

K,n3+5,trtx,trty ! K35
KBETW,n4,n3,n4-1,Dist,spacing ! K39

L,n3,n3+1 ! L6
L,n3+1,n3+2 ! L7
L,n3+2,n3+3 ! L8
L,n3+3,n3+4 ! L9
L,n3+4,n3+5 ! L10
L,n3+5,n4-1 ! L11
L,n4-1,n4 ! L12

! Right rafter-----
K,n5,span-rbc,z ! K50 start of rafter at int with bottom chord
K,n6,midsp,h ! K60 Apex for Left rafter
KBETW,n5,n6,n5+1,Dist,spacing ! K51
K,n5+2,span-vbc,vr ! K52
K,n5+3,span-trbx,trby ! K53
K,n5+4,span-cr,col ! K54
K,n5+5,span-trtx,trty ! K55
KBETW,n6,n5,n6-1,Dist,spacing ! K59

L,n5,n5+1 ! L13
L,n5+1,n5+2 ! L14
L,n5+2,n5+3 ! L15
L,n5+3,n5+4 ! L16
L,n5+4,n5+5 ! L17
L,n5+5,n6-1 ! L18
L,n6-1,n6 ! L19

! Left vertical truss-----
K,n7,vbc,z ! K70 L vert to bottom chord ON vert
K,n8,vbc,vr ! K80 L vert to L rafter chord ON vert
KBETW,n7,n8,n7+1,Dist,spacing ! K71
KBETW,n8,n7,n8-1,Dist,spacing ! K79

L,n7,n7+1 ! L20
L,n7+1,n8-1 ! L21
L,n8-1,n8 ! L22

! Right vertical truss-----
K,n9,span-vbc,z ! K90 L vert to bottom chord ON vert
K,n10,span-vbc,vr ! K100 L vert to L rafter chord ON vert
KBETW,n9,n10,n9+1,Dist,spacing ! K91
KBETW,n10,n9,n10-1,Dist,spacing ! K99

L,n9,n9+1 ! L23
L,n9+1,n10-1 ! L24
L,n10-1,n10 ! L25

! / scissor brace-----
K,n11,trbx,trby ! K110
K,n12,span-trtx,trty ! K120

KBETW,n11,n12,n11+1,Dist,spacing ! K111
KBETW,n12,n11,n12-1,Dist,spacing ! K119
K,n11+3,ct,col ! K113
KBETW,n11+3,n11,n11+2,Dist,spacing ! K112
KBETW,n11+3,n12,n11+4,Dist,spacing ! K114
K,n11+6,midsp,tt ! K116 scissor truss crossing point
KBETW,n11+6,n11,n11+5,Dist,spacing ! K115
KBETW,n11+6,n12,n11+7,Dist,spacing ! K117

L,n11,n11+1 ! L26
L,n11+1,n11+2 ! L27
L,n11+2,n11+3 ! L28
L,n11+3,n11+4 ! L29
L,n11+4,n11+5 ! L30
L,n11+5,n11+6 ! L31
L,n11+6,n11+7 ! L32
L,n11+7,n12-1 ! L33
L,n12-1,n12 ! L34

! \ scissor brace-----
K,n13,span-trbx,trby ! K130
K,n14,trtx,trty ! K140
KBETW,n13,n14,n13+1,Dist,spacing ! K131
KBETW,n14,n13,n14-1,Dist,spacing ! K139
K,n13+3,span-ct,col ! K133
KBETW,n13+3,n13,n13+2,Dist,spacing ! K132
KBETW,n13+3,n14,n13+4,Dist,spacing ! K134
K,n13+6,midsp,tt ! K136 scissor truss crossing point
KBETW,n13+6,n13,n13+5,Dist,spacing ! K135
KBETW,n13+6,n14,n13+7,Dist,spacing ! K137

L,n13,n13+1 ! L35
L,n13+1,n13+2 ! L36
L,n13+2,n13+3 ! L37
L,n13+3,n13+4 ! L38
L,n13+4,n13+5 ! L39
L,n13+5,n13+6 ! L40
L,n13+6,n13+7 ! L41
L,n13+7,n14-1 ! L42
L,n14-1,n14 ! L43

! Collar Tie-----
K,n15,cr,col ! K150
K,n16,span-cr,col ! K160
KBETW,n15,n16,n15+1,Dist,spacing ! K151
KBETW,n16,n15,n16-1,Dist,spacing ! K159
K,n15+3,ct,col ! K153
KBETW,n15+3,n15,n15+2,Dist,spacing ! K152
KBETW,n15+3,n16,n15+4,Dist,spacing ! K154
K,n15+6,span-ct,col ! K156
KBETW,n15+6,n15,n15+5,Dist,spacing ! K155
KBETW,n15+6,n16,n15+7,Dist,spacing ! K157

L,n15,n15+1 ! L44
L,n15+1,n15+2 ! L45
L,n15+2,n15+3 ! L46
L,n15+3,n15+4 ! L47
L,n15+4,n15+5 ! L48
L,n15+5,n15+6 ! L49
L,n15+6,n15+7 ! L50
L,n15+7,n16-1 ! L51
L,n16-1,n16 ! L52

!-----Spring nodes

NKPT,n3,n3
NKPT,n4,n4
NKPT,n5,n5
NKPT,n6,n6
NKPT,n7,n7
NKPT,n8,n8
NKPT,n9,n9
NKPT,n10,n10
NKPT,n11,n11
NKPT,n11+3,n11+3
NKPT,n11+6,n11+6
NKPT,n12,n12
NKPT,n13,n13
NKPT,n13+3,n13+3
NKPT,n13+6,n13+6
NKPT,n14,n14
NKPT,n15,n15
NKPT,n15+3,n15+3
NKPT,n15+6,n15+6
NKPT,n16,n16

!-----

! Define the element types

ET,1,BEAM188 ! 3D beam elements for wood members
ET,2,COMBIN14,0,6 ! ROTZ - 1D linear spring damper
ET,3,COMBIN14,0,1 ! UX - 1D linear longitudinal spring for X disp
ET,4,COMBIN14,0,2 ! UY- 1D linear longitudinal spring for Y disp

! Real constants for springs

! NOTCHED DOVETAIL CONSTANTS-----

! Regular Dovetail Lap (ASSUME 20MM DOWEL FOR TENSION)

R,2,40000 ! (+) rotational stiffness DOVETAIL
!R,3,-40000 ! (-) rotational stiffness DOVETAIL

! Derived from Kitamori spring equations

R,4,50000000 ! X COMPRESSION Translation Stiffness Constants
R,5,50000000 ! Y COMPRESSION Translation

! From Kunecky and Hanaj paper on dowel tension Stiffness

```
! interpolated from 18mm and 22mm dowels
R,6,1200000 ! X TENSION Translation Stiffness Constants
R,7,1200000 ! Y TENSION Translation Stiffness Constants

! HALF LAP CONSTANTS-----
R,8,0.1 ! (+) rotational stiffness DOVETAIL
R,9,50000000 ! X Translation Stiffness Constants
R,10,50000000 ! Y Translation Stiffness Constants

! Rafter end mortise and tenon-----
! Derived from Kitamori spring equations
R,11,40000 ! (+) rotational stiffness
R,12,120000 ! (-) rotational stiffness
R,13,60000000 ! x longitudinal stiffness
R,14,60000000 ! y longitudinal stiffness

! Apex forked bridle joint-----
! Derived from Kitamori spring equations
R,15,40000 ! (+) rotational stiffness
R,16,50000000 ! x longitudinal stiffness
R,17,50000000 ! y longitudinal stiffness

! Properties of C24 and Spruce
MP,DENS,1,420 ! Density kg/m3
MP,EX,1,11e9 ! E_0,mean [Pa]
MP,EY,1,0.4e9 ! E_90,mean [Pa]
MP,EZ,1,0.4e9 ! E_90,mean [Pa]
MP,GXY,1,.7e9 ! Shear modulus
MP,GYZ,1,0.1e9
MP,GXZ,1,0.7e9
MP,PRXY,1,0.4 ! Poisson's ratio per US Forestry service for Spruce
MP,PRYZ,1,0.05
MP,PRXZ,1,0.4

! define the cross-sections
SECTYPE,1,BEAM,RECT
SECDATA,0.22,0.2 ! bottom chord
SECTYPE,2,BEAM,RECT
SECDATA,0.15,0.19 ! rafters
SECTYPE,3,BEAM,RECT
SECDATA,0.17,0.14 ! end verticals
SECTYPE,4,BEAM,RECT
SECDATA,0.13,0.14 ! diagonals
SECTYPE,5,BEAM,RECT
SECDATA,0.13,0.13 ! collar tie

!-----
!! MESHING !!
LESIZE,ALL,10*spacing ! set line element mesh size

! Mesh the wood members first
! all members will be material and element type 1
```

```
MAT,1
TYPE,1

! Bottom chord / tie beam-----
LSEL,S,LOC,Y,0 ! select bottom chord
LSEL,U,LENGTH,,spacing ! ensure no hinge segments are selected
SECNUM,1 ! set the section
LMESH,all !
CM,bottomchord_lines,line
CM,bottomchord_nodes,node
CM,bottomchord_elems,elem
ESEL,none

! RAFTERS-----
! Left rafter
LSEL,S,,6,12
LSEL,U,LENGTH,,spacing
SECNUM,2
LMESH,all
CM,rafterl_lines,line
CM,rafterl_nodes,node
CM,rafterl_elems,elem
LOCAL,11,0,rbc,z,,lrafang
EMODIF,all,ESYS,11
CSYS,0
ESEL,none

! Right rafter
LSEL,S,,13,19
LSEL,U,LENGTH,,spacing
SECNUM,2
LMESH,all
CM,rafterr_lines,line
CM,rafterr_nodes,node
CM,rafterr_elems,elem
LOCAL,12,0,midsp,h,,rrafang
EMODIF,all,ESYS,12
CSYS,0
ESEL,none

! vertical braces-----
LSEL,S,,20,22
LSEL,U,LENGTH,,spacing
SECNUM,3
LMESH,all
CM,vertl_lines,line
CM,vertl_nodes,node
CM,vertl_elems,elem
LOCAL,13,0,vbc,z,,90
EMODIF,all,ESYS,13
ESEL,none
```

```
LSEL,S,,,23,25
LSEL,U,LENGTH,,spacing
SECNUM,3
LMESH,all
CM,vertr_lines,line
CM,vertr_nodes,node
CM,vertr_elems,elem
EMODIF,all,ESYS,13
CSYS,0
ESEL,none

! cross braces
LSEL,S,,,26,34
LSEL,U,LENGTH,,spacing
SECNUM,4
LMESH,all
CM,crossl_lines,line
CM,crossl_nodes,node
CM,crossl_elems,elem
LOCAL,14,0,trbx,trby,,lcbang
EMODIF,all,ESYS,14
CSYS,0
ESEL,none

LSEL,S,,,35,43
LSEL,U,LENGTH,,spacing
SECNUM,4
LMESH,all
CM,crossr_lines,line
CM,crossr_nodes,node
CM,crossr_elems,elem
LOCAL,15,0,trtx,trty,,rcbang
EMODIF,all,ESYS,15
CSYS,0
ESEL,none

! collar tie
LSEL,S,LOC,Y,col
LSEL,U,LENGTH,,spacing
SECNUM,5
LMESH,all
CM,collartie_lines,line
CM,collartie_nodes,node
CM,collartie_elems,elem
ESEL,all
!nummrg,all

! Define spring elements-----
ESEL,none
ALLSEL
! bottom chord to L rafter-
! Notched dovetail Comp
```

MAT,1
TYPE,2
REAL,11
E,162,n3 ! rotational spring
TYPE,3
REAL,13
E,162,n3 ! X longitudinal spring
TYPE,4
REAL,14
E,162,n3 ! Y longitudinal spring

! bottom chord to L vert truss-
! Notched dovetail T
MAT,1
TYPE,2
REAL,2
E,166,n7 ! rotational spring
TYPE,3
REAL,6
E,166,n7 ! X longitudinal spring
TYPE,4
REAL,7
E,166,n7 ! Y longitudinal spring

! bottom chord to R vert truss-
! Notched dovetail T
MAT,1
TYPE,2
REAL,2
E,179,n9 ! rotational spring
TYPE,3
REAL,6
E,179,n9 ! X longitudinal spring
TYPE,4
REAL,7
E,179,n9 ! Y longitudinal spring

! bottom chord to R rafter-
MAT,1
TYPE,2
REAL,11
E,241,n5 ! rotational spring
TYPE,3
REAL,13
E,241,n5 ! X longitudinal spring
TYPE,4
REAL,14
E,241,n5 ! Y longitudinal spring

! L rafter to R rafter-
MAT,1
TYPE,2

```
REAL,15
E,n4,n6 ! rotational spring
TYPE,3
REAL,16
E,n4,n6 ! X longitudinal spring
TYPE,4
REAL,17
E,n4,n6 ! Y longitudinal spring

! L rafter to L vert truss-
MAT,1
TYPE,2
REAL,2
E,259,n8 ! rotational spring
TYPE,3
REAL,6
E,259,n8 ! X longitudinal spring
TYPE,4
REAL,7
E,259,n8 ! Y longitudinal spring

! R rafter to R vert truss-
MAT,1
TYPE,2
REAL,2
E,356,n10 ! rotational spring
TYPE,3
REAL,6
E,356,n10 ! X longitudinal spring
TYPE,4
REAL,7
E,356,n10 ! Y longitudinal spring

! L rafter to lower cross brace-
MAT,1
TYPE,2
REAL,2
E,286,n11 ! rotational spring
TYPE,3
REAL,4
E,286,n11 ! X longitudinal spring
TYPE,4
REAL,5
E,286,n11 ! Y longitudinal spring

! / cross brace int with collar tie-
MAT,1
TYPE,2
REAL,8
E,n15+3,n11+3 ! rotational spring
TYPE,3
REAL,9
```

E,n15+3,n11+3 ! X longitudinal spring
TYPE,4
REAL,10
E,n15+3,n11+3 ! Y longitudinal spring

! / cross brace to \ cross brace-
MAT,1
TYPE,2
REAL,8
E,n13+6,n11+6 ! rotational spring
TYPE,3
REAL,9
E,n13+6,n11+6 ! X longitudinal spring
TYPE,4
REAL,10
E,n13+6,n11+6 ! Y longitudinal spring

! / cross brace to R rafter-
MAT,1
TYPE,2
REAL,2
E,412,n12 ! rotational spring
TYPE,3
REAL,4
E,412,n12 ! X longitudinal spring
TYPE,4
REAL,5
E,412,n12 ! Y longitudinal spring

! R vert truss to R rafter-
MAT,1
TYPE,2
REAL,2
E,356,n10! rotational spring
TYPE,3
REAL,6
E,356,n10 ! X longitudinal spring
TYPE,4
REAL,7
E,356,n10 ! Y longitudinal spring

! \ cross brace to collar tie-
MAT,1
TYPE,2
REAL,8
E,n15+6,n13+3 ! rotational spring
TYPE,3
REAL,9
E,n15+6,n13+3 ! X longitudinal spring
TYPE,4
REAL,10
E,n15+6,n13+3 ! Y longitudinal spring

```
! \ cross brace to R rafter-
MAT,1
TYPE,2
REAL,2
E,383,n13 ! rotational spring
TYPE,3
REAL,4
E,383,n13 ! X longitudinal spring
TYPE,4
REAL,5
E,383,n13 ! Y longitudinal spring

! \ cross brace to L rafter-
MAT,1
TYPE,2
REAL,2
E,315,n14 ! rotational spring
TYPE,3
REAL,4
E,315,n14 ! X longitudinal spring
TYPE,4
REAL,5
E,315,n14 ! Y longitudinal spring

! collar tie to L rafter-
MAT,1
TYPE,2
REAL,2
E,n15,302 ! rotational spring
TYPE,3
REAL,4
E,n15,302 ! X longitudinal spring
TYPE,4
REAL,5
E,n15,302 ! Y longitudinal spring

! collar tie to R rafter-
MAT,1
TYPE,2
REAL,2
E,n16,399 ! rotational spring
TYPE,3
REAL,4
E,n16,399 ! X longitudinal spring
TYPE,4
REAL,5
E,n16,399 ! Y longitudinal spring

/eshape,1
EPLOT
```


ALLSEL

02_CEs

! Connection types:

! TYPE 1 - half lap into continuous member or mortise and tenon (1 hinge segment)

! TYPE 2 - Corner bridle joint(2 hinge segments)

! TYPE 3 - half lap between two continuous members (4 hinge segments)

! Set CEs for overlapping nodes

! Apply constraint equations to the hinge segments such that the deform the same at both ends

! Set BCs to link the overlapping nodes at the joint

! BCs restrict all but ROTZ

! may have to adjust later if we want UX or UY springs to work

! Bottom Chord to L rafter-----

! spring rotational constraints

CE,NEXT,0,162,rotx,1,n3,rotx,-1 ! CE1

CE,NEXT,0,162,roty,1,n3,roty,-1 ! CE2

ALLSEL,all

! TYPE 1 hinge segment

LSEL,S,,6

NSLL,S,1

NSEL,A,NODE,,n3 ! because the keypoint at the spring end is not meshed and directly associated with the line we have to manually select it here

*get,node1,NODE,0,NUM,MIN

*get,node2,NODE,0,NUM,MAX

CE,NEXT,0,node1,ux,1,node2,ux,-1 ! CE3

CE,NEXT,0,node1,uy,1,node2,uy,-1 ! CE4

CE,NEXT,0,node1,rotx,1,node2,rotx,-1 ! CE6

CE,NEXT,0,node1,roty,1,node2,roty,-1 ! CE7

CE,NEXT,0,node1,rotz,1,node2,rotz,-1 ! CE8

ALLSEL,all

! bottom chord to L vert truss-----

CE,NEXT,0,166,rotx,1,n7,rotx,-1 ! CE

CE,NEXT,0,166,roty,1,n7,roty,-1 ! CE

ALLSEL,all

! TYPE 1 - bottom chord to L vert truss

LSEL,S,,20

NSLL,S,1

NSEL,A,NODE,,n7

*get,node1,NODE,0,NUM,MIN

*get,node2,NODE,0,NUM,MAX

CE,NEXT,0,node1,ux,1,node2,ux,-1 ! CE

CE,NEXT,0,node1,uy,1,node2,uy,-1 ! CE

CE,NEXT,0,node1,rotx,1,node2,rotx,-1 ! CE

CE,NEXT,0,node1,roty,1,node2,roty,-1 ! CE

CE,NEXT,0,node1,rotz,1,node2,rotz,-1 ! CE

ALLSEL,all

! bottom chord to R vert truss -----

```

CE,NEXT,0,179,rotx,1,n9,rotx,-1 ! CE
CE,NEXT,0,179,roty,1,n9,roty,-1 ! CE
ALLSEL,all
LSEL,S,,,23
NSLL,S,1
NSEL,A,NODE,,n9
*get,node1,NODE,0,NUM,MIN
*get,node2,NODE,0,NUM,MAX
CE,NEXT,0,node1,ux,1,node2,ux,-1 ! CE
CE,NEXT,0,node1,uy,1,node2,uy,-1 ! CE
CE,NEXT,0,node1,rotx,1,node2,rotx,-1 ! CE
CE,NEXT,0,node1,roty,1,node2,roty,-1 ! CE
CE,NEXT,0,node1,rotz,1,node2,rotz,-1 ! CE
ALLSEL,all
! bottom chord to R rafter-----
CE,NEXT,0,241,rotx,1,n5,rotx,-1
CE,NEXT,0,241,roty,1,n5,roty,-1
ALLSEL,all

! TYPE 1 - R rafter meets bottom chord
LSEL,S,,,13
NSLL,S,1
NSEL,A,NODE,,n5 ! because the keypoint at the spring end is not meshed and directly associated with
the line we have to manually select it here
*get,node1,NODE,0,NUM,MIN
*get,node2,NODE,0,NUM,MAX
CE,NEXT,0,node1,ux,1,node2,ux,-1
CE,NEXT,0,node1,uy,1,node2,uy,-1
CE,NEXT,0,node1,rotx,1,node2,rotx,-1
CE,NEXT,0,node1,roty,1,node2,roty,-1
CE,NEXT,0,node1,rotz,1,node2,rotz,-1
ALLSEL,all
! APEX / L rafter to R rafter-----
CE,NEXT,0,n4,rotx,1,n6,rotx,-1
CE,NEXT,0,n4,roty,1,n6,roty,-1
ALLSEL,all
! TYPE 2 hinge - Apex Left
LSEL,S,,,12
NSLL,S,1
NSEL,A,,,n4
*get,node1,NODE,0,NUM,MIN
*get,node2,NODE,0,NUM,MAX
CE,NEXT,0,node1,ux,1,node2,ux,-1
CE,NEXT,0,node1,uy,1,node2,uy,-1
CE,NEXT,0,node1,rotx,1,node2,rotx,-1
CE,NEXT,0,node1,roty,1,node2,roty,-1
CE,NEXT,0,node1,rotz,1,node2,rotz,-1
ALLSEL,all
! TYPE 2 - Apex Right
LSEL,S,,,19
NSLL,S,1
NSEL,A,,,n6

```

```

*get,node1,NODE,0,NUM,MIN
*get,node2,NODE,0,NUM,MAX
CE,NEXT,0,node1,ux,1,node2,ux,-1
CE,NEXT,0,node1,uy,1,node2,uy,-1
CE,NEXT,0,node1,rotx,1,node2,rotx,-1
CE,NEXT,0,node1,roty,1,node2,roty,-1
CE,NEXT,0,node1,rotz,1,node2,rotz,-1
! L rafter to L vert truss-----
CE,NEXT,0,259,rotx,1,n8,rotx,-1
CE,NEXT,0,259,roty,1,n8,roty,-1
ALLSEL,all
! TYPE 1
LSEL,S,,22
NSLL,S,1
NSEL,A,NODE,,n8
*get,node1,NODE,0,NUM,MIN
*get,node2,NODE,0,NUM,MAX
CE,NEXT,0,node1,ux,1,node2,ux,-1
CE,NEXT,0,node1,uy,1,node2,uy,-1
CE,NEXT,0,node1,rotx,1,node2,rotx,-1
CE,NEXT,0,node1,roty,1,node2,roty,-1
CE,NEXT,0,node1,rotz,1,node2,rotz,-1
ALLSEL,all
! R rafter to R vert truss-----
CE,NEXT,0,356,rotx,1,n10,rotx,-1
CE,NEXT,0,356,roty,1,n10,roty,-1
ALLSEL,all
LSEL,S,,25
NSLL,S,1
NSEL,A,NODE,,n10
*get,node1,NODE,0,NUM,MIN
*get,node2,NODE,0,NUM,MAX
CE,NEXT,0,node1,ux,1,node2,ux,-1
CE,NEXT,0,node1,uy,1,node2,uy,-1
CE,NEXT,0,node1,rotx,1,node2,rotx,-1
CE,NEXT,0,node1,roty,1,node2,roty,-1
CE,NEXT,0,node1,rotz,1,node2,rotz,-1
ALLSEL,all
! / cross brace to L rafter-----
CE,NEXT,0,286,rotx,1,n11,rotx,-1
CE,NEXT,0,286,roty,1,n11,roty,-1
ALLSEL,all
LSEL,S,,26
NSLL,S,1
NSEL,A,NODE,,n11
*get,node1,NODE,0,NUM,MIN
*get,node2,NODE,0,NUM,MAX
CE,NEXT,0,node1,ux,1,node2,ux,-1
CE,NEXT,0,node1,uy,1,node2,uy,-1
CE,NEXT,0,node1,rotx,1,node2,rotx,-1
CE,NEXT,0,node1,roty,1,node2,roty,-1
CE,NEXT,0,node1,rotz,1,node2,rotz,-1

```

```

ALLSEL,all
! / cross brace int with collar tie-----
CE,NEXT,0,n15+3,rotx,1,n11+3,rotx,-1
CE,NEXT,0,n15+3,roty,1,n11+3,roty,-1
ALLSEL,all
! TYPE 3
LSEL,S,,,28
NSLL,S,1
NSEL,A,NODE,,113
*get,node1,NODE,0,NUM,MIN
*get,node2,NODE,0,NUM,MAX
CE,NEXT,0,node1,ux,1,node2,ux,-1
CE,NEXT,0,node1,uy,1,node2,uy,-1
CE,NEXT,0,node1,rotx,1,node2,rotx,-1
CE,NEXT,0,node1,roty,1,node2,roty,-1
CE,NEXT,0,node1,rotz,1,node2,rotz,-1
allsel,all
LSEL,S,,,29
NSLL,S,1
NSEL,A,NODE,,113
*get,node1,NODE,0,NUM,MIN
*get,node2,NODE,0,NUM,MAX
CE,NEXT,0,node1,ux,1,node2,ux,-1
CE,NEXT,0,node1,uy,1,node2,uy,-1
CE,NEXT,0,node1,rotx,1,node2,rotx,-1
CE,NEXT,0,node1,roty,1,node2,roty,-1
CE,NEXT,0,node1,rotz,1,node2,rotz,-1
allsel,all
LSEL,S,,,46
NSLL,S,1
NSEL,A,NODE,,153
*get,node1,NODE,0,NUM,MIN
*get,node2,NODE,0,NUM,MAX
CE,NEXT,0,node1,ux,1,node2,ux,-1
CE,NEXT,0,node1,uy,1,node2,uy,-1
CE,NEXT,0,node1,rotx,1,node2,rotx,-1
CE,NEXT,0,node1,roty,1,node2,roty,-1
CE,NEXT,0,node1,rotz,1,node2,rotz,-1
allsel,all
LSEL,S,,,47
NSLL,S,1
NSEL,A,NODE,,153
*get,node1,NODE,0,NUM,MIN
*get,node2,NODE,0,NUM,MAX
CE,NEXT,0,node1,ux,1,node2,ux,-1
CE,NEXT,0,node1,uy,1,node2,uy,-1
CE,NEXT,0,node1,rotx,1,node2,rotx,-1
CE,NEXT,0,node1,roty,1,node2,roty,-1
CE,NEXT,0,node1,rotz,1,node2,rotz,-1
allsel,all
! / cross brace to \ cross brace-----
CE,NEXT,0,n13+6,rotx,1,n11+6,rotx,-1

```

```

CE,NEXT,0,n13+6,roty,1,n11+6,roty,-1
ALLSEL,all
LSEL,S,,,31 ! / hinge segments
NSLL,S,1
NSEL,A,NODE,,116
*get,node1,NODE,0,NUM,MIN
*get,node2,NODE,0,NUM,MAX
CE,NEXT,0,node1,ux,1,node2,ux,-1
CE,NEXT,0,node1,uy,1,node2,uy,-1
CE,NEXT,0,node1,rotx,1,node2,rotx,-1
CE,NEXT,0,node1,roty,1,node2,roty,-1
CE,NEXT,0,node1,rotz,1,node2,rotz,-1
allsel,all
LSEL,S,,,32 ! / hinge segments
NSLL,S,1
NSEL,A,NODE,,116
*get,node1,NODE,0,NUM,MIN
*get,node2,NODE,0,NUM,MAX
CE,NEXT,0,node1,ux,1,node2,ux,-1
CE,NEXT,0,node1,uy,1,node2,uy,-1
CE,NEXT,0,node1,rotx,1,node2,rotx,-1
CE,NEXT,0,node1,roty,1,node2,roty,-1
CE,NEXT,0,node1,rotz,1,node2,rotz,-1
allsel,all
LSEL,S,,,40 ! \ hinge segments
NSLL,S,1
NSEL,A,NODE,,136
*get,node1,NODE,0,NUM,MIN
*get,node2,NODE,0,NUM,MAX
CE,NEXT,0,node1,ux,1,node2,ux,-1
CE,NEXT,0,node1,uy,1,node2,uy,-1
CE,NEXT,0,node1,rotx,1,node2,rotx,-1
CE,NEXT,0,node1,roty,1,node2,roty,-1
CE,NEXT,0,node1,rotz,1,node2,rotz,-1
allsel,all
LSEL,S,,,41 ! \ hinge segments
NSLL,S,1
NSEL,A,NODE,,136
*get,node1,NODE,0,NUM,MIN
*get,node2,NODE,0,NUM,MAX
CE,NEXT,0,node1,ux,1,node2,ux,-1
CE,NEXT,0,node1,uy,1,node2,uy,-1
CE,NEXT,0,node1,rotx,1,node2,rotx,-1
CE,NEXT,0,node1,roty,1,node2,roty,-1
CE,NEXT,0,node1,rotz,1,node2,rotz,-1
allsel,all
! / cross brace to R rafter-----
CE,NEXT,0,412,rotx,1,n12,rotx,-1
CE,NEXT,0,412,roty,1,n12,roty,-1
ALLSEL,all
LSEL,S,,,34
NSLL,S,1

```

```

NSEL,A,NODE,,n12
*get,node1,NODE,0,NUM,MIN
*get,node2,NODE,0,NUM,MAX
CE,NEXT,0,node1,ux,1,node2,ux,-1
CE,NEXT,0,node1,uy,1,node2,uy,-1
CE,NEXT,0,node1,rotx,1,node2,rotx,-1
CE,NEXT,0,node1,roty,1,node2,roty,-1
CE,NEXT,0,node1,rotz,1,node2,rotz,-1
ALLSEL,all
! \ cross brace to collar tie-----
CE,NEXT,0,n15+6,rotx,1,n13+3,rotx,-1
CE,NEXT,0,n15+6,roty,1,n13+3,roty,-1
ALLSEL,all
LSEL,S,,,37 ! \ segments
NSLL,S,1
NSEL,A,NODE,,133
*get,node1,NODE,0,NUM,MIN
*get,node2,NODE,0,NUM,MAX
CE,NEXT,0,node1,ux,1,node2,ux,-1
CE,NEXT,0,node1,uy,1,node2,uy,-1
CE,NEXT,0,node1,rotx,1,node2,rotx,-1
CE,NEXT,0,node1,roty,1,node2,roty,-1
CE,NEXT,0,node1,rotz,1,node2,rotz,-1
ALLSEL,all
LSEL,S,,,38 ! \ segments
NSLL,S,1
NSEL,A,NODE,,133
*get,node1,NODE,0,NUM,MIN
*get,node2,NODE,0,NUM,MAX
CE,NEXT,0,node1,ux,1,node2,ux,-1
CE,NEXT,0,node1,uy,1,node2,uy,-1
CE,NEXT,0,node1,rotx,1,node2,rotx,-1
CE,NEXT,0,node1,roty,1,node2,roty,-1
CE,NEXT,0,node1,rotz,1,node2,rotz,-1
ALLSEL,all
LSEL,S,,,49 ! - segments
NSLL,S,1
NSEL,A,NODE,,156
*get,node1,NODE,0,NUM,MIN
*get,node2,NODE,0,NUM,MAX
CE,NEXT,0,node1,ux,1,node2,ux,-1
CE,NEXT,0,node1,uy,1,node2,uy,-1
CE,NEXT,0,node1,rotx,1,node2,rotx,-1
CE,NEXT,0,node1,roty,1,node2,roty,-1
CE,NEXT,0,node1,rotz,1,node2,rotz,-1
LSEL,S,,,50 ! - segments
NSLL,S,1
NSEL,A,NODE,,156
*get,node1,NODE,0,NUM,MIN
*get,node2,NODE,0,NUM,MAX
CE,NEXT,0,node1,ux,1,node2,ux,-1
CE,NEXT,0,node1,uy,1,node2,uy,-1

```

```

CE,NEXT,0,node1,rotx,1,node2,rotx,-1
CE,NEXT,0,node1,roty,1,node2,roty,-1
CE,NEXT,0,node1,rotz,1,node2,rotz,-1
! \ cross brace to R rafter-----
CE,NEXT,0,383,rotx,1,n13,rotx,-1
CE,NEXT,0,383,roty,1,n13,roty,-1
ALLSEL,all
LSEL,S,,35
NSLL,S,1
NSEL,A,NODE,,n13
*get,node1,NODE,0,NUM,MIN
*get,node2,NODE,0,NUM,MAX
CE,NEXT,0,node1,ux,1,node2,ux,-1
CE,NEXT,0,node1,uy,1,node2,uy,-1
CE,NEXT,0,node1,rotx,1,node2,rotx,-1
CE,NEXT,0,node1,roty,1,node2,roty,-1
CE,NEXT,0,node1,rotz,1,node2,rotz,-1
allsel,all
! \ cross brace to L rafter-----
CE,NEXT,0,315,rotx,1,n14,rotx,-1
CE,NEXT,0,315,roty,1,n14,roty,-1
ALLSEL,all
LSEL,S,,43
NSLL,S,1
NSEL,A,NODE,,n14
*get,node1,NODE,0,NUM,MIN
*get,node2,NODE,0,NUM,MAX
CE,NEXT,0,node1,ux,1,node2,ux,-1
CE,NEXT,0,node1,uy,1,node2,uy,-1
CE,NEXT,0,node1,rotx,1,node2,rotx,-1
CE,NEXT,0,node1,roty,1,node2,roty,-1
CE,NEXT,0,node1,rotz,1,node2,rotz,-1
allsel,all
! collar tie to L rafter-----
CE,NEXT,0,n15,rotx,1,302,rotx,-1
CE,NEXT,0,n15,roty,1,302,roty,-1
ALLSEL,all
LSEL,S,,44
NSLL,S,1
NSEL,A,NODE,,n15
*get,node1,NODE,0,NUM,MIN
*get,node2,NODE,0,NUM,MAX
CE,NEXT,0,node1,ux,1,node2,ux,-1
CE,NEXT,0,node1,uy,1,node2,uy,-1
CE,NEXT,0,node1,rotx,1,node2,rotx,-1
CE,NEXT,0,node1,roty,1,node2,roty,-1
CE,NEXT,0,node1,rotz,1,node2,rotz,-1
allsel,all
! collar tie to R rafter-----
CE,NEXT,0,n16,rotx,1,399,rotx,-1
CE,NEXT,0,n16,roty,1,399,roty,-1 ! CE34
ALLSEL,all

```

```

LSEL,S,,,52
NSLL,S,1
NSEL,A,NODE,,n16
*get,node1,NODE,0,NUM,MIN
*get,node2,NODE,0,NUM,MAX
CE,NEXT,0,node1,ux,1,node2,ux,-1
CE,NEXT,0,node1,uy,1,node2,uy,-1
CE,NEXT,0,node1,rotx,1,node2,rotx,-1
CE,NEXT,0,node1,roty,1,node2,roty,-1
CE,NEXT,0,node1,rotz,1,node2,rotz,-1
!-----
! Set BCs to link the ends of the hinge segments
! cross brace intersection constraint between braces
! Needed for the rigid case but commented out until then
!LSEL,S,,,41
!LSEL,A,,,31
!NSLL,S,1
!*get,node1,NODE,0,NUM,MIN
!*get,node2,NODE,0,NUM,MAX
!CE,NEXT,0,node1,ux,1,node2,ux,-1
!CE,NEXT,0,node1,uy,1,node2,uy,-1
!CE,NEXT,0,node1,rotx,1,node2,rotx,-1
!CE,NEXT,0,node1,roty,1,node2,roty,-1
!CE,NEXT,0,node1,rotz,1,node2,rotz,-1 ! CE40
!ALLSEL,all
! cross brace intersection constraint with collar tie (L)
! Needed for the rigid case but commented out until then
!LSEL,S,,,29
!LSEL,A,,,47
!NSLL,S,1
!*get,node1,NODE,0,NUM,MIN
!*get,node2,NODE,0,NUM,MAX
!CE,NEXT,0,node1,ux,1,node2,ux,-1
!CE,NEXT,0,node1,uy,1,node2,uy,-1
!CE,NEXT,0,node1,rotx,1,node2,rotx,-1
!CE,NEXT,0,node1,roty,1,node2,roty,-1
!CE,NEXT,0,node1,rotz,1,node2,rotz,-1 ! CE46
!ALLSEL,all
! cross brace intersection constraint with collar tie (R)
! Needed for the rigid case but commented out until then
!LSEL,S,,,38
!LSEL,A,,,49
!NSLL,S,1
!*get,node1,NODE,0,NUM,MIN
!*get,node2,NODE,0,NUM,MAX
!CE,NEXT,0,node1,ux,1,node2,ux,-1
!CE,NEXT,0,node1,uy,1,node2,uy,-1
!CE,NEXT,0,node1,rotx,1,node2,rotx,-1
!CE,NEXT,0,node1,roty,1,node2,roty,-1
!CE,NEXT,0,node1,rotz,1,node2,rotz,-1 ! CE52
!ALLSEL,all
!-----

```


ALLSEL,all
ANTYPE,0 ! Set as a static analysis

03 BCs

! GLOBAL BOUNDARY CONDITIONS

!-----

! Set the far left node as a pin, and restrain from OOP rotation

NSEL,S,LOC,X,0 ! sel far left node

D,all,UX ! Left end defined as pin

D,all,UY ! Left end defined as pin

D,all,UZ ! Left end defined as pin

D,all,ROTX

D,all,ROTY

! Set the far right node as a roller, and restrain from OOP rotation

NSEL,S,LOC,X,span

D,all,UY ! other end defined as roller

D,all,ROTX

D,all,ROTY

NSEL,ALL

D,all,UZ

D,all,ROTX

D,all,ROTY

ALLSEL,all

04 loads:

! DEFINE LOADING AND LOAD STEPS

wfac=1.5 ! combination factor for wind

dfac=1.35 ! combination factor for dead load and self weight

lfac=1 ! combination factor for live load

tribwidth=1.1 ! [m]

windFGH=273*wfac ! [N/m²] Windward pressure

windI=78*wfac ! [N/m²] Leeward suction

windJ=117*wfac ! [N/m²] Leeward suction

! LOADSTEP 1: PERMANENT LOAD

dead=550*dfac ! [N/m²]

ACEL,0,9.81*dfac,0 ! gravity load / self weight

LSEL,S,,6,19

NSLL,S

*GET,nonodes,NODE,,COUNT

F,all,FY,-dead*tribwidth/nonodes

```
ALLSEL,all
/input,03_BCs
LSWRITE,1
FDELE,all
ALLSEL,all
```

```
! LOADSTEP 2: LIVE LOAD
live=600*lfac ! [N/m^2]
```

```
LSEL,S,,,6,19
NSLL,S
*GET,nonodes,NODE,,COUNT
F,all,FY,-live*tribwidth/nonodes
ALLSEL,all
/input,03_BCs
LSWRITE,2
FDELE,all
ALLSEL,all
```

```
! LOADSTEP 3: WIND LOAD
! Apply EUROCODE Wind Loads according to EN-1991-1-1-4
lrafang = atan(h/(midsp-rbc))
```

```
! Start with windward side (LEFT), constant normal pressure along length
LSEL,S,,,7,11
NSLL,S,1
*GET,nonodes,NODE,,COUNT
F,all,FY,-windFGH*sin(lrafang)*tribwidth/nonodes ! Project normal load into the Y axis
F,all,FX,windFGH*cos(lrafang)*tribwidth/nonodes ! Project normal load into the X axis
ALLSEL,all
/input,03_BCs
allsel,all
```

```
! Leeward side (RIGHT UPPER), constant normal pressure along length
LSEL,S,,,14,19
NSLL,S
NSEL,R,LOC,X,midsp,midsp+2.4
*GET,nonodes,NODE,,COUNT
F,all,FY,windJ*sin(lrafang)*tribwidth/nonodes ! Project normal load into the Y axis
F,all,FX,windJ*cos(lrafang)*tribwidth/nonodes ! Project normal load into the X axis
ALLSEL,all
allsel,all
```

```
! Leeward side (RIGHT LOWER), constant normal pressure along length
LSEL,S,,,14,19
NSLL,S
NSEL,R,LOC,X,midsp+2.4,span-rbc
*GET,nonodes,NODE,,COUNT
F,all,FY,windI*sin(lrafang)*tribwidth/nonodes ! Project normal load into the Y axis
F,all,FX,windI*cos(lrafang)*tribwidth/nonodes ! Project normal load into the X axis
ALLSEL,all
```

LSWRITE,3

ALLSEL,all
FDELE,all
ALLSEL,all

05 post:

! DEFINE LOAD COMBINATIONS

LCOPER,zero

SET,1

LCWRITE,1

LCDEF,2,2

LCDEF,3,3

LCOPER,ADD,2

LCOPER,ADD,3

LCWRITE,4

RAPPND,4

SET,4 ! (where N is 1-4)

!/SHOW,PNG ! send plots to PNG file

!/GFILE,500 ! plot file resolution

!/RGB,INDEX,100,100,100,0 ! switch the

!/RGB,INDEX,0,0,0,15 ! B/W colors

!/VIEW,1,1,1,1 ! set the viewing direction

allsel

ESEL,S,ENAME,,188 ! select only BEAM188 elements

ETABLE,Fx-i,SMISC,1 ! axial force in BEAM188, node I

ETABLE,Fx-j,SMISC,14 ! axial force in BEAM188, node J

ETABLE,My-i,SMISC,2 ! y-bending moment in BEAM188, node I

ETABLE,My-j,SMISC,15 ! y-bending moment in BEAM188, node J

ETABLE,Mz-i,SMISC,3 ! z-bending moment in BEAM188, node I

ETABLE,Mz-j,SMISC,16 ! z-bending moment in BEAM188, node J

ETABLE,SFy-i,SMISC,6 ! y-shear force in BEAM188, node I

ETABLE,SFy-j,SMISC,19 ! y-shear force in BEAM188, node J

ETABLE,SFz-i,SMISC,5 ! z-shear force in BEAM188, node I

ETABLE,SFz-j,SMISC,18 ! z-shear force in BEAM188, node J

/TSPEC,0,10

/PLOPTS,INFO,3 ! controls display of legend, 3 is default when GUI is on

/PLOPTS,LEG1,1 ! Header portion of legend column is on

```

/PLOPTS,LEG2,1 ! view portion of legend column is on
/PLOPTS,LEG3,1 ! contour portion of legend column is on
/PLOPTS,FRAME,0 ! turn off frame border lines around windows
/PLOPTS,TITLE,1 ! Turn on bottom left text title
/PLOPTS,MINM,0 ! turns off min-max symbols
/PLOPTS,FILE,0 ! do not include jobname in the legend
/PLOPTS,WINS,1 ! autosize graphics window
/PLOPTS,WP,0 ! working plane off
/PLOPTS,DATE,0 ! no date shown
/VSCALE,1,0.5,0 ! scale length of displayed vectors in window 1 to half, using relative length scaling
/eshape,1 ! display elems with shapes scaled by real constants, section defs, etc
/dev,font,1,Courier*New,400,0,-24,0,0,,
/SHOW,png,,0
PNGR,color,2
PNGR,COMP,1,-1
PNGR,ORIENT,HORIZ
/GFILE,800
!*
/contour,,38 ! assigns the number of contours, max = 128
PLDISP,2 ! Plot deformed shape over the undeformed shape
PLNSOL,U,SUM,0,1 ! Contour plot of sum total deflection
/CMAP,_TEMPCMAP_,CMP,,SAVE
/RGB,INDEX,100,100,100,0
/RGB,INDEX,80,80,80,13
/RGB,INDEX,60,60,60,14
/RGB,INDEX,0,0,0,15
/VIEW,1,0,0,1
/REPLOT
/CMAP,_TEMPCMAP_,CMP
/DELETE,_TEMPCMAP_,CMP
/SHOW,CLOSE
/DEVICE,VECTOR,0 ! turns off vector graphics
/SHOW,TERM !
/REPLOT

!PLLS,My-i,My-j
!PLLS,Mz-i,Mz-j
!PLLS,SFz-i,SFz-j
!PLLS,SFy-i,SFy-j

/dev,font,1,Courier*New,400,0,-24,0,0,,
/SHOW,png,,0
pngr,color,2
PNGR,COMP,1,-1
PNGR,ORIENT,HORIZ
/GFILE,800
!*
/contour,,38 ! assigns the number of contours, max = 128
PLLS,Fx-i,Fx-j
/CMAP,_TEMPCMAP_,CMP,,SAVE
/RGB,INDEX,100,100,100,0
/RGB,INDEX,80,80,80,13

```

```
/RGB,INDEX, 60, 60, 60,14
/RGB,INDEX, 0, 0, 0,15
/VIEW,1,0,0,1
/REPLOT
/CMAP,_TEMPCMAP_,CMP
/DELETE,_TEMPCMAP_,CMP
/SHOW,CLOSE
/DEVICE,VECTOR,0 ! turns off vector graphics
/SHOW, TERM !

/dev,font,1,Courier*New,400,0,-24,0,0,,
/SHOW,png,,0
png,color,2
PNGR,COMP,1,-1
PNGR,ORIENT,HORIZ
/GFILE,800
!*
/contour,,38 ! assigns the number of contours, max = 128
PLLS,Mz-i,Mz-j
/CMAP,_TEMPCMAP_,CMP,,SAVE
/RGB,INDEX,100,100,100, 0
/RGB,INDEX, 80, 80, 80,13
/RGB,INDEX, 60, 60, 60,14
/RGB,INDEX, 0, 0, 0,15
/VIEW,1,0,0,1
/REPLOT
/CMAP,_TEMPCMAP_,CMP
/DELETE,_TEMPCMAP_,CMP
/SHOW,CLOSE
/DEVICE,VECTOR,0 ! turns off vector graphics
/SHOW, TERM !

/dev,font,1,Courier*New,400,0,-24,0,0,,
/SHOW,png,,0
png,color,2
PNGR,COMP,1,-1
PNGR,ORIENT,HORIZ
/GFILE,800
!*
/contour,,38 ! assigns the number of contours, max = 128
PLLS,SFy-i,SFy-j
/CMAP,_TEMPCMAP_,CMP,,SAVE
/RGB,INDEX,100,100,100, 0
/RGB,INDEX, 80, 80, 80,13
/RGB,INDEX, 60, 60, 60,14
/RGB,INDEX, 0, 0, 0,15
/VIEW,1,0,0,1
/REPLOT
/CMAP,_TEMPCMAP_,CMP
/DELETE,_TEMPCMAP_,CMP
/SHOW,CLOSE
/DEVICE,VECTOR,0 ! turns off vector graphics
```

/SHOW, TERM !

! Partition windows for displays

/WIND,ALL,OFF

/WIND,1,LTOP

/WIND,2,RTOP

/WIND,3,LBOT

/WIND,4,RBOT

/GCMD,1,PLDISP,2 ! Plot deformed shape over the undeformed shape

/GCMD,1,PLNSOL,U,SUM,0,1 ! Contour plot of sum total deflection

/GCMD,2,PLLS,Fx-i,Fx-j

/GCMD,3,PLLS,Mz-i,Mz-j

/GCMD,4,PLLS,SFy-i,SFy-j

GPLOT